SUBSPACE BASED CARRIER FREQUENCY OFFSET ESTIMATIONS FOR OFDM SYSTEMS

KYAWT KYAWT KHAING

NATIONAL UNIVERSITY OF SINGAPORE

2004

SUBSPACE BASED CARRIER FREQUENCY OFFSET ESTIMATIONS FOR OFDM SYSTEMS

KYAWT KYAWT KHAING

(B.Eng., Yangon Technological University)

A THESIS SUBMITTED

FOR THE DEGREE OF MASTER OF ENGINEERING

DEPARTMENT OF ELECTRICAL&COMPUTER ENGINEERING

NATIONAL UNIVERSITY OF SINGAPORE

2004

ACKNOWLEDGMENT

I would like to express my deepest thanks and gratitude to my supervisor, Dr. A. Rahim Leyman, for his invaluable guidance, patience and encouragement in me during the course of this research work. His encouragement and keen insight helped me to stay focused and to complete this research. I am also indebted to Dr. Chew Yong Huat for his support and encouragement.

Specially thanks to Suwandi Rusli Lie for his invaluable suggestions as well as his encouragements. I owe a great thank to all of the friends and colleagues for all of the good times, assistance and friendship during my academic years.

To my husband, Nyein Chan Soe Win, I would like to thank you for your support during my studies and your enriching companionship through the years. Finally I thank my parents and grandmother for their love, continued support encouragement and sacrifice throughout the years, and I will be forever indebted to them for all that they have done.

TABLE OF CONTENTS

SUMMARY

Orthogonal Frequency Division Multiplexing (OFDM) has been of tremendous interest in wire-line and wireless applications. This is because of its resistance to multipath delay spread, its high data rate transmission capability, and high bandwidth efficiency. However, synchronization is a challenge which must be overcome to make OFDM competitive for use in wireless applications. The, OFDM receiver can tolerate only a small fraction of the carrier frequency offset (CFO) without impairing seriously its performance.

CFO estimation is an important design issue for OFDM system. This issue has been receiving wide attention in the communications literature. Since most of the methods are based on correlation and maximum likelihood approach, CFO estimation with subspace-based methods is still an open issue. The accuracy of a super resolution subspace-based method has motivated this work. In this thesis, the CFO estimations are proposed and analyzed for both conventional OFDM system and OFDM based Wireless Local Area Network (WLAN) structure.

For conventional OFDM system, Matrix Pencil method, one of the subspace-based methods, is exploited to estimate the CFO effectively. The proposed technique uses only one OFDM symbol with equispacing. Why the proposed method requires the equispaced structure for the transmitted signal and performs better than Estimation of Signal Parameters Via Rotational Invariance Technique (ESPRIT) method is explained. In addition, how to improve the performance of the proposed method is also shown. The

simulation results show that the performance of the proposed method is superior to that of the ESPRIT method under frequency selective fading channel and the impact of the covariance matrix in ESPRIT method.

For the OFDM based WLAN system, the signal model of the preamble section is derived as the signal model of the direction of arrival (DOA) estimation in the uniform linear array signal processing. This potentially leads us to the possible exploitation of the plethora of DOA estimation algorithms for CFO estimation. Thus, one of the subspace-based DOA estimations, called Multiple Signal Classification (MUSIC), is applied to estimate the CFO over frequency selective fading channel. A first order perturbation analysis for this method is also derived.

Since the signal model of the preamble section is identical to a uniform linear array signal model, maximum entropy method can also be used for CFO estimation. Next, extensive computer simulations have been performed to validate the MUSIC and the maximum entropy method. The resolution of the spectrum and the mean, variance and standard deviation of the estimation error of the MUSIC method with different signal to noise ratio (SNR) are also analyzed. Minimum mean square error (MMSE) result that the performance of the MUSIC estimator is comparable with that of the nonlinear least square (NLS) estimator even with small data size and low SNR. Simulation results show that the MUSIC method, the maximum entropy method and the NLS method have the same CFO estimation range, and that the maximum entropy method needs a longer data than the MUSIC method to obtain accurate estimation results although both methods have the same estimation range.

NOTATIONS

4G	Fourth Generation
ADSL	Asynchronous Digital Subscriber Line
AR	Auto Regressive
AWGN	Additive White Gaussian Noise
BPSK	Binary Phase Shift Keying
CDMA	Code Division Multiple Access
CFO	Carrier Frequency Offset
CRB	Cramer-Rao Bound
DAB	Digital Audio Broadcasting
DFT	Discrete Fourier Transform
DOA	Direction of Arrival
DVB	Digital Video Broadcasting
ESPRIT	Estimation of Signal Parameters Via Rotational Invariance Technique
FDM	Frequency Division Multiplexing
FFT	Fast Fourier Transform
FIM	Fisher Information Matrix
GE	Generalized Eigenvalue
GI	Guard Interval

HIPERLAN/2	High Performance Local Area Network 2
ICI	Inter Carrier Interference
IDFT	Inverse Discrete Fourier Transform
IFFT	Inverse Fast Fourier Transform
iid	independent and identically distributed
ISI	Inter-Symbol Interference
MAC	Medium Access Control
Mbps	Mega Bit Per Second
MC-CDMA	Multi-Carrier Code Division Multiple Access
ME	Maximum Entropy
ML	Maximum Likelihood
MMSE	Minimum Mean Square Error
MP	Matrix Pencil
MPDU	MAC Protocol Data Unit
M-PSK	M-array Phase Shift Keying
MUSIC	Multiple Signal Classification
NLS	Nonlinear Least Square
OFDM	Orthogonal Frequency Division Multiplexing
PHY	Physical Layer
PLCP	Physical Layer Convergence Procedure
POF	Pencil of Function
PPDU	PLCP Protocol Data Unit
PSDU	PLCP Service Data Unit
QAM	Quadrature Amplitude Modulation
QPSK	Quadrature Phase Shift Keying

S/P	Serial to Parallel
SNR	Signal to Noise Ratio
SVD	Singular Value Decomposition
TLS	Total Least Square
TLS-ESPRIT	Total Least Square- Estimation of Signal Parameters Via Rotational Invariance Technique
wireless ATM	wireless Asymmetric Transport Mode
WLAN	Wireless Local Area Network

Mathematical Notations

$[.]^*$	Complex Conjugate of $[.]$
$[.]^T$	Transpose of $[.]$
$[.]^H$	Hermitian of $[.]$
$\left[\hat{.}\right]$	Estimation of $[.]$
$[.]^+$	Pseudoinverse of $[.]$
$E[.]$	Expectation of $[.]$
$\mathrm{Re}[.]$	Real part of $[.]$
$diag[x]$	Diagonal matrix with x on its main diagonal
$*$	Linear convolution
$\otimes$	Circular convolution
$\delta_{i,j}$	Dirac delta which is equal to 1 if $i = j$ and 0 otherwise

LIST OF FIGURES

LIST OF TABLES

CHAPTER 1

INTRODUCTION

From an electrical engineer's point of view, communication is the transferring of messages or information from a source to destination or in the case of broadcasting to many other individual users [1]. Many of the recent developments in communication techniques made it possible to transmit and receive information on local and wide area networks at maximum data rates with low probability of error. Development in wireless communications is more difficult than that in wire-line access due to design factors ranging from channel impairments security issues to synchronization problems. However, wireless communication has a great advantage: it allows the mobility of users often over a very large area. In Digital Audio Broadcasting (DAB) and terrestrial Digital Video Broadcasting (DVB) systems [2]-[3], the signals are transmitted to many dispersed users passing through the multipath environments which are found mostly in urban areas. Multipath propagation causes the powers of these received signals to fluctuate with time. Therefore, systems must be designed to be robust against large path losses, frequency selective channel behavior and large multipath delay spreads, which lead to Inter-Symbol Interference (ISI). This is a challenge for traditional single-carrier transmission because adaptive equalization can be enormously complex for channels

with a large delay spread compared to the symbol period. An attractive alternative method to combat delay spread is Orthogonal Frequency Division Multiplexing (OFDM), which transmits the data over many parallel low speed subcarriers.

OFDM is being employed in many communication areas such as Asynchronous Digital Subscriber Line (ADSL) [4], Digital Audio Broadcasting (DAB) system standard [2], terrestrial Digital Video Broadcasting (DVB) system standard [3], Wireless Local Area Network (WLAN) of IEEE 802.11a [5], HiperLAN/2 standard [6], wireless Asymmetric Transport Mode (wireless ATM) [7] and fourth generation (4G) wireless communication systems [8]. As a promising modulation technique, OFDM has been combined with Code Division Multiple Access (CDMA) to form a new system called Multi-Carrier (MC) CDMA system [9]. In addition, several European projects have also investigated OFDM in broadband mobile communications.

OFDM has become an increasingly attractive modulation technique in high data rate communication areas because of the advantages of OFDM [10]; (i) efficient way to deal with multipath effect (ii) simple equalization (iii) high bandwidth efficiency and (iv) suppression of intersymbol interference (ISI) using a guard interval. By implementing OFDM, one can ascertain these advantages.

Despite the many advantages of OFDM, it also has some disadvantages. Two of its major disadvantages are high sensitivity to frequency errors [11] and timing synchronization [12].

1.1 Overview of OFDM System

1.1.1 OFDM transmitter

The principle of OFDM transmission is to divide the available bandwidth into several narrow band subcarriers so that the channel looks flat on each subcarrier. Figure 1.1 shows an OFDM transmitter. The serial data stream $\{S_o, S_1, ..., S_{N-2}, S_{N-1}\}$ is passed through a serial to parallel converter (S/P) which splits the serial data stream into parallel data stream. The symbol period of each data on the parallel data stream becomes N times larger than the symbol period of each data on the serial data stream as shown in Figure 1.1. Due to this reason, Inter-Symbol Interference (ISI) can be reduced and for a given delay spread, and only a one-tap equalizer is required in an OFDM system which significantly decreases the implementation complexity in the receiver.

Subsequently, the parallel data stream is modulated by different subcarriers, which form an orthogonal set to provide a minimum frequency space between subcarriers without having Inter-Carrier Interference (ICI). A more efficient way to modulate and demodulate a large number of subcarriers is equivalently using the Fast Fourier Transform (FFT) [13] where the signal spectrum of a subcarrier can actually overlap with that of adjacent subcarriers. Because of overlapping adjacent subcarrier signal spectrum, OFDM has a higher bandwidth efficiency compare to Frequency Division Multilexing (FDM).

The OFDM symbol is obtained after base-band modulation of parallel data stream $\{S_o, S_1, ..., S_{N-2}, S_{N-1}\}$ as follows:

$$x(n) = \frac{1}{\sqrt{N}} \sum_{k=0}^{N-1} S_k \, e^{j\frac{2\pi}{N}kn}, \quad n = 0,1,...,N-1. \tag{1.1}$$

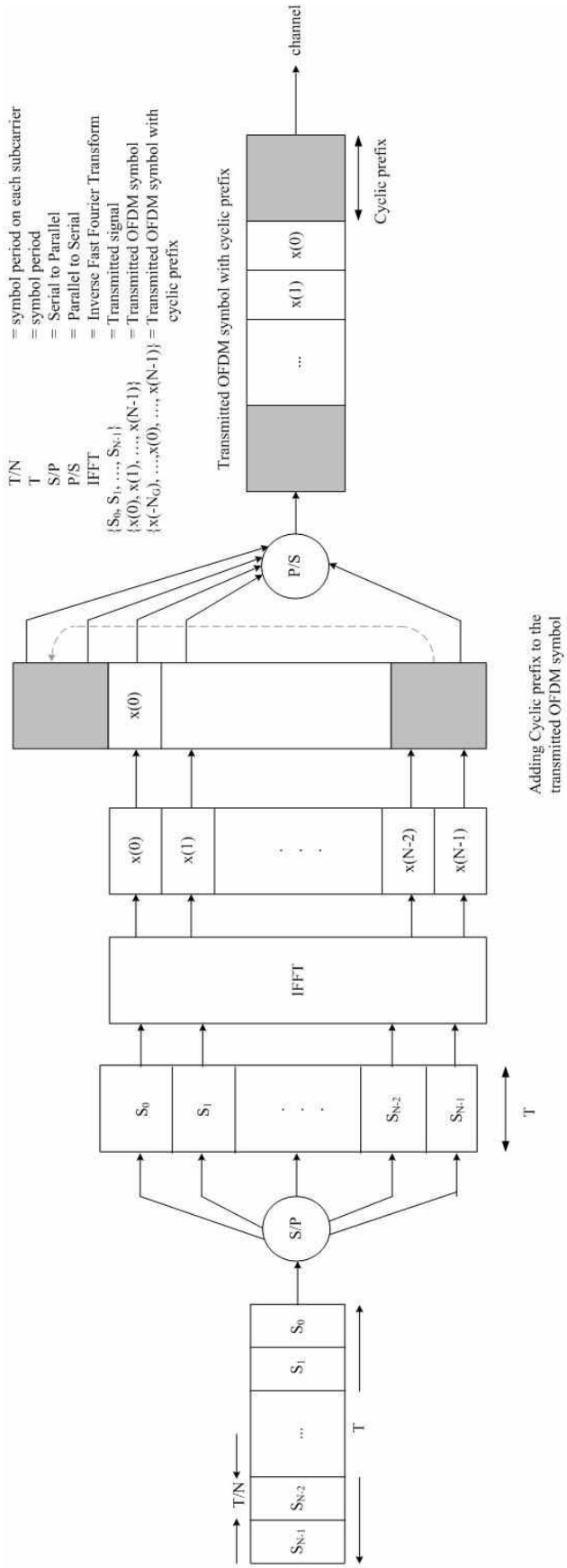

Figure 1.1 Basic block diagram of OFDM transmitter.

When the OFDM samples are converted to serial and transmitted through the channel, the channel gains and the OFDM samples are linearly convolved as

$$x'(n) = x(n) * h(n)$$

or

$$x'(n) = \sum_{m=0}^{N-1} x(m)\, h(n-m), \quad n = 0, 1, \ldots, N+M-1 \tag{1.2}$$

where $h(n)$ is the channel impulse response, which has M multipaths. Due to the presence of multipath, there is ISI between the adjacent OFDM symbols. One way to avoid ISI is to add cyclic prefix/postfix extension whose length is greater than or equal to the duration of delay spread between the symbols. After adding the cyclic prefix/postfix extensions to each OFDM symbol, the linear convolution changes to the circular convolution as

$$x'(n) = x(n) \otimes h(n)$$

or

$$FFT\{x'(n)\} = FFT\{x(n) \otimes h(n)\} = FFT\{x(n)\} \times FFT\{h(n)\} \tag{1.3}$$

The received sequence length of the circular convolution is equal to the transmitted symbol length and so the ISI is eliminated. Instead of using both prefix and postfix extensions, some systems use prefix extension alone. The samples of cyclic prefix extension are copied from the end of the OFDM symbol as shown in Figure 1.1. Typically, a cyclic prefix length which is not more than 10% of the OFDM symbol's duration is employed [10]. The OFDM symbol with cyclic prefix becomes

$$x(n) = \frac{1}{\sqrt{N}} \sum_{k=0}^{N-1} S_k\, e^{j\frac{2\pi}{N}kn}, \quad n = -N_G, -N_G+1, \ldots, 0, 1, \ldots, N-1. \tag{1.4}$$

The OFDM symbol after adding cyclic prefix is passed through a parallel to serial converter to transmit to the destination.

1.1.2 Communication Channel

In mobile communication systems, the signals are usually reflected from buildings, hills and irregular terrains. Therefore, we observe the signals at different angles of arrival with different delays. These multipath components cause amplitude, time and phase variations in the received signal, i.e., signal fading. There are different types of fading according to the relation between the signal and channel parameters [14].

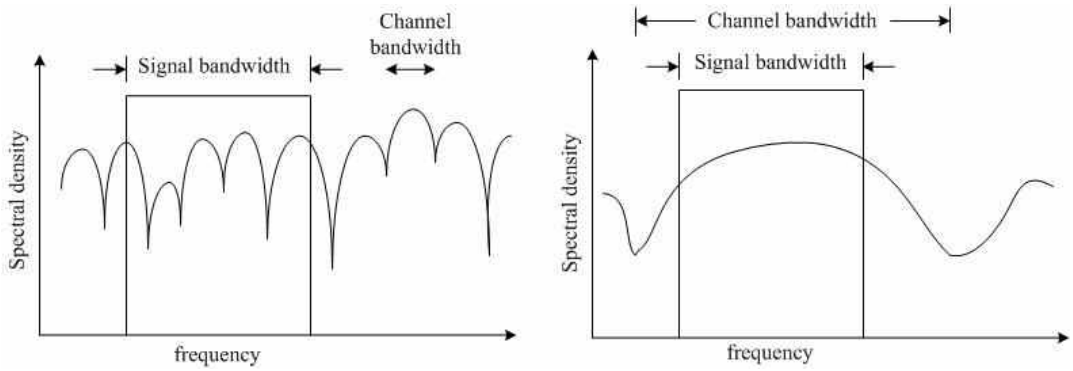

Figure 1.2 Channels (a) frequency selective fading (b) flat fading.

Based on multipath time delay spread, signal fading can be either flat fading or frequency selective fading as shown in Figure 1.2. The transmitted signal undergoes frequency selective fading, when the signal bandwidth is larger than the coherence bandwidth. Coherence bandwidth is the frequency range over which frequency components have strong correlation in amplitude and are affected by the channel in a similar manner. Otherwise, the transmitted signal undergoes flat fading. In this research we assume that the channels are slow time varying and the signal bandwidth is wide enough so that the channels experience frequency selective fading because

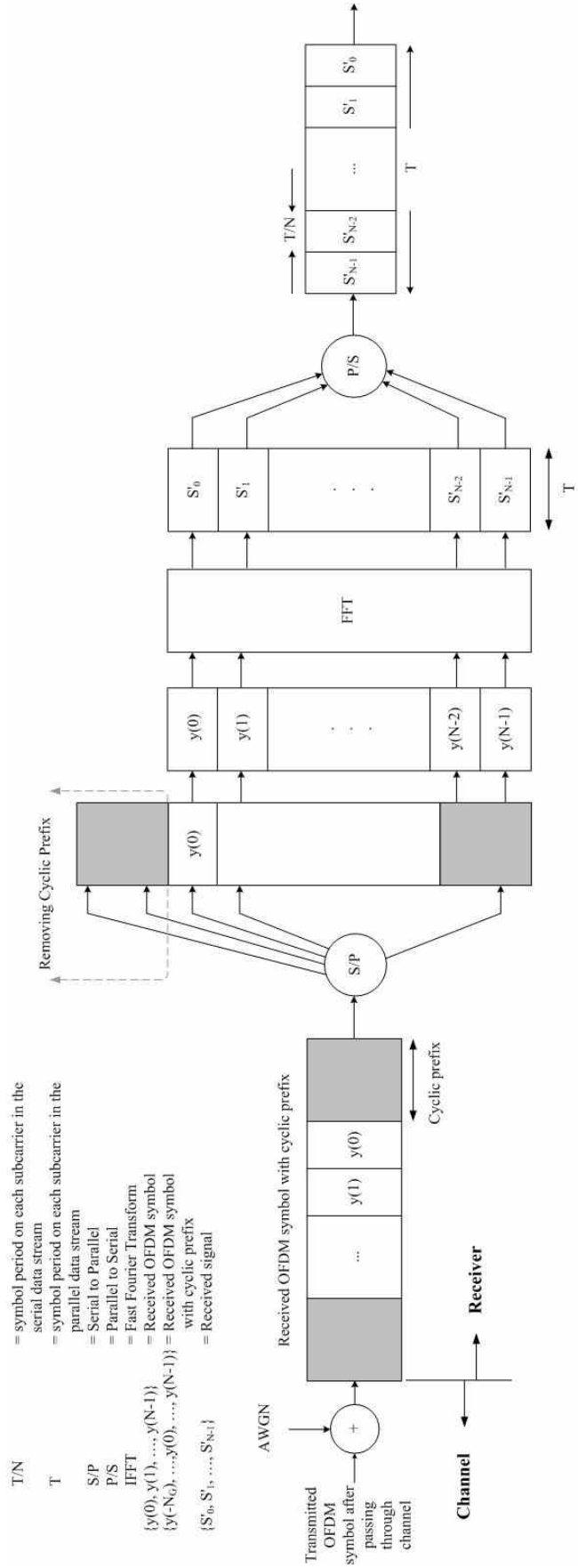

Figure 1.3 Basic block diagram of OFDM receiver.

OFDM has been originally conceived to transmit data reliably in frequency selective channels without using a complex channel equalizer [10]. Moreover, the transmitter and receiver are assumed to be stationary or slowly moving, and hence the Doppler shifts over an OFDM symbol can be ignored.

1.1.3 OFDM receiver

After passing through the channel, the OFDM symbol with cyclic prefix will be received as

$$y(n) = \frac{1}{\sqrt{N}} \sum_{k=0}^{N-1} H_k S_k \, e^{j\frac{2\pi}{N}kn} + w(n) \tag{1.5}$$

where $n = -N_G, -N_G+1, \ldots, 0, 1, \ldots, N-1$, N_G is the length of leakage from the previous frame, $H_k = \sum_{l=0}^{L_c-1} h(l)\exp\left(-j(2\pi/N)kl\right)$, is the transfer function of the channel at the frequency of the kth subcarrier and $w(n)$ is the zero-mean complex envelope of Additive White Gaussian Noise (AWGN) with variance σ_w^2. For each received OFDM symbol, only the cyclic prefix extension will be affected by leakage from the previous received OFDM symbol if the channel delay spread is shorter than the length of cyclic prefix. The basic OFDM receiver system is illustrated in Figure 1.3. After receiving the OFDM symbol, the received serial data stream $\{y(-N_G), \ldots, y(-1), y(0), y(1), \ldots, y(N-2), y(N-1)\}$ is passed through a serial to parallel converter (S/P) to convert into the parallel data stream. Before taking FFT of $y(n)$ for base-band demodulation, the cyclic prefix is removed from the parallel data stream. Therefore, the OFDM symbol after removing the cyclic prefix becomes

$$y(n) = \frac{1}{\sqrt{N}} \sum_{k=0}^{N-1} H_k S_k \, e^{j\frac{2\pi}{N}kn} + w(n), \; n = 0,1,\ldots,N-1. \tag{1.6}$$

In fact, the base-band demodulation process is a simple FFT, a reverse of the IFFT used in the baseband modulation. Therefore, each subcarrier can be recovered to a scalar factor by applying FFT to $y(n)$.

1.2 Problems in OFDM system

In the OFDM system we have just examined, synchronization is a critical issue. Synchronization in OFDM system usually includes 3 types: symbol timing synchronization, carrier frequency offset (CFO) synchronization and sampling clock synchronization. The first two have consequences that are more serious in OFDM system.

Timing synchronization is the process of finding the initialization point of the OFDM symbol. If the starting point of the OFDM symbol is not chosen correctly, there will be a timing offset. If the timing offset range is within the cyclic prefix length, this timing offset does not destroy the orthogonality among the subcarriers and introduces only a phase rotation in every subcarrier at the FFT output [15]. If the timing offset is greater than the length of the cyclic prefix, there will be ISI. Time effect is shown in Figure 1.4.

The second problem, CFO is mainly caused by the local oscillator mismatch between the transmitter and receiver. The local oscillators at the transmitter and receiver will usually not generate exactly the same frequency, and this difference can lead to degradations in demodulation of the signal at the receiver. Moreover, CFO is also caused by the Doppler Effect which arises from non-stationary of source/destination and obstacles between them i.e. the relative motion between the transmitter and receiver. In

our work, we assume that CFO is not caused by any Doppler Effect because we consider that the transmitter and receiver are stationary or slowly moving.

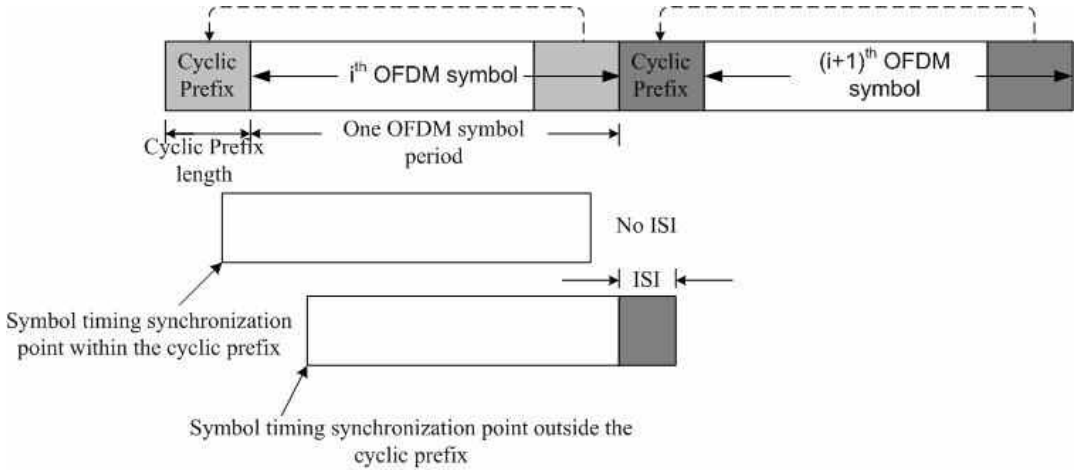

Figure 1.4 Timing offset in OFDM.

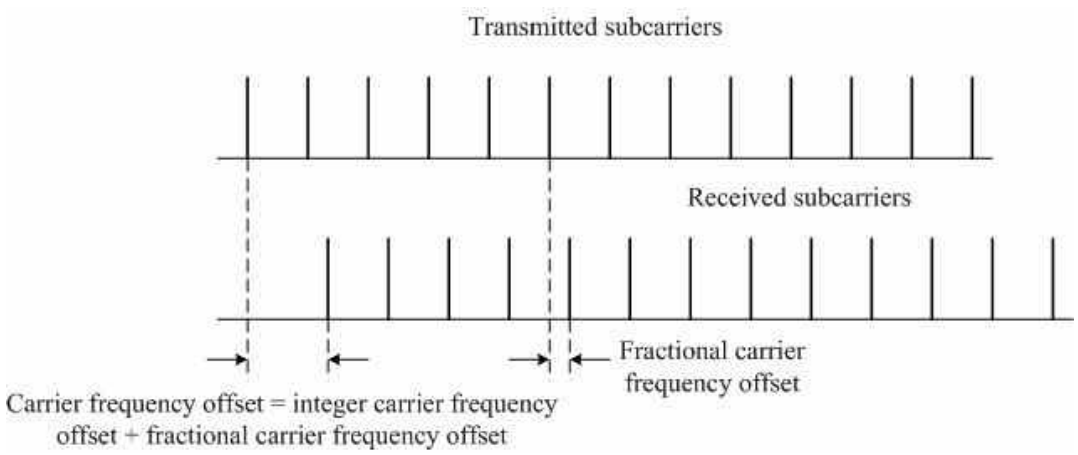

Figure 1.5 Carrier frequency offset in OFDM.

CFO is undesirable. It shifts the received signal spectrum in the frequency domain. CFO can be decomposed as the summation of the integer multiple of subcarrier spacing and the fractional value of subcarrier spacing as shown in Figure 1.5. If there is

an integer CFO in the received subcarriers, these subcarriers will still be mutually orthogonal. But the signal will be in the phase rotation after the FFT demodulation. However, if the CFO is fractional, the orthogonality between adjacent subcarriers is destroyed. Therefore, the existence of fractional CFO in an OFDM system violates the orthogonality between subcarriers. Breaking the orthogonality causes ICI at the FFT output, and degrades the system performance as compared to the single carrier system [11, 15]. When there is CFO, the received OFDM symbol admits the following equation instead of Eqn. (1.4)

$$y(n) = \frac{1}{\sqrt{N}} \sum_{k=0}^{N-1} H_k S_k \, e^{j\frac{2\pi}{N}(k+\varepsilon)n} + w(n) \tag{1.7}$$

where $n = 0,1,\ldots,N-1$, and ε is the CFO.

1.3 Research Motivation

OFDM has generated a tremendous interest in wire-line and wireless applications because of its resistance to multipath delay spread, its high data rate transmission capability with high bandwidth efficiency and the feasibility in applying adaptive modulation and/or power distribution across the subcarriers according to the channel conditions. However, synchronization is the one major issue in OFDM system. Among them, OFDM receiver can tolerate only a small fraction of the CFO without impairing seriously its performance. If the CFO is eliminated before taking FFT, the system performance will not be degraded. Therefore, the aim of this research work is to introduce accurate estimation methods to eliminate the CFO effect for both continuous type OFDM transmission system as in a broadcast application (e.g. DAB, DVB) and

burst type OFDM transmission as in a WLAN (e.g. IEEE 802.11a, HIPERLAN/2). In our research work, we assume that timing synchronization is perfect.

1.4 Contributions

- We develop the signal model for conventional OFDM system with equispacing structure and develop an accurate CFO estimation method by using only one OFDM symbol. In addition, we improve the performance of the proposed method by using oversampling. We show that the performance of the proposed Matrix Pencil (MP) method is superior to that of the Estimation of Signal Parameters Via Rotational Invariance Technique (ESPRIT) method [36] under frequency selective fading channel. The proposed method approaches the Cramer-Rao bound (CRB) except at low signal to noise ratio (SNR).
- We show in a clear way how an OFDM preamble data frame in WLAN can be modeled in accordance with the widely used uniform linear array direction of arrival (DOA) estimation. This potentially leads us to the possible exploitation of the plethora of DOA estimation algorithms for CFO estimation. We show how a subspace-based DOA algorithm, called MUltiple SIgnal Classification (MUSIC), can be successfully applied to the CFO estimation in OFDM based WLAN. It uses the preamble section in OFDM based WLAN. We also derive the theoretical performance, which indicates the strength of the proposed estimation method.
- We present a maximum entropy method for CFO estimation. Secondly, we perform extensive computer simulations in order to validate the MUSIC CFO estimation method and the maximum entropy estimator.

1.5 Outline of the Thesis

This thesis investigates the estimation methods for CFO in OFDM systems. The research work includes the estimation methods for OFDM based WLANs and conventional OFDM systems and the performances of the proposed methods. Standard Mathematical notations are given at page (ix).

In Chapter 1, a basic OFDM modulation system is introduced, and subsequently the main design issue in OFDM system is revealed along with the effects of synchronization.

Chapter 2 introduces the OFDM based WLANs structure and reviews the literature on some of the frequency offset estimation methods for OFDM based WLANs and the conventional OFDM systems. Moreover, this chapter includes a literature survey on subspace based methods to estimate CFO.

Using the matrix pencil method, Chapter 3 proposes a novel subspace based method of CFO estimation in conventional OFDM system with only one OFDM symbol. Oversampling is also used to achieve more accurate results. The performances of the matrix pencil method with and without oversampling are presented and also compare with the performance of ESPRIT method [36].

Chapter 4 explains how to reconstruct the signal model so that the DOA estimation algorithms of uniform linear array signal processing can be exploited in the preamble section of the OFDM based WLAN. Moreover, a first order performance analysis on the MUSIC method for CFO estimation is also derived.

In Chapter 5, maximum entropy method is applied for CFO estimation. Extensive computer simulations have been performed to validate the MUSIC CFO estimation method and the maximum entropy method. The CFO estimation ranges of

the MUSIC method and the maximum entropy method are also presented and also compared with that of Nonlinear Least Square (NLS) method [40].

Finally, Chapter 6 provides the conclusions and gives recommendations for future work.

CHAPTER 2

BACKGROUND PRELIMINARIES- CARRIER FREQUENCY OFFSET ESTIMATION METHODS

This chapter reviews the existing CFO estimation methods for conventional OFDM, OFDM based WLANs systems, and the subspace-based DOA estimation methods used in uniform linear array signal processing. Section 2.1 presents the literature survey for the conventional OFDM case. A literature survey of OFDM based WLANs is given in Section 2.2. The subspace-based methods are also discussed in Section 2.3.

2.1 Literature survey for conventional OFDM system

The definition of CFO and the OFDM signal model have been discussed in Chapter 1. All OFDM systems have to eliminate the CFO to prevent degradation in system performance. Therefore, the CFO estimation method is one of the most important issues in designing the OFDM systems. This issue is briefly discussed in this section.

There are a number of techniques used to estimate the CFO. Most of the existing methods are based on Maximum Likelihood (ML) [16]-[28]. However, there are other non-ML methods that are useful for CFO estimation [29, 31, 32, 34, 36].

2.1.1 Maximum Likelihood methods

There are a number of CFO estimation methods, which are based on ML. First, Moose [16] discussed the effects of CFO on the performance of OFDM digital communications, and evaluated the statistical properties of the Inter-Carrier Interference (ICI) due to CFO. He then developed the correlation based ML method for CFO estimation in the frequency domain. For the correlation based ML method, two identical OFDM symbols are transmitted. Therefore, at the receiver, the two received OFDM symbols are

$$y(n) = r(n) + w(n),\ n = 0,\ 1,\ 2,\ ...,\ 2N-1 \tag{2.1}$$

where $r(n) = \frac{1}{\sqrt{N}} \sum_{k=0}^{N-1} H_k S_k\ e^{j2\pi n(k+\varepsilon)/N}$, $n = 0,\ 1,\ 2,\ ..., N-1$ constitute the first symbol and $n = N,\ 1,\ 2,\ ..., 2N-1$ constitute the second symbol.

In the absence of noise, the Discrete Fourier Transform (DFT) of the first received OFDM symbol is

$$R_{1,k} = \sum_{n=0}^{N-1} r(n) e^{-j2\pi nk/N},\ k = 0,1,2,...,N-1 \tag{2.2}$$

and the DFT of the second received OFDM symbol is

$$R_{2,k} = \sum_{n=N}^{2N-1} r(n) e^{-j2\pi nk/N}$$

$$R_{2,k} = \sum_{n=0}^{N-1} r(n+N) e^{-j2\pi nk/N},\ k = 0,1,2,...,N-1. \tag{2.3}$$

Since two identical OFDM symbols are transmitted, the relationship between the two DFTs is $R_{2,k} = R_{1,k} e^{j2\pi\varepsilon}$ as $r(n+N) = r(n) e^{j2\pi\varepsilon}$. Therefore, the received OFDM symbols with noise are expressed as

$$Y_{1,k} = R_{1,k} + W_{1,k}$$

$$Y_{2,k} = R_{1,k} e^{j2\pi\varepsilon} + W_{2,k} \tag{2.4}$$

where $W_{1,k} = \sum_{n=0}^{N-1} w(n) e^{-j2\pi nk/N}$ and $W_{2,k} = \sum_{n=N}^{2N-1} w(n) e^{-j2\pi nk/N}$ are the DFT of $w(n)$, which is the noise contribution at the receiver. By taking the correlation between the above equations, the CFO can be estimated as

$$\hat{\varepsilon} = \frac{1}{2\pi} \tan^{-1} \left\{ \frac{\sum_{k=0}^{N-1} \mathrm{Im}\left(Y_{2,k} Y_{1,k}^{*}\right)}{\sum_{k=0}^{N-1} \mathrm{Re}\left(Y_{2,k} Y_{1,k}^{*}\right)} \right\} \tag{2.5}$$

Since Moose method [16] is defined by taking the correlation between the repeated OFDM symbols after DFT, their estimated CFO range is limited to $\pm 1/2$ of the subcarrier spacing. If the phase drift between two samples is greater than $\pm\pi$ ($\pm 1/2$ of the subcarrier spacing), the CFO estimation will not be possible. The basic strategy for initial frequency offset acquisition, which exceeds $\pm 1/2$ the subcarrier spacing, is to shorten the DFT period and use larger carrier spacing such that the phase drift does not exceed $\pm\pi$.

Schmidl and Cox [17] presented joint estimation of timing and carrier frequency offset by using two training OFDM symbols for either continuous or burst type transmission over a frequency selective fading channel. As for the CFO, the actual CFO is considered as the combination of fractional CFO and integer CFO. Schmidl [17] developed two steps for CFO estimation: one step is for fractional CFO, ε_f, and another

step is for integer CFO, ε_i. To obtain these two estimations, Schmidl and Cox [17] also suggested transmitting two OFDM training symbols. The first OFDM training symbol, where the first half is identical to the second half, is used to estimate the fractional CFO. The fractional CFO is estimated by taking the correlation between the two halves of the first received OFDM training symbol before taking DFT as follows:

$$\hat{\varepsilon}_f = \frac{1}{\pi}\arg\left(\sum_{n=0}^{N/2-1} y^*(n)\, y(n+N/2)\right) \tag{2.6}$$

By multiplying the samples of OFDM symbols with $\exp(-j2\pi/N\,\hat{\varepsilon}_f)$, the fractional CFO is eliminated. After eliminating the fractional CFO, the two received OFDM training symbols are discrete Fourier transformed. These DFT OFDM training symbols ($Y_{1,k}$ and $Y_{2,k}$) will be shifted by ε_i positions due to the uncompensated integer CFO, ε_i. Since this phase shift is the same for each pair of frequencies, the integer CFO, ε_i, can be estimated by finding g, which is the maximum position of

$$B(g) \triangleq \frac{\left|\sum_{k=0}^{N/2-1} Y^*_{1,2k+2g} Y_{2,2k+2g} v_k^*\right|^2}{2\left(\sum_{k=0}^{N/2-1} \left|Y_{2,2k}\right|^2\right)^2} \tag{2.7}$$

where g is an integer, spanning the range of possible frequency offsets, $v_k \triangleq \sqrt{2}\left(S_{2,k}/S_{1,k}\right)$ is the sequence, the differential coding structure, which is taken at the transmitter, and $S_{1,k}$ and $S_{2,k}$ are the two consecutive data symbols in the kth subcarriers, taken from a finite constellation such as QAM or M-PSK, to create the two transmitted OFDM training symbols.

Morelli and Mengali [18] modified the method of [17] by taking more than two identical portions in the first OFDM training symbol to increase the CFO estimation range although using the same ML method [17]. CFO range is extended by $\pm L/2$

subcarrier spacing without losing the estimation accuracy where L is the number of identical portion in the OFDM training symbol.

Lim and Lee [19] also updated the method of [17] to estimate the fractional and integer CFO with only one OFDM training symbol without degrading the variance of the estimation error, and it can achieve the same estimation range as Schmidl and Cox method [17]. For the fractional CFO estimation, [19] is identical with Schmidl and Cox method [17]. However, for the integer CFO, instead of using two training symbols as in [17], the authors [19] use only one OFDM training symbol. The main difference between [19] and [17] in the integer CFO estimation is the definition of the signature sequence. While Schmidl and Cox [17] define the signature sequence, $v_k \triangleq \sqrt{2}\left(S_{2,k}/S_{1,k}\right)$, at the transmitter, Lim and Lee [19] define the sequence

$$v_k \triangleq \frac{S^*{}_k S_{k+2}}{\left|S^*{}_k S_{k+2}\right|} \tag{2.8}$$

at the transmitter, where S_k is the QAM or M-PSK data symbol in the kth subcarriers to create the transmitted OFDM training symbol. At the receiver

$$u_l \triangleq \begin{cases} \dfrac{Y_{2l}^* Y_{2l+2}}{\left|Y_{2l}^* Y_{2l+2}\right|}, & l=0,1,\ldots,(N-4)/2 \\ \dfrac{Y_{l-2}^* Y_0}{\left|Y_{l-2}^* Y_0\right|}, & l=(N-2)/2 \end{cases} \tag{2.9}$$

where $Y_l = \sum_{n=0}^{N-1} y(n) e^{-j\frac{2\pi ln}{N}}$, $l = 0, 1, ..., (N-2)/2$, is the DFT of the received OFDM training symbol after eliminating the fractional CFO.

To estimate the integer CFO, the correlation between the signature sequences from the transmitter and receiver is taken as follows:

$$B(m) \triangleq \frac{\left| \sum_{l=0}^{N/2-1} u_l \, v_{l+m}^* \right|^2}{\left(\sum_{l=0}^{N/2-1} |u_l|^2 \right)^2} \tag{2.10}$$

where m is an even integer. Therefore, the integer CFO, ε_i, can be estimated by taking the position of the maximum value of $B(m)$ as

$$\hat{\varepsilon}_i = \arg_m \left\{ \max\left(B(m) \right) \right\}. \tag{2.11}$$

Kim et al. [20] proposed a new frequency synchronization algorithm, which is based on Schmidl and Cox method [17]. This new method is specifically designed to find the integer CFO by using one training OFDM symbol only. The main difference between the method in [20] and the method in [17] is the definition of the sequence at the transmitter. While [17] defines the sequence as, $v_k = \sqrt{2}\left(S_{2,k} / S_{1,k} \right)$, the new method [20] defines the sequence as, $v_k = S_{2k} / S_{2k+2}$, where $k = 0,1,2,...,(N-4)/2$ where S_k is the data symbol in the kth subcarrier. Therefore, the integer CFO is g, which is the maximum position of

$$B(g) = \frac{\left| \sum_{k=0}^{N/2-2} Y^*_{2k+2g+2} Y_{2k+2g} v_k^* \right|^2}{\left(\sum_{k=0}^{N/2-2} \left| Y_{2k+2g} \right|^2 \right)^2} \tag{2.12}$$

where $Y_l = \sum_{n=0}^{N-1} y(n) e^{-j\frac{2\pi ln}{N}}$, $l = 0, 1, ..., (N-2)/2$, is the DFT of the received OFDM training symbol after eliminating the fractional CFO.

By comparing the sequences, $v_k = S_{2k} / S_{2k+2}$ for $k = 0, 1, 2, ..., (N-4)/2$ from [20] and $v_k = \sqrt{2}\left(S_{2,k} / S_{1,k} \right)$ from [17], we can also see that this new method [20] takes the sequence between the two data symbols transmitted through two adjacent

subcarriers in one OFDM symbol, while [17] defines the sequence between the two data symbols transmitted through the same subcarrier in two adjacent OFDM symbols. The method in [20] reduces the number of the training symbols than the Schmidl and Cox method [17] without increasing the complexity.

The integer CFO estimation method with two training symbols using M-PSK (M-array Phase Shift Keying) modulation is also presented in [21]. The authors define the transmitted signal with M-PSK as follows:

$$S_{l,k} = \begin{cases} e^{j2\pi m_l(k)/M} & k = 0, 2, ..., N-2 \\ 0 & k = 1, 3, ..., N-1 \end{cases} \tag{2.13}$$

where $l = \{1,\ 2\}$ defines the first or second OFDM training symbol and $m_l(k) \in \{0, 1, ..., M-1\}$ is determined to satisfy the following equation for each OFDM symbol

$$m_l(k+4) - 2m_l(k+2) + m_l(k) = (-1)^{l+1}$$

$$\left[m_l(k+4) - m_l(k+2)\right] - \left[m_l(k+2) - m_l(k)\right] = (-1)^{l+1}. \tag{2.14}$$

Eqn. (2.13) shows that the subcarriers are differentially modulated so that the phase difference of the two adjacent subcarriers linearly increases when $m_l(k)$ of each subcarrier increases for first OFDM training symbol and decreases for second training OFDM symbol respectively. However, they [21] assume that the channel impulse response does not change within two OFDM symbol periods. Even if the channel and timing offset effects are not removed perfectly, the new integer CFO estimation method [21] can eliminate the phase due to these effects by subtracting the phases, one phase is obtained from the correlation of second training OFDM symbol and the other phase is obtained from the correlation of first training OFDM symbol as follows:

$$\hat{\varepsilon}_i = \frac{M}{2\pi}\frac{2}{N}\left[\sum_{k=0(2)}^{N-2} Y_{2,k}^{*} Y_{2,k+2}\left(S_{2,k}S_{2,k+2}^{*}\right) - \sum_{k=0(2)}^{N-2} Y_{1,k}^{*} Y_{1,k+2}\left(S_{1,k}S_{1,k+2}^{*}\right)\right] \tag{2.15}$$

where $Y_{1,k} = \sum_{n=0}^{N-1} y_1(n) e^{-j\frac{2\pi kn}{N}}$ and $Y_{2,k} = \sum_{n=0}^{N-1} y_2(n) e^{-j\frac{2\pi kn}{N}}$ are the DFT of $y_1(n)$ and $y_2(n)$, respectively.

Although the performances of this method are comparable with the performances of Schmidl and Cox method [17], the CFO range totally depends on *M* from the M-PSK modulation, while Schmidl and Cox method [17] has the CFO range which depends on *N*, the total number of subcarrier.

Schmidl and Cox [22] also presented a blind synchronization ML method for an OFDM system operating over a frequency selective fading channel. However, there are two restrictions to the proposed method: (i) the constellation on each subcarrier must have its signal points equally spaced in their phases and (ii) the length of the Guard Interval (GI) or cyclic prefix must be chosen from a subset of allowed values. The frequency offset acquisition range is $\pm 1/8$ of the total OFDM symbol bandwidth. The synchronization information is derived by taking samples from any window with a length of about three OFDM symbols so that two full OFDM symbols are contained.

To derive the joint ML method [23] for timing and carrier frequency offset, Van De Beek et al. takes the $(2N+L)$ consecutive samples form the receiver where N is the total number of samples within one OFDM symbol and L is the length of cyclic prefix. They assumed that there is one complete OFDM symbol within this observation period (one transmitted OFDM symbol + cyclic prefix), $(N+L)$. The channel is non-dispersive, and that the transmitted signal is only affected by complex additive white Gaussian noise. Due to the redundant information contained within the cyclic prefix, the

samples in the cyclic prefix and the samples which are copied for the cyclic prefix are correlated as

$$E\left\{y(k)\,y^{*}(k+m)\right\}=\begin{cases}\sigma_s^2+\sigma_w^2 & m=0\\ \sigma_s^2\,e^{-j2\pi\varepsilon} & m=N\\ 0 & otherwise\end{cases} \tag{2.16}$$

By using the probability density function of the received OFDM symbol in observation period, $(2N+L)$, Van De Beek et al. [23] derived the joint ML symbol time and carrier frequency offset estimation. However, this joint ML method [23] is considered only for the AWGN channel. Although this joint ML method [23] can perform for the time dispersive channel, this method will not be the optimal estimation method because it does not consider the time dispersive channel environment during optimization.

A globally optimum ML estimator for carrier frequency and symbol timing synchronization of OFDM systems is presented in [24]. The proposed joint ML method [24] is an extension of the joint ML method described in [23]. The authors [24] indicated that the Van De Beek et al.'s method [23] does not globally characterize the estimation problem. Since Van De Beek et al. [23] assumed that there is one complete OFDM symbol, $(N+L)$, within the observation interval, $(2N+L)$, the timing offset (θ) range becomes $1\le\theta\le N$. If the timing offset is beyond this range, Van De Beek et al.'s method [23] cannot estimate the timing offset correctly. Based on this observation, a new ML method for the joint timing and frequency offset estimation was derived in [24] with new timing offset (θ) range, $1\le\theta\le N+L$. Furthermore, an estimation method for CFO regardless of noise distribution and timing offset values is also proposed in [24]. The authors [24] concluded that although there is no optimum criteria

associated with this estimation method, it could be globally used as an initial estimate for other estimators such as ML estimators.

Choi et al. [25] proposed another ML estimation method of CFO for both AWGN and frequency selective fading channels by utilizing the nature of cyclic prefix and null subcarriers (virtual subcarriers). If null subcarriers are not used in this ML method, this ML method is identical to the ML method in [23]. Due to the virtual subcarrier, the autocorrelation function of the transmitted OFDM symbol is not an impulse function, i.e. it is a colored Gaussian process. This property makes the ML method to have wider CFO estimation range, $\pm N/2$, than the ML method [23] which has estimation range, $\pm 1/2$. However, there is some difficulty in the CFO estimation that minimizes the cost function or maximizes the ML method. One way to overcome this condition is by letting z to be $\exp\left(j2\pi\varepsilon / N\right)$ so that the cost function becomes a polynomial in z. Therefore, the CFO can be identified as the root of the cost function on the unit circle. Since the order of the polynomial is *2*(*M-1*), where *M* is the number of samples in the observation period, the computational complexity will be high. The other approach for implementation is an exhaustive search over a predetermined region. This also requires many computations. Therefore, in order to reduce the complexity of the proposed ML method, a suboptimum method is presented. However the estimation range of the suboptimum method is limited to $\pm 1/2$ of the subcarrier spacing, same as the estimation range of ML method [23]. Therefore, the proposed ML method, which has high computational complexity, is needed to use again for the estimation of the remaining integer offset.

Chen and Wang [26] proposed a CFO estimation method using oversampling. This method is motivated by the perfect retrieval of the CFO in the absence of noise. At the receiver, the continuous-time complex base-band OFDM symbol is sampled to

obtain the discrete-time OFDM symbol. Normally, initial time shift, τ, is assumed as zero. Therefore, the discrete-time received OFDM symbol is as in Eqn. (1.5). However, Chen and Wang [26] defined the initial time shift, τ, to obtain the oversampled data. When the initial time shift is assumed $\tau=0$ and $\tau=1/2$, an oversampling rate of 2, the discrete-time received OFDM symbol becomes

at $\tau=0$,

$$y_1(n)=\frac{1}{\sqrt{N}}\sum_{k=0}^{N-1}H_kS_k\,e^{j\frac{2\pi}{N}(k+\varepsilon)n}+\ w_1(n)\,,\qquad n=0,\ 1,\ 2,\ ...,N-1$$

or

$$\mathbf{y_1}\triangleq\mathbf{P}(\varepsilon)\mathbf{W}\mathbf{s}'+\mathbf{w_2} \tag{2.17}$$

at $\tau=\frac{1}{2}$

$$y_2(n)=\frac{1}{\sqrt{N}}\sum_{k=0}^{N-1}H_kS_ke^{j\frac{2\pi}{N}(k+\varepsilon)(n+1/2)}+w_2(n)\,,\qquad n=0,\ 1,\ 2,\ ...,N-1$$

or

$$\mathbf{y}_2\triangleq e^{j2\pi\varepsilon/N}\mathbf{P}(\varepsilon)\mathbf{W}\mathbf{E}\mathbf{s}'+\mathbf{w}_2 \tag{2.18}$$

where $\mathbf{y_1}\triangleq\left[y_1(0),\quad y_1(1),\quad ...,\quad y_1(N-1)\right]^T$,

$\mathbf{y_2}\triangleq\left[y_2(0),\quad y_2(1),\quad ...,\quad y_2(N-1)\right]^T$,

$\mathbf{P}(\varepsilon)\triangleq diag\left[1\quad e^{j2\pi\varepsilon/N}\quad ...\quad e^{j(N-1)2\pi\varepsilon/N}\right]$,

$\mathbf{E}\triangleq diag\left[1\quad e^{j\pi/N}\quad ...\quad e^{j(N-1)\pi/N}\right]$,

$$\mathbf{W} \triangleq \begin{bmatrix} 1 & 1 & \dots & 1 \\ 1 & e^{j\frac{2\pi}{N}} & \dots & e^{j\frac{2\pi(N-1)}{N}} \\ . & . & \dots & . \\ . & . & \dots & . \\ . & . & \dots & . \\ 1 & e^{j\frac{2\pi(N-1)}{N}} & \dots & e^{j\frac{2\pi(N-1)^2}{N}} \end{bmatrix}$$

$$\mathbf{s}' \triangleq \left[H_0 S_0,\ H_1 S_1,\ \dots,\ H_{N-1} S_{N-1}\right]^T,$$

$$\mathbf{w}_1 = \left[w_1(0) \quad w_1(1) \quad \dots \quad w_1(N-1)\right]^T,$$

$$\mathbf{w}_2 = \left[w_2(0) \quad w_2(1) \quad \dots \quad w_2(N-1)\right]^T.$$

Therefore, by using the two different initial time shift, τ, $\tau=0$ and $\tau=1/2$, the two set of OFDM symbols, given by Eqn. (2.16) and Eqn. (2.17) are obtained. To estimate the CFO perfectly in the absence of noise, Chen and Wang [26] define the following

$$\mathbf{z_1} \triangleq \mathbf{W^H P^H}(\phi)\,\mathbf{y_1} \tag{2.19}$$

$$\mathbf{z_2} \triangleq e^{-j\phi/2}\,\mathbf{E^H}\,\mathbf{W^H P^H}(\phi)\,\mathbf{y_2}. \tag{2.20}$$

When $\phi=\varepsilon$, $\mathbf{z_1} = \mathbf{z_2} = \mathbf{s}'$ will be obtained in the noiseless condition. Therefore, by varying the phase, ϕ, from *0* to 2π the CFO, ε, can be estimated perfectly in the absence of noise.

In the presence of noise, $\mathbf{z_1}$ and $\mathbf{z_2}$ will not be identical for any value of ϕ. Therefore, instead of finding the condition above, $\mathbf{z_1} = \mathbf{z_2}$, the minimum distance between $\mathbf{z_1}$ and $\mathbf{z_2}$ is sought to estimate the CFO by varying ϕ from *0* to 2π as follows:

$$\hat{\varepsilon} = \min_{\phi} \quad \left(\mathbf{z}_1 - \mathbf{z}_2\right)^H \left(\mathbf{z}_1 - \mathbf{z}_2\right) \tag{2.21}$$

Moreover, Chen and Wang showed that the proposed method is indeed the ML estimation via oversampling by assuming the noise is zero mean, uncorrelated, circularly symmetric complex white Gaussian and there is no virtual carrier.

Table 2.1 Summary of the three types of null subcarriers placement.

Placemen Type of the null subcarriers	**Consecutive null subcarriers method**	**Equispaced null subcarriers (N_z) (or) equispaced active subcarriers (N_a) method**	**Null subcarriers with distinct spacing method**
Robustness to location of the channel zeros	Most vulnerable	Most robust	Slightly more vulnerable than the equispaced null subcarriers
Identifiable range for CFO	$-N/2 \sim N/2$	$-N/2N_z \sim N/2N_z$ (or) $-N/2N_a \sim N/2N_a$	$-N/2 \sim N/2$

A deterministic ML estimation method [27] for the CFO is considered based on the presence of null subcarriers over the frequency selective fading channel. If the active subcarriers are equispaced, this ML method is identical with Schmidl and Cox method [17]. However, the main issue in [27] is the necessary and sufficient conditions on the number of null subcarriers and their placement to ensure the identifiability of the CFO. The problem of non-identifiability appears due to the location of the channel zeros when the channel is unknown and the placement of the null subcarriers. The authors [27] discussed three types of the null subcarriers placement. The summary of the three types of the null subcarriers is presented in Table 2.1.

In addition, Ghogho and Swami [28] proposed a semi-blind ML approach where a few pilots are inserted in the OFDM symbol. The semi-blind ML estimator is shown to significantly outperform the blind estimator even with a few pilots, provided they are equispaced. If the entire pilot symbols, which are inserted in the OFDM symbol are zero the semi-blind ML estimator reduces to the null subcarrier (zero pilots) based ML estimator [27]. The authors [28] preferred to use non-zero pilots instead of null subcarrier when the reliable estimation of an unknown frequency-selective channel is required. It was shown that if the number of pilots is larger than the channel order, the ML method [27] which uses zero pilots and the semi-blind method [28] which uses non-zero pilots lead to almost the same CFO estimation performance.

2.1.2 Non-ML CFO estimation methods

In Section 2.1.1, we have studied some CFO estimation techniques, which are based on ML methods. In this section, we will review non-ML based CFO estimation methods.

Bolcskei [29] introduced an algorithm for the blind estimation of symbol timing and carrier frequency offset in wireless OFDM systems. The proposed estimator is an extension of the Gini-Giannakis's estimator for single-carrier systems [30]. The main idea exploits the cyclostationarity of OFDM signals, and this method relies on second-order statistics only. Moreover, the author [29] proposed the use of different subcarrier transmit powers (subcarrier weighting) and periodic transmitter precoding to achieve a carrier frequency acquisition range of the entire bandwidth of the OFDM signal, and a symbol timing acquisition range of arbitrary length. This approach applies to non-integer timing errors as well, and demonstrated that it needs neither pilot symbols nor a cyclic prefix.

When the CFO is around ± 0.5 of the subcarrier spacing, conventional coarse carrier recovery algorithms are unable to exactly estimate the CFO because the offset estimation resolution is 1. In addition, conventional fine carrier synchronization algorithms require many symbols to compensate for the remaining CFO of ± 0.5. Therefore, a new coarse CFO algorithm [31] is proposed to solve a CFO problem that is around ± 0.5 of subcarrier spacing by using two OFDM training symbols and consists of two estimation procedures. In the first step, the proposed algorithm [31] estimates the integer CFO by detecting the maximum correlation between two pilots with the same k^{th} subcarriers from two OFDM training symbols in the frequency domain based on shifting the pilot positions as follows:

$$C_m \triangleq \left| \sum_{k=P_m} Y_{j+1,k} Y_{j,k}^* \right|, \quad m = 0, \pm 1, \pm 2, ..., \tag{2.22}$$

where $P_m = [p_1 + m, p_2 + m, ..., p_L + m]$ are the positions of the pilot subcarriers to be correlated in two OFDM training symbols and m is the subcarrier offset from P_0. The integer part of the CFO, ε_i, is estimated by detecting the offset position m where the value C_m is maximized as

$$\hat{\varepsilon}_i = \max_m (C_m). \tag{2.23}$$

In the second step, the proposed algorithm uses the maximum correlation value, C_M, among C_m and the adjacent value C_{M-1} or C_{M+1} to determine a CFO of around ± 0.5, as follows:

$$\rho = \max (C_{M-1} / C_M, C_{M+1} / C_M). \tag{2.24}$$

When the CFO is near ± 0.5, the adjacent value of C_M, C_{M-1} or C_{M+1}, is also very large compared to C_M. By using this property, the CFO can be estimated as

$$\varepsilon_f = \begin{cases} \varepsilon_i - 0.5, & if\ C_{M-1} > C_{M+1}\ and\ C_{M-1}/C_M > \mu \\ \varepsilon_i + 0.5, & if\ C_{M-1} < C_{M+1}\ and\ C_{M+1}/C_M > \mu \\ \varepsilon_i, & elsewhere \end{cases} \tag{2.25}$$

where μ is a pre-defined threshold.

When the pre-defined threshold, μ, is set at 0.2, the range of the remaining offset is from -0.23 to 0.29. This range can vary according to the multipath channel conditions. Since the proposed algorithm reduces the CFO to between +0.25 and -0.25, the +0.5 or -0.5 CFO problems can be solved. Within this reduced offset range, the fine carrier frequency synchronization algorithm can estimate a CFO, and thus reduce the acquisition time.

A non-data aided CFO estimation algorithm is developed in [32] over a frequency selective fading channel. This algorithm is a variant of Oerder-Meyr's Feedforward clock recovery algorithm [33], which is known to be resistant to time selective fading. The main idea behind the proposed algorithm in [32] is to exploit the time-frequency domain exchange inherent to the modulation scheme. A CFO therefore has a similar impact on OFDM as a clock timing offset has in a QAM system. From this similarity, the authors [32] applied the timing recovery algorithms developed for QAM transmissions over time selective channels to CFO estimation in OFDM.

Liu and Tureli [34] present a MUSIC-like algorithm in the time domain by exploiting the orthogonality between the null subcarriers (virtual subcarriers) and information bearing subcarriers. Since MUSIC-like algorithm uses virtual subcarriers, only M out of N subcarriers are used for data transmission, and Eqn. (1.5) becomes

$$y(n) = \frac{1}{\sqrt{N}} \sum_{k=0}^{M-1} H_k S_k\, e^{j\frac{2\pi}{N}kn} + w(n), \qquad n = 0,1,\ldots,N-1$$

$$\Rightarrow \quad \mathbf{y} \triangleq \mathbf{W}_p\, \mathbf{s}' \tag{2.26}$$

where $\mathbf{y} \triangleq \left[y(0),\ y(1),\ ...,\ y(N-1) \right]^T$

$$\mathbf{W} \triangleq \begin{bmatrix} 1 & 1 & ... & 1 \\ 1 & e^{j\frac{2\pi}{N}} & ... & e^{j\frac{2\pi(N-1)}{N}} \\ . & . & ... & . \\ . & . & ... & . \\ . & . & ... & . \\ 1 & e^{j\frac{2\pi(N-1)}{N}} & ... & e^{j\frac{2\pi(N-1)^2}{N}} \end{bmatrix}_{N\times N} \triangleq \left[\mathbf{W_p}\ \mathbf{W_c} \right]$$

$\mathbf{W_p}$ contains the first M columns of $\mathbf{W}$ and $\mathbf{W_c}$, which is called the orthogonal complement of $\mathbf{W_p}$, consists of last $(N-M)$ columns of $\mathbf{W}$.

Due to the orthogonality between the virtual subcarriers and information bearing subcarriers, the multiplication of complex conjugate orthogonal complement $\mathbf{W_c}^H$ and the received OFDM symbol will be zero in the absence of noise, and if there is no CFO, i.e. $\mathbf{W_c}^H \boldsymbol{y} = 0$. However, if there is a CFO contribution, the received OFDM symbol becomes

$$y(n) = \frac{1}{\sqrt{N}} \sum_{k=0}^{M-1} H_k S_k\, e^{j\frac{2\pi(k+\varepsilon)}{N}n} + w(n)$$

$$\mathbf{y} \triangleq \mathbf{E}\,\mathbf{W}\,\tilde{\mathbf{s}} \tag{2.27}$$

where $\mathbf{E} \triangleq diag\left[1 \quad e^{j2\pi\varepsilon/N} \quad ... \quad e^{j(N-1)2\pi\varepsilon/N} \right]$.

Since there is CFO, the multiplication of the received OFDM symbol and the orthogonal complement will no longer be zero ($\mathbf{W_c}^H \boldsymbol{y} \neq 0$). Therefore, Liu and Tureli [34] define $\mathbf{Z} = diag\left[1 \quad z \quad z^2 \quad\quad z^{N\text{-}1} \right]$, where $z = \exp(j2\pi\theta/N)$. When $\theta = \varepsilon$, the multiplication value will be zero $\left(\mathbf{W}'^H \mathbf{Z}^{-1} \boldsymbol{y} = 0 \right)$ again in the noiseless case, and will have a minimum value at the presence of noise. From this observation, Liu and Tureli [34] find the CFO by varying θ from *0* to 2π. They indicated that this algorithm offers

the accuracy of a super resolution subspace method, MUSIC, without involving computationally intensive subspace decompositions. Actually, this proposed algorithm is not really a MUSIC algorithm [45] because the authors did not use any subspace processing.

Chen [35] derived an ML algorithm for CFO at the presence of virtual carriers. The resulting CFO estimate of this ML algorithm has an identical form to that of the MUSIC like algorithm [34]. Thus, Chen explained that these two algorithms are equivalent and showed the equivalence between these two algorithms.

Trueli et al.[36] take the advantage of the presence of the null subcarriers (virtual carriers) to use ESPRIT, one of the subspace-based methods. From the received OFDM blocks, each block is subdivided into $(N-M)$ blocks where N is the total number of subcarriers within one OFDM block or symbol, $M > P$ and P is the total number of used subcarriers in one OFDM block. Next, the vectors for both the forward and backward directions are constructed as follows:

$$\mathbf{y}_{Fk}^{i} \triangleq \left[y_k(i-1), \quad ..., \quad y_k(i+M-1) \right]^T$$

$$\mathbf{y}_{Bk}^{i} \triangleq \left[y_k(N-i), \quad ..., \quad y_k(M-i-M) \right]^H \tag{2.28}$$

where $i = 1,\ 2,\ ...,\ N-M$. By using these forward backward vectors, the estimated correlation matrix can be formed as

$$\hat{\mathbf{R}}_{M+1} \triangleq \frac{1}{K(N-M)} \sum_{k=1}^{K} \sum_{i=1}^{N-M} \left[y^{i}{}_{Fk} \left(y^{i}{}_{Fk} \right)^H + y^{i}{}_{Bk} \left(y^{i}{}_{Bk} \right)^H \right]. \tag{2.29}$$

The eigenvectors of $\hat{\mathbf{R}}_{M+1}$, which span the signal subspace, are obtained by using Spectral Value Decomposition (SVD). The ESPRIT method for CFO estimation is exploited from the shift invariant structure of the eigenvectors of $\hat{\mathbf{R}}_{M+1}$. However, ESPRIT method requires more than one OFDM symbol to obtain reliable estimation.

Although the ESPRIT used more than one OFDM symbol (10 OFDM symbols are used in simulation), the Minimum Mean Square Error (MMSE) of this algorithm is still high.

From the literature survey, subspace-based method to estimate the CFO in OFDM system is still an open problem. Therefore, using the subspace-based method in CFO estimation is precisely the goal of this research work.

2.2 Literature survey for OFDM based WLANs structure

WLANs require a transmission technique that is capable of having a low bit error rate in a multipath fading environment whilst maintaining a high transmission bit rate. OFDM is therefore a useful technology for packet-based communication as required in WLANs system. The objective of the IEEE 802.11 standard is to provide identical services in a WLAN similar to that in the wire-line networks, i.e. high throughput, highly reliable data delivery, and continuous network connections. The architecture of the IEEE 802.11 network and the concepts can be found in [37].

PLCP Preamble	**SIGNAL**	**DATA**
12 symbols	One OFDM Symbol	Variable Number of OFDM Symbols

Figure 2.1 PLCP Protocol Data Unit (PPDU) Frame format.

IEEE 802.11a Physical Layer (PHY) is one of the PHY extensions of IEEE 802.11 and is referred to as the OFDM PHY. The OFDM PHY provides the capability to transmit PLCP Service Data Unit (PSDU) frames at multiple data rates up to 54 Mbps for WLANs where multimedia services provision is a consideration. The OFDM

modulation system in WLANs is same as that mentioned in Chapter 1. However, WLANs use a burst transmission. During transmission, each data packet contains a certain number of OFDM data symbols preceded by a Physical Layer Convergence Procedure (PLCP) preamble that is used to acquire the incoming OFDM signal for synchronization at the demodulator. OFDM frame consists of a PLCP preamble, signal and data fields as shown in Figure 2.1.

The main parameters of the OFDM based WLAN are listed in Table 2.2. The WLAN IEEE 802.11a provides 8 kinds of data rates up to 54 Mbps by using the modulation systems, which is shown in Table 2.2. There are three types of guard interval: $0\mu s$ for short training sequence, $0.8\mu s$ for long training sequence and $0.8\mu s$ for data symbols. These guard intervals provide robustness to channel delay spread up to several hundreds of nanoseconds, depending on modulation used in the system. The subcarrier frequency spacing, 0.3125MHz, is the inverse of the OFDM symbol interval, $4\mu s$, minus the guard interval duration, $0.8\mu s$. The number of data subcarriers is 48 but each OFDM symbol adds 4 pilot subcarriers, which can be used to track the remaining CFO after an initial frequency correction during the training symbol. Therefore, the total number of subcarriers is 52. More details of the OFDM based WLAN are available in [5]. The common synchronization method for WLAN CFO is by using pilot symbols, which are usually transmitted as the header of the OFDM information frame.

Table 2.2 Parameters of the OFDM base WLAN.

Data rate	6, 9, 12, 18, 24, 36, 48, 54 (Mb/s)
Modulation	BPSK, QPSK, 16-QAM, 64-QAM
Channel spacing	20 MHz
Subcarrier frequency spacing	0.3125 MHz
IFFT/FFT period	3.2 μs
Preamble duration	16 μs
Short training sequence duration	8 μs
Long training sequence duration	8 μs
Training symbol GI duration	1.6 μs
OFDM Symbol interval	4 μs
Number of data subcarriers	48
Number of pilot subcarriers	4
Total number of subcarriers	52
Duration of the SIGNAL symbol	4 μs
GI duration	0.8 μs

In [38], a MMSE based joint timing and frequency synchronization algorithm is proposed for fast burst synchronization in OFDM systems. The authors utilize only one OFDM symbol. This symbol is exploited in the time domain to give an estimate of coarse frame starting position and fine frequency offset in the frequency domain.

An optimum frame and carrier frequency synchronization method [39] is proposed for a burst type OFDM application in a frequency selective fading channel. The authors used both short and long symbols from a preamble structure of WLAN for

CFO estimation. As for the carrier frequency synchronization, coarse CFO is estimated by using the ML method proposed in [16] before applying the DFT. The fine CFO is performed after DFT. The fine CFO is estimated by finding the maximum of the correlation value of the DFT output and the expected output. By using pre and post DFT CFO estimation method, the frequency offset, which is more than $\pm 1/2$ of the subcarrier spacing, can be estimated.

Li et al. [40] proposed an efficient CFO estimation algorithm for OFDM based WLAN. Nonlinear Least Square (NLS) approach is used in the preamble section. When the additive noise is white and Gaussian, this NLS method is basically ML method. The authors found that using the nine short and two long OFDM training symbols yields better performance than using only the nine short OFDM training symbols or using only the two long OFDM training symbols. Moreover, the new preamble structure is constructed by replacing the guard interval and the two long OFDM training symbols with the ten short OFDM training symbols so that to obtain the twenty identical short training symbol within the preamble section. Using the nineteen short OFDM training symbols yields better performance than either using nine short and two long OFDM training symbols or only using nine short OFDM training symbols or only using two long OFDM training symbols. A more detailed treatment will be given in Chapter 4.

Liu and Chong [41] present three tracking algorithms for joint estimation of carrier frequency and sampling clock offsets for OFDM-based WLAN systems, such as IEEE 802.11a standard. The first method is performed by one-dimensional least square estimation, which is applied over the difference of rotated phases between two adjacent symbols and averaged over L number of OFDM symbols. The second algorithm compares the phase difference of the current OFDM symbol with the subsequent D^{th} OFDM symbol so that the effects of noise may be reduced to some extent, and thus

gives better performance especially with low SNR or small synchronization offset. And the third method uses two-dimensional linear least square estimation within the frequency and time domains. The first method on frequency domain was shown to have less computational complexity, but has lower estimation accuracy, especially in the case of low SNR. The second method can improve the estimation performance for lower SNR where consecutive observation of more symbols at one time is allowed. The third method showed steady estimation performance and it increases computational complexity to a small extent. However the estimation performance of third method degrades as SNR become large while first method and second method have better estimation performance. Detailed explanation can be found in [41].

Acquisition and tracking stages for CFO estimation and compensation are provided in [42]. For the acquisitions stage, the authors suggest to use the NLS method [40] to estimate CFO. Although CFO is estimated, and compensated in acquisition stage, there will be a residual CFO, which should be as small as possible. Therefore, a tracking stage is required because even a very small CFO will cause phase shift. The authors proposed to adaptively estimate and compensate CFO by means of pilots within the data section shown in Figure 2.1. In the tracking stage, phase shift instead of frequency offset is directly estimated in the data section by ML method. To obtain the adaptive estimate, the authors used 4 pilots, which exist in each OFDM symbol of data section to estimate the remaining phase shift by taking ML estimation of these 4 pilots.

A time domain correlation on the preamble of HIPERLAN/2 WLANs is proposed in [43] for coarse CFO estimation. While comparing with the training symbol based CFO estimation [16], this estimator is a time domain ML estimator that uses the short preamble section of the physical burst instead of training symbols. Due to the preamble structure, the frequency offset estimation range is extended four times in

comparison to previous work in [16]. However, the authors indicated that the proposed algorithm does not provide the required accuracy for HIPERLAN/2. Therefore, to achieve the required accuracy, a CFO correction architecture is proposed. This architecture consists of two parts. The first part performs coarse CFO correction that feeds a numerically controlled oscillator to remove a part of CFO. The second part implements the fine CFO correction that uses linear phase extrapolation to correct the phase shift caused by the remaining CFO. This architecture is a feed forward structure, with no feedback to the analog front end. This results in reduced implementation complexity.

In the literature, subspace based methods have not been sufficiently studied for CFO estimation in OFDM based WLAN structure. In the next section, we will review the subspace-based methods in order to estimate the CFO.

2.3 Subspace-based DOA methodologies

Subspace-based methods, which are discussed in this section, are basically the spectral estimation techniques. These methods result from the successful implementation of subspace processing in a number of array processing problems.

Due to the OFDM symbol format that will be used in Chapter 3, we can apply one of the subspace-based methods to the CFO estimation for conventional OFDM system. For OFDM based WLAN, we derive the signal model, and explain how this signal model is similar to the signal model in array signal processing in Chapter 4. From this similarity, we would be able to apply the subspace-based estimations for DOA or frequency estimation in array signal processing to the estimation of CFO in

OFDM based WLAN. Therefore, in the sequel we review the existing subspace processing strategies used for DOA/frequency estimation.

2.3.1 MUSIC DOA Estimation Technique

The tremendous interest in the subspace-based approaches was triggered by the introduction of the MUSIC algorithm [44]. In 1977, Schmidt [44] developed the MUSIC algorithm by taking a geometric view of the signal parameter estimation problem. MUSIC was indeed originally presented as a DOA estimator. Consider the following noise corrupted sinusoidal signal received at the M uniform linear array elements:

$$\mathbf{x}(n)=\mathbf{A}(\theta)\mathbf{s}(n)+\mathbf{w}(n)\ ,\quad n=0,\,1,\,2,\,...,\,N-1 \tag{2.30}$$

$$\mathbf{A}(\theta)=\left[\mathbf{a}(\theta_1),\,\mathbf{a}(\theta_2),\,...,\,\mathbf{a}(\theta_d)\right] \tag{2.31}$$

$$\mathbf{a}(\theta_i)=\left[1,\,e^{j\omega_0\triangle\sin(\theta_i)/c},\,...,\,e^{j\omega_0\triangle(M-1)\sin(\theta_i)/c}\right] \tag{2.32}$$

where $\mathbf{x}(n)$ is the received signal vector, $\mathbf{A}(\theta)$ is the steering matrix, $\triangle$ is the distance between the two adjacent antenna elements, θ_i is the direction of arrival of the ith signal, M is the total number of antennas, c is the propagation speed, $\mathbf{s}(n)$ is the narrow band signal vector, $\mathbf{w}(n)$ is a zero mean Gaussian noise vector, N is the total number of snapshots or samples, and $d\,(d<M)$ is the total number of narrow band signals.

The MUSIC algorithm is summarized to the following steps:

(1) Collect the data from the M sensors and estimate the covariance matrix, $\hat{\mathbf{R}}_{\mathbf{xx}}$ where $\hat{\mathbf{R}}_{\mathbf{xx}}\triangleq(1/N)\sum_{n=0}^{N-1}\mathbf{x}(n)\mathbf{x}^H(n)=\mathbf{A}\,\hat{\mathbf{R}}_{\mathbf{ss}}\,\mathbf{A}^H+\sigma^2\mathbf{I}$ is the estimated covariance matrix of the received signal, $\hat{\mathbf{R}}_{\mathbf{ss}}=(1/N)\sum_{n=0}^{N-1}\mathbf{s}(n)\mathbf{s}^H(n)$ is the estimated

covariance matrix of the transmitted signal, σ^2 is the noise variance, and $\mathbf{I}$ is the identity matrix.

(2) Compute the eigendecomposition of $\hat{\mathbf{R}}_{\mathbf{xx}}$, we have

$$\hat{\mathbf{R}}_{\mathbf{xx}} = \hat{\mathbf{E}}\hat{\mathbf{\Omega}}\hat{\mathbf{E}} \tag{2.33}$$

with $\hat{\mathbf{E}} = [\mathbf{e}_1, \mathbf{e}_2, ..., \mathbf{e}_M]$ is the eigenvectors and $\hat{\mathbf{\Omega}} = diag\ [\omega_1, \omega_2, ..., \omega_M]$ is the eigenvalues of the estimated covariance matrix $\hat{\mathbf{R}}_{xx}$ with $\omega_1 \geq \omega_2 \geq ... \geq \omega_M$.

(3) Estimate the number of signals, d, from the eigendecomposition and then compute the matrices $\hat{\mathbf{E}}_s$ and $\hat{\mathbf{E}}_n$ whose columns span the signal and noise subspaces, respectively: $\hat{\mathbf{E}}_s = [\mathbf{e}_1, \quad \mathbf{e}_2, \quad ..., \quad \mathbf{e}_d]$ and $\hat{\mathbf{E}}_n = [\mathbf{e}_{d+1}, \quad \mathbf{e}_{d+2}, \quad ..., \quad \mathbf{e}_M]$.

(4) Compute the MUSIC spectrum defined according to the following formula:

$$P(\theta) = \frac{1}{\mathbf{a}^{\mathrm{H}}(\theta)\hat{\mathbf{E}}_n\hat{\mathbf{E}}_n^H\mathbf{a}(\theta)}. \tag{2.34}$$

(5) Find the d (largest) peaks of $P(\theta)$ to obtain the estimated values of the parameters θ.

Since the unknown parameter is θ in the DOA estimation, MUSIC method requires a major search over $\theta \in [0, 2\pi]$. This is the practical problem of MUSIC method. Moreover, the MUSIC estimates of θ are computed from the eigenelements of $\hat{\mathbf{R}}_{\mathbf{xx}}$. Thus, it is intuitively clear that their statistical properties will depend on the random fluctuations of these eigenelements.

The performance of the MUSIC method has been extensively studied in many papers. When the number of samples becomes very large, the MUSIC algorithm yields unbiased estimates whose variances match the Cramer Rao Bound (CRB). However, with a limited number of samples and/or high noise, the variances of the MUSIC

algorithm will not match the CRB. For only limited number of samples and/or high noise power, the performance criterion of the MUSIC algorithm is derived in [45]. For the performance criterion, two types of estimation errors, namely local and global are considered. Local errors are described by the deviation of the shape of the observed peak, which will be rounded and perhaps shifted due to the loss of orthogonality between the signal subspace and the noise subspace, from the peak at the true direction angle. Global errors are defined as "false" peaks, which are not within some small neighborhood of the true directions. The main interest in [45] is the relationship between the error performance and the design of the array manifold or equivalently the array geometry.

Friedlander [46] also analyzed the sensitivity of the MUSIC algorithm due to system errors, which cause differences between the array manifold, used by MUSIC and the true manifold. The effect of such errors on the DOA estimation is investigated. In addition, the MUSIC algorithm is analyzed for the case of two closely spaced sources at the presence of phase and gain errors in the array elements or errors in the element locations. Moreover, the author also derived the formula to correctly estimate the effect of such errors on the accuracy and resolving power of the MUSIC algorithm. From [46], we note that linear arrays are relatively insensitive to phase errors and do not suffer from failure due to merging of the spectral peaks. Their sensitivity to gain error is similar to that of nonlinear arrays. The phase sensitivity of linear arrays decreases with increasing array aperture and is constant for sources separated by a fixed fraction of a beam width. From these observations, we conclude that increasing the array aperture will reduce the sensitivity of the system to modeling errors. However, all the analyses in [46] assume that the covariance matrix is based on the infinite data case.

Stoica and Soderstrom [47] are concerned with the analysis of the large sample second order properties of MUSIC and subspace rotation method, such as ESPRIT, for sinusoidal frequency estimation. Both MUSIC and subspace rotation estimation are based on the eigendecomposition of a sample data covariance matrix. Firstly, they derived explicit expressions for the covariance of the estimation errors. Next, they used these expressions to analyze and compare the statistical performances of both methods. The expressions for the estimation error variances are also used to study the dependence of MUSIC and subspace rotation performances on the dimension of covariance matrix. We note that the accuracy of both methods increases significantly with increasing the number of sensors. Moreover, it has been shown that usually subspace rotation method, such as ESPRIT, is slightly more accurate than MUSIC method. However, in the array processing case, subspace rotation method is always less accurate than MUSIC method in large samples.

Stoica and Nehorai [48] - [49] studied the performance of the MUSIC and ML methods and analyzed their statistical efficiency. CRB is also derived to compare with the above estimation methods. Moreover, the authors investigated the relationship between the MUSIC and ML estimators. In 1990, the authors [49] extended the results of [48]. Firstly, a Weighted MUSIC estimator is established but the unweighted MUSIC achieves the best performance in large samples. Next, it derives the covariance matrix of the ML estimator and presented detailed analytical studies of the statistical efficiency of MUSIC and ML estimators. These studies include performance comparisons of MUSIC and ML estimators as well as with the ultimate performance corresponding to the CRB. Finally, some numerical examples, which provide a more quantitative study of performance for the problem of finding two directions with uniform linear sensor arrays, are presented in [49].

From [48] and [49], we note that the MUSIC is a large sample (for $N>>0$) realization of the ML estimator if and only if the signals are uncorrelated. It was also shown that in the uncorrelated signals case the MUSIC error variance monotonically decreases with increasing the number of sensors, m. Moreover, when the covariance matrix is the Hermitian positive definite square root of the inverse matrix $\left(A^{*}A\right)^{-1}$, the MUSIC estimator will be more accurate than the ML estimator for sufficiently large values of sigma. As for ML estimator, it has been shown that the ML estimator does not achieve the CRB for $N \to \infty$ if $m < \infty$. For undamped signal model, the ML estimator approaches the CRB performance if the number of sensors, m, is increased. Furthermore, for highly correlated sources the performance of MUSIC degrades significantly compared to ML estimator and CRB, whereas for weakly correlated sources MUSIC and ML estimator provide similar performance that is close to the CRB for reasonably high SNR.

2.3.2 Matrix Pencil DOA Estimation Technique

The Matrix Pencil (MP) method is a variation of either ESPRIT [50] or Pencil of Function (POF) method. Hua and Sarkar [51] developed the MP method following a generalized idea of POF method, present several variations of the MP method and discuss techniques for the generalized eigenvalue problem. Generally, MP method estimates poles or frequencies from exponentially damped or undamped sinusoidal sequences which can be described by

$$\begin{aligned} y(n) &= x(n) + w(n) \\ &= \sum_{i=1}^{M} b_i \exp(s_i n) + w(n) \end{aligned} \tag{2.35}$$

where $y(n)$ is the observed data sequence, $x(n)=\sum_{i=1}^{M} b_i \exp(s_i n)$ is the sum of M number of complex exponential signals, b_i is the complex amplitude, $s_i = -\alpha_i + j\omega_i$; $\alpha_i \geq 0$ is the damping factor of the ith signal, ω_i is the angular frequency of the ith signal, $w(n)$ is the complex value white Gaussian noise, $n=0, 1, 2, ..., N-1$, N is the total number of samples, and M is the total number of signals.

Another famous technique for pole retrieval is the Prony method or Polynomial method [52]. MP method and Prony method are two of the popular linear methods. In the MP method, there is a main parameter, called pencil parameter, L. This parameter should satisfy $M \leq L \leq N-M$ so that the span of any L of $\mathbf{y}_l$ has rank no less than M. For the polynomial method, there is also a free parameter, often called polynomial degree. The free polynomial degree and the free pencil parameter bear interesting similarities as can be seen in [51] and [52].

Our work will only focus on the MP method. Matrix Pencil algorithm can be summarized as follows:

(1) Construct the vectors from the received data sequence $y(n)$ as $\mathbf{y}_l = \left[y(l), \quad y(l+1), ..., \quad y(N-L+l-1) \right]^T$, where $l = 0,1, ..., L$ and L is the pencil parameter.

(2) In the absence of noise $y(n) = x(n)$, the matrices are formed by using the above vectors

$$\mathbf{Y}_1 \triangleq \left[\mathbf{y}_0, \quad \mathbf{y}_1, ..., \quad \mathbf{y}_{L-1} \right] \triangleq \mathbf{Z}_L \mathbf{B} \mathbf{Z}_R \tag{2.36}$$

$$\mathbf{Y}_2 \triangleq \left[\mathbf{y}_1, \quad \mathbf{y}_2, ..., \quad \mathbf{y}_L \right] \triangleq \mathbf{Z}_L \mathbf{B} \mathbf{Z} \mathbf{Z}_R \tag{2.37}$$

where $\mathbf{Z}_{\mathrm{L}} \triangleq \begin{bmatrix} 1 & \dots & 1 \\ z_1 & \dots & z_M \\ & \dots & \\ z_1^{N-L-1} & \dots & z_M^{N-L-1} \end{bmatrix}$

$$\mathbf{B} \triangleq diag\left[b_1,\ b_2,\ ...,\ b_M\right]$$

$$\mathbf{Z}_{\mathrm{R}} \triangleq \begin{bmatrix} 1 & z_1 & \dots & z_1^{L-1} \\ 1 & z_2 & \dots & z_2^{L-1} \\ & & \dots & \\ 1 & z_M & \dots & z_M^{L-1} \end{bmatrix}$$

$$\mathbf{Z} \triangleq diag\left[z_1,\ z_2,\ ...,\ z_d\right], \qquad z_i = e^{(-\alpha_i + j\omega_i)}.$$

(3) Consider the matrix pencil based on the above decomposition of $\mathbf{Y}_1$ and $\mathbf{Y}_2$

$$\mathbf{Y}_2 - \lambda\mathbf{Y}_1 = \mathbf{Z}_L\mathbf{B}\left[\mathbf{Z} - \lambda\mathbf{I}\right]\mathbf{Z}_R \tag{2.38}$$

and the rank of $\left[\mathbf{Y}_2 - \lambda\mathbf{Y}_1\right]$ will be M because of $M \le L \le N - M$. However, if $\lambda = z_i$, $i = 1, 2, ..., M$, the ith row of $\mathbf{B}\left[\mathbf{Z} - \lambda\mathbf{I}\right]\mathbf{Z}_R$ is zero and the rank of this matrix is $M - 1$. Hence the parameters $\left[z_i;\ i = 1,\ 2,\ ...,M\right]$ can be estimated as the generalized eigenvalues of the matrix pair $\left[\mathbf{Y}_1, \mathbf{Y}_2\right]$.

(4) At the presence of noise, define the vector $\mathbf{y}_l$ the same way as in the noiseless case and the matrix $\mathbf{Y}$ is defined as

$$\mathbf{Y} \triangleq \left[\mathbf{y}_0,\quad \mathbf{y}_1,\ ....,\quad \mathbf{y}_L\right] \tag{2.39}$$

and take the SVD on $\mathbf{Y}$ to form $\mathbf{Y}_1$ and $\mathbf{Y}_2$ as follows:

$$\mathbf{Y}_{[N-L]\times[\mathrm{L}+1]} \triangleq \mathbf{U}\mathbf{S}\mathbf{V}^H \tag{2.40}$$

$$\mathbf{U} \triangleq \left[\mathbf{u}_1,\quad \mathbf{u}_2,\quad ...,\quad \mathbf{u}_{N-L}\right] \tag{2.41}$$

$$\mathbf{V} \triangleq \left[\mathbf{v}_1,\quad \mathbf{v}_2,\quad ...,\quad \mathbf{v}_{L+1}\right] \tag{2.42}$$

$$\mathbf{S} \triangleq \left[\mathbf{s}_1,\quad \mathbf{s}_2,\quad ...,\quad \mathbf{s}_{L+1}\right] \tag{2.43}$$

where $\mathbf{U}$ and $\mathbf{V}$ are left and right singular matrices respectively of $\mathbf{Y}$, and $\mathbf{s}_i = [0 \quad ... \quad 0 \quad \lambda_i \quad 0 \quad ... \quad 0]^T$ is a column vector consisting of all zeros except a singular value at the ith element.

Let
$$\mathbf{Y}_1 = \sum_{i=1}^{M} \lambda_i \mathbf{u}_i \mathbf{v}_i^H \tag{2.44}$$

$$\mathbf{Y}_2 = \sum_{i=2}^{M+1} \lambda_i \mathbf{u}_i \mathbf{v}_i^H \ . \tag{2.45}$$

By using $\mathbf{Y}_1$ and $\mathbf{Y}_2$, the parameters $[z_i; i = 1, 2, ..., M]$ are estimated as the generalized eigenvalues of the matrix pair $[\mathbf{Y}_1, \mathbf{Y}_2]$.

The objective of [53] is to compare the matrix pencil method originally presented in [51] to the polynomial method presented in [52]. The comparison in [53] showed that MP method and the polynomial method are two special cases of a matrix prediction approach, but MP method is more efficient in computation and less restrictive about the signal poles. It is found through perturbation analysis and simulation that, for signals with unknown damping factors, MP method is less sensitive to noise than the polynomial method [52].

Hua and Sarkar [54] reviewed the direct matrix pencil algorithm, the Pro-ESPRIT and the TLS-ESPRIT algorithms for estimating Generalized Eigenvalues (GE) of singular matrix pencils perturbed by noise. They showed that all the SVD steps in ESPRIT and MP methods have the same first-order perturbations in their estimated GE since the SVD is explored as the common structure in ESPRIT and MP methods. However, while comparing the eigendecomposition or SVD based steps inherent in the ESPRIT and the MP method, the effect of covariance filtering is not considered in these methods [55]. In fact, the main difference between ESPRIT method [50] and MP method [51] is the construction of the matrix structure. Both ESPRIT method and MP

method use the same sequence of data samples and vary only, but importantly, in how those samples are used in estimating the parameters. While ESPRIT method obtains the covariance matrix from the received signal, MP method obtains only the Hankel matrix from the received signal.

2.4 Maximum Entropy DOA Estimation Technique

Maximum entropy is a method for computing the power density spectrum that corresponds to the most random or the most unpredictable time series whose autocorrelation function agrees with a set of known values. This condition is equivalent to an extrapolation of the autocorrelation function of the available time series by maximizing the entropy of the process. We can obtain an estimate of the power spectrum of the process which is identical to the Auto-Regressive (AR) spectrum. This technique is originally developed by Burg [55]. We can apply this technique to estimate the DOA of planewaves of a linear phased array sensor system [56] and [57]. The summary of the maximum entropy for DOA estimation is as follows:

(1) Determine a set of filter weights, $\{w_i\}$, applied to the output of the array sensors data vector, $\mathbf{y}(n)$, in such a way that the mth element of $\mathbf{y}(n)$, $\mathbf{y}_m(n)$, is estimated in a least square sense by a linear combination of the other $(M-1)$ sensors. i.e

$$\underset{\mathbf{w}}{MINIMISE}\left\{\mathbf{w}^H\mathbf{R}_{yy}\mathbf{w}\right\} \text{ subject to } \mathbf{w}^H\mathbf{1}_m = 1 \tag{2.46}$$

where $\mathbf{1}_m$ is a real vector consisting of all zeros except a one at the mth element, and $\mathbf{R}_{yy}$ is the covariance matrix of the received signal.

(2) From the above constraint, Eqn.(2.46), the optimized weights are obtained as

$$\mathbf{w}_{ME} = \frac{\mathbf{R}_{yy}^{-1}\mathbf{1}_m}{\mathbf{1}_m^H \mathbf{R}_{yy}^{-1}\mathbf{1}_m} \tag{2.47}$$

and the minimized power is given by

$$\sigma_{ME}^2 = \frac{1}{\mathbf{1}_m^H \mathbf{R}_{yy}^{-1}\mathbf{1}_m}. \tag{2.48}$$

(3) Consider the smoothing error as

$$\begin{aligned}\psi_m(n) &= y_m(n) - \hat{y}_m(n) \\ &= y_m(n) + \sum_{\substack{i=0 \\ i\neq m}}^{M-1} w_i^* y_i(n)\end{aligned} \tag{2.49}$$

The above equation mimics an AR process generated by an all pole filter excited by a white noise, $\psi_m(n)$.

(4) Since the noise has a power given by Eqn. (2.48), the AR spectrum and the maximum entropy spectrum are indeed equivalent, that is, the maximum entropy power spectral estimate of $y(t)$ at $m=0$ is given as

$$P_{MEM}(\omega) = \frac{\left(\mathbf{1}_0^H \mathbf{R}_{yy}^{-1}\mathbf{1}_0\right)^{-1}}{\left|1 + \sum_{i=1}^{M} w_i e^{-j\omega i}\right|^2} \tag{2.50}$$

If $\mathbf{e}(\theta)$ is defined as the steering vector of Eqn. (2.31), the ME spatial spectrum can be deduced as follows:

$$P_{MEM}(\theta) = \frac{\left(\mathbf{1}_0^H \mathbf{R}_{yy}^{-1}\mathbf{1}_0\right)^{-1}}{\left|\mathbf{w}_{ME}^H \mathbf{e}(\theta)\right|^2} \tag{2.51}$$

where the smoothing-error filter weights, $\mathbf{w}_{ME}$ is given by Eqn. (2.46) and $1_0 = [1, 0, ..., 0]$.

(5) Find the largest peak of $P_{MEM}(\theta)$ to obtain the estimated value of the parameters θ.

In [58], the maximum entropy spectral estimator based on modified covariance is used to estimate the frequencies of several sinusoids in AWGN channel. The frequencies are estimated from the peak positions of the ME spectrum which is computed from the observed data of the random process. Analytical expressions for the variance of the estimated peak positions are derived for the high SNR value. This variance expression is considered for two special cases; (1) single frequency or multiple well separated frequencies and (2) two closely spaced frequencies. For the former case, the peak position variance can approach the CRB when the ME model order is about 1/3 of the data length. For the latter case, the peak position variance depends on frequency separation and phase difference. ME spectral estimator is called "high resolution" estimators due to their resolving ability for the closely spaced frequencies.

A theoretical approach of the maximum entropy spectral estimator properties for one or two pure frequencies with AWGN noise is presented in [59] under the assumption that the AR filter coefficients are estimated without error. By assuming that the AR filter coefficients are accurate with no uncertainties, the poles of the AR filter transfer function can be categorized in two types: the pure frequencies and the white noise. This allows to propose the pure frequency estimation and to relate the apparent bandwidth of the pure frequency to the SNR. This result also shows that a better resolution is achieved when the AR filter order is increased. For the two frequencies case, a theoretical approach of the poles for the pure frequencies location is presented. This gives the theoretical results on the bias and the resolution power of the ME spectral estimator as a function of the SNR, AR filter order and pure frequencies separation.

Maximum entropy has been suggested by numerous authors as a good objective measure for optimally modeling the power spectrum of a wide-sense stationary random process.

2.5. Conclusion

This chapter reviews the existing CFO estimation methods for conventional OFDM system and OFDM-based WLAN. There is still ample work that needs to be done in the subspace processing arena for CFO estimation. Thus, this thesis focuses on subspace methods. We review the existing subspace processing strategies used for DOA/frequency estimation. We have identified the key performance indicators of subspace based methods. In the following chapters, we will use our experiences in subspace processing to develop a new method that is useful and computationally attractive. For completeness, we will also study the usefulness of maximum entropy method to CFO estimation.

CHAPTER 3

CARRIER FREQUENCY OFFSET ESTIMATION FOR THE CONVENTIONAL OFDM SYSTEMS

As mentioned in earlier chapter, CFO estimation is an important design issue for OFDM system. This issue has been receiving wide attention in the communications literature. Most of the methods are based on correlation and ML approach. CFO estimation with subspace-based method is still an open problem because ESPRIT [36] requires more than one OFDM symbol although this method can be used to estimate CFO.

In this chapter, we propose a matrix pencil based method that can effectively estimate the CFO. The proposed technique uses only a single OFDM symbol with equispacing. This chapter is organized as follows. Section 3.1 develops the signal model of the OFDM system used for our proposed method, and explains why equispaced structure is needed for signal transmission in the proposed method. In Section 3.2, we propose a MP method to estimate the CFO and show how to improve the performance of the proposed MP method. Section 3.3 includes the simulation results of the proposed MP method and discusses the performances of both MP method and ESPRIT method. This chapter concludes some final remarks in Section 3.4.

3.1 Signal Model

In this section, the signal model for conventional OFDM system is explained in detail.

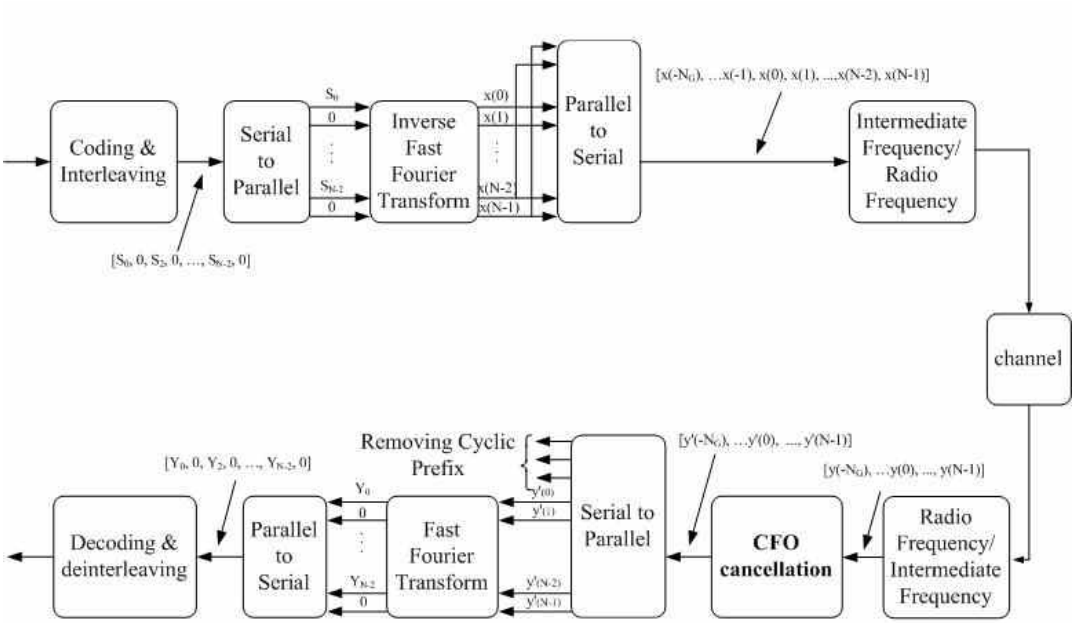

Figure 3.1 The OFDM system

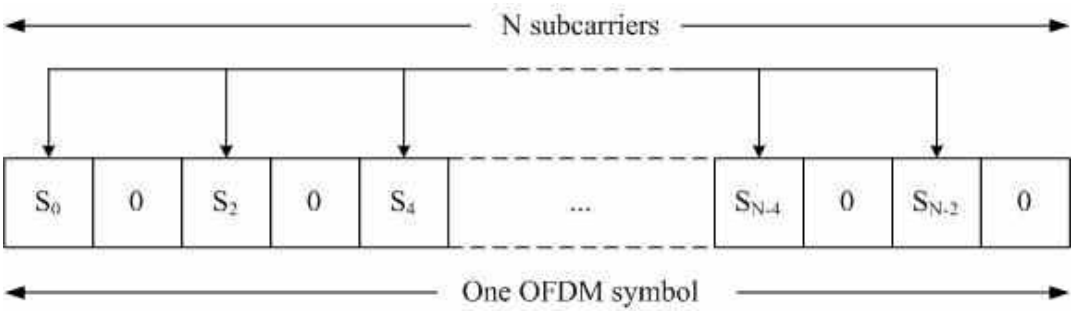

Figure 3.2 Transmitted signal structure for proposed Matrix Pencil method.

The OFDM system is illustrated in Figure 3.1. A data stream $\{S_i\}$ belonging to a QAM or M-PSK constellation is fed into an IFFT which produce the time domain sequence $\mathbf{x} \triangleq \left[x(0) \quad x(1) \quad \ldots \quad x(N-1)\right]^T$. We define the transmitted data stream as $\mathbf{S} \triangleq \left[S_0 \quad 0 \quad S_2 \quad 0 \quad \ldots \quad S_{N-2} \quad 0\right]^T$ as shown in Figure 3.2. That means the data symbols are transmitted on the even frequencies as mentioned in [17] in order to obtain equispaced active subcarriers and $N(=P+V)$ is the total number of subcarriers, V is the number of null subcarriers, and $P = N/2$ is the number of active subcarriers in the system.

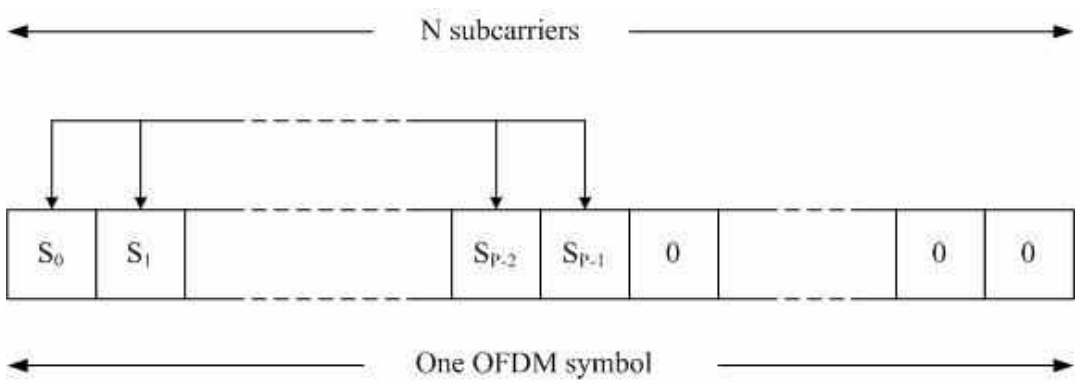

Figure 3.3 Transmitted signal structure for ESPRIT method.

Consecutive data structure of the transmitted signal in ESPRIT method [36] is shown in Figure 3.3. The frequency spacing for this structure is $2\pi/N$ where N is the total number of subcarriers. Although the proposed MP method is able to estimate small frequency spacing, it requires large number of samples or subcarriers to obtain an accurate CFO estimation. This issue will be discussed in the sequel. For the OFDM case, the number of samples cannot be taken arbitrary as in the sinusoidal case [52, 53] since the number of samples in OFDM symbol is the number of subcarriers. The MP

method, with an inadequate number of samples for small frequency spacing, will result in poor CFO estimate. Since the number of samples cannot be increased in the OFDM case, maximizing the frequency spacing between the adjacent subcarriers is the alternative way to obtain better accuracy. By employing equispaced structure, as illustrated in Figure 3.2, frequency spacing becomes double of the original spacing. Therefore the frequency spacing between the adjacent subcarriers for the MP method is $2(2\pi/N)$. Because of this frequency spacing, the maximum number of active subcarriers that can be used in the proposed method is $N/2$.

Details on the OFDM transmitter and receiver systems are available in Chapter 1. In the sequel, we assume that time synchronization is perfect, and the channel has L_c multipath fading whose variations are negligible during transmission of the single OFDM symbol. Due to the equispacing structure of the transmitted data stream, the received OFDM symbol with CFO after removing cyclic prefix can now be shown as follows:

$$y(n) = \frac{1}{\sqrt{N}} \sum_{k=0:2}^{N-1} H_k S_k \exp\left(j2\pi/N\,(k+\varepsilon)n \right) + w(n) \tag{3.1}$$

In vector form, we get the following:

$$\begin{bmatrix} y(0) \\ y(1) \\ . \\ . \\ . \\ y(N-1) \end{bmatrix}_{N\times 1} \triangleq \frac{1}{\sqrt{N}} \begin{bmatrix} 1 & 0 & \dots & 0 \\ 0 & e^{j\frac{2\pi}{N}\varepsilon} & \dots & 0 \\ 0 & 0 & e^{j2\frac{2\pi}{N}\varepsilon} & . \\ 0 & 0 & \dots & . \\ 0 & 0 & \dots & . \\ 0 & 0 & \dots & e^{j(N-1)\frac{2\pi}{N}\varepsilon} \end{bmatrix}_{N\times N} \begin{bmatrix} 1 & 1 & \dots & 1 \\ 1 & e^{j\frac{2\pi}{N}} & \dots & e^{j\frac{2\pi}{N}(N-1)} \\ . & . & \dots & . \\ . & . & \dots & . \\ . & . & \dots & . \\ 1 & e^{j\frac{2\pi}{N}(N-1)} & \dots & e^{j\frac{2\pi}{N}(N-1)(N-1)} \end{bmatrix}_{N\times N}$$

$$\begin{bmatrix} H_0 S_0 \\ 0 \\ H_2 S_2 \\ 0 \\ \dots \\ H_{N-2} S_{N-2} \\ 0 \end{bmatrix}_{N\times 1} + \begin{bmatrix} w(0) \\ w(1) \\ . \\ . \\ . \\ . \\ w(N-1) \end{bmatrix}_{N\times 1}$$

or

$$\Rightarrow \begin{bmatrix} y(0) \\ y(1) \\ . \\ . \\ . \\ y(N-1) \end{bmatrix}_{N\times 1} \triangleq \frac{1}{\sqrt{N}} \begin{bmatrix} 1 & 0 & \dots & 0 \\ 0 & e^{j\frac{2\pi}{N}\varepsilon} & \dots & 0 \\ 0 & 0 & e^{j2\frac{2\pi}{N}\varepsilon} & . \\ 0 & 0 & \dots & . \\ 0 & 0 & \dots & . \\ 0 & 0 & \dots & e^{j(N-1)\frac{2\pi}{N}\varepsilon} \end{bmatrix}_{N\times N} \begin{bmatrix} 1 & 1 & \dots & 1 & 1 \\ 1 & e^{j2\frac{2\pi}{N}} & \dots & e^{j\frac{2\pi}{N}(N-4)} & e^{j\frac{2\pi}{N}(N-2)} \\ . & . & \dots & . & . \\ . & . & \dots & . & . \\ . & . & \dots & . & . \\ 1 & e^{j2\frac{2\pi}{N}(N-1)} & \dots & e^{j\frac{2\pi}{N}(N-4)(N-1)} & e^{j\frac{2\pi}{N}(N-2)(N-1)} \end{bmatrix}_{N\times N/2}$$

$$\begin{bmatrix} H_0 S_0 \\ H_2 S_2 \\ . \\ . \\ . \\ H_{N-2} S_{N-2} \end{bmatrix}_{N/2\times 1} + \begin{bmatrix} w(0) \\ w(1) \\ . \\ . \\ . \\ . \\ w(N-1) \end{bmatrix}_{N\times 1}$$

or

$$\begin{aligned} \mathbf{y} &\triangleq \frac{1}{\sqrt{N}} \mathbf{E}\mathbf{W}\mathbf{s}' + \mathbf{w} \\ &\triangleq \mathbf{d} + \mathbf{w} \end{aligned} \tag{3.2}$$

where $\mathbf{d} \triangleq \frac{1}{\sqrt{N}} \mathbf{E}\,\mathbf{W}\,\mathbf{s}'$ with the following definitions

$$\mathbf{E} = diag\begin{bmatrix} 1 & e^{j\frac{2\pi}{N}\varepsilon} & e^{j2\frac{2\pi}{N}\varepsilon} & \dots & e^{j(N-1)\frac{2\pi}{N}\varepsilon} \end{bmatrix},$$

$$\mathbf{W} = \begin{bmatrix} 1 & 1 & \dots & 1 & 1 \\ 1 & e^{j2\frac{2\pi}{N}} & \dots & e^{j\frac{2\pi}{N}(N-4)} & e^{j\frac{2\pi}{N}(N-2)} \\ . & . & \dots & . & . \\ . & . & \dots & . & . \\ . & . & \dots & . & . \\ 1 & e^{j2\frac{2\pi}{N}(N-1)} & \dots & e^{j\frac{2\pi}{N}(N-4)(N-1)} & e^{j\frac{2\pi}{N}(N-2)(N-1)} \end{bmatrix}, \text{ and}$$

$$\mathbf{s}' = \begin{bmatrix} H_0 S_0 & H_2 S_2 & \dots & H_{N-2} S_{N-2} \end{bmatrix}^T.$$

Without eliminating the CFO and by applying DFT on the received OFDM symbol, we obtain

$$Y_k = \sum_{n=0}^{N-1} y(n) e^{-j\frac{2\pi kn}{N}} \tag{3.3}$$

$$Y_k = (S_k H_k)\left\{ \left(sin(\pi\varepsilon)\right) / \left(Nsin(\pi\varepsilon/N) \right) \right\} e^{j\pi\varepsilon(N-1)/N} + I_k + W_k. \tag{3.4}$$

The proof of the Eqn. (3.4) is given in Appendix A. The first term of the above equation is the modulation value S_k modified by the channel transfer function, H_k, and experiences an attenuation, $\left\{ \left(sin(\pi\varepsilon)\right) / \left(Nsin(\pi\varepsilon/N) \right) \right\}$, and phase shift, $e^{j\pi\varepsilon(N-1)/N}$, due to the frequency offset. The second term, I_k, is the ICI due to the CFO and is given by

$$I_k = \frac{1}{N} \sum_{\substack{l=0 \\ l \neq k}}^{N-1} H_l S_l \frac{\sin\left(\pi\left(l-k-\varepsilon\right)\right)}{\sin\left(\frac{\pi}{N}\left(l-k-\varepsilon\right)\right)} e^{j\frac{\pi}{N}(l-k-\varepsilon)(N-1)}. \tag{3.5}$$

Therefore, there are two effects caused by CFO: one is the amplitude reduction at the output of FFT and the second is ICI from the other subcarriers that are now no longer orthogonal to each other.

3.2 Carrier Frequency Offset Estimation using Matrix Pencil Technique

In this section, we study a MP strategy [54] for estimating the CFO of the OFDM system. We recall that MP has been successfully exploited in the general parameter estimation of exponentially damped and/or undamped sinusoids in noise. See [56, 57] for more details. Also, in Code Division Multiple Access (CDMA) system, the MP algorithm has been shown to provide accurate DOA estimates with a single snapshot [60] and with extremely low computation burden.

The main parameter in MP algorithm is the pencil parameter, L. The choice of the pencil parameter L is critical in any matrix pencil based algorithm. In our OFDM system, the pencil parameter L is chosen as $N/2$ so that the hankel matrix $\mathbf{Y}_i$, $i=1, 2$, which is taken from the received data, has rank no less than $N/2$ ($N/2$ is the total number of active subcarriers in the proposed MP method). To use the MP method, we first consider the OFDM system in the absence of noise. From Eqn. (3.2) we develop the forward backward matrix as

$$\mathbf{D} \triangleq \begin{bmatrix} \mathbf{d}_L & \mathbf{d}_{L-1} & \dots & \mathbf{d}_0 \\ \mathbf{d}_0^* & \mathbf{d}_1^* & \dots & \mathbf{d}_L^* \end{bmatrix} \tag{3.6}$$

where the vector $\mathbf{d}_i \triangleq [d_i, d_{i+1}, ..., d_{i+N-L-1}]^T$, $i = 0, 1, 2, ..., L$, is taken from Eqn. (3.2) .

To apply the MP method, we form 2 submatrices, $\mathbf{D}_1$ and $\mathbf{D}_2$ taken from $\mathbf{D}$ by deleting the last column and first column respectively as

$$\mathbf{D}_1 \triangleq \frac{1}{\sqrt{N}} \mathbf{Z_L R\ Z_R} = \begin{bmatrix} \mathbf{d}_L & \mathbf{d}_{L-1} & \dots & \mathbf{d}_1 \\ \mathbf{d}_{L-1}^* & \mathbf{d}_1^* & \dots & \mathbf{d}_{L-1}^* \end{bmatrix} \tag{3.7}$$

$$\mathbf{D}_2 \triangleq \frac{1}{\sqrt{N}} \mathbf{Z_L R\ Z Z_R} = \begin{bmatrix} \mathbf{d}_{L-1} & \mathbf{d}_{L-2} & \dots & \mathbf{d}_0 \\ \mathbf{d}_L^* & \mathbf{d}_2^* & \dots & \mathbf{d}_L^* \end{bmatrix} \tag{3.8}$$

where $\mathbf{R} \triangleq diag\left[H_0S_0 \quad H_2S_2 \quad \ldots \quad H_{N-2}S_{N-2}\right]$

$$\mathbf{Z} \triangleq diag\left[e^{-j\frac{2\pi}{N}\varepsilon} \quad e^{-j\frac{2\pi}{N}(\varepsilon+2)} \quad \ldots \quad e^{-j\frac{2\pi}{N}(\varepsilon+N-2)}\right]$$

$$\mathbf{Z}_{\mathrm{L}} \triangleq \begin{bmatrix} e^{j\frac{2\pi}{N}\varepsilon L} & e^{j\frac{2\pi}{N}(\varepsilon+2)L} & \ldots & e^{j\frac{2\pi}{N}(\varepsilon+N-2)L} \\ e^{j\frac{2\pi}{N}\varepsilon(L+1)} & e^{j\frac{2\pi}{N}(\varepsilon+2)(L+1)} & \ldots & e^{j\frac{2\pi}{N}(\varepsilon+N-2)(L+1)} \\ . & . & \ldots & . \\ . & . & \ldots & . \\ . & . & \ldots & . \\ e^{j\frac{2\pi}{N}\varepsilon(N-1)} & e^{j\frac{2\pi}{N}(\varepsilon+2)(N-1)} & \ldots & e^{j\frac{2\pi}{N}(\varepsilon+N-2)(N-1)} \\ 1 & 1 & \ldots & 1 \\ e^{-j\frac{2\pi}{N}\varepsilon} & e^{-j\frac{2\pi}{N}(\varepsilon+2)} & \ldots & e^{-j\frac{2\pi}{N}(\varepsilon+N-2)} \\ . & . & \ldots & . \\ . & . & \ldots & . \\ . & . & \ldots & . \\ e^{-j\frac{2\pi}{N}\varepsilon(N-L-1)} & e^{-j\frac{2\pi}{N}(\varepsilon+2)(N-L-1)} & \ldots & e^{-j\frac{2\pi}{N}(\varepsilon+N-2)(N-L-1)} \end{bmatrix}$$

$$\mathbf{Z}_{\mathbf{R}} \triangleq \begin{bmatrix} 1 & e^{-j\frac{2\pi}{N}\varepsilon} & e^{-j\frac{2\pi}{N}\varepsilon 2} & \ldots & e^{-j\frac{2\pi}{N}\varepsilon(L-1)} \\ 1 & e^{-j\frac{2\pi}{N}(\varepsilon+2)} & e^{-j\frac{2\pi}{N}(\varepsilon+2)2} & \ldots & e^{-j\frac{2\pi}{N}(\varepsilon+2)(L-1)} \\ . & . & . & \ldots & . \\ . & . & . & \ldots & . \\ . & . & . & \ldots & . \\ 1 & e^{-j\frac{2\pi}{N}(\varepsilon+N-2)} & e^{-j\frac{2\pi}{N}(\varepsilon+N-2)} & \ldots & e^{-j\frac{2\pi}{N}(\varepsilon+N-2)(L-1)} \end{bmatrix}.$$

By applying the MP method onto $\mathbf{D}_1$ and $\mathbf{D}_2$, we can perfectly retrieve $\exp\left(-j\,2\pi/N\,(\varepsilon+2k)\right)$, $k=0,\ 1,\ \ldots, N/2-1$, which are the eigenvalues of $\mathbf{P}$, where $\mathbf{P}=\mathbf{D}_1^{+}\mathbf{D}_2$, in the absence of noise. We estimate the CFO from the estimated $\exp\left(-j\,2\pi/N\,(\varepsilon+2k)\right)$ as follows:

$$\hat{\varphi} = -\frac{2}{N}\sum_{k=0}^{\frac{N}{2}-1}\left[arg\left(e^{-j\frac{2\pi}{N}(\varepsilon+2k)}\right) + \frac{2\pi}{N}(2k)\right] \tag{3.9}$$

$$\Rightarrow \quad \hat{\varepsilon} = \frac{\hat{\phi}}{(\frac{2\pi}{N})}. \tag{3.10}$$

For the noisy data, we apply the Total Least Square (TLS) technique on the MP method to minimize the noise effect. The forward backward matrix $\mathbf{Y}$ is defined from Eqn. (3.2) as follows:

$$\mathbf{Y} \triangleq \begin{bmatrix} \mathbf{y}_L & \mathbf{y}_{L-1} & \cdots & \mathbf{y}_0 \\ \mathbf{y}_0^* & \mathbf{y}_1^* & \cdots & \mathbf{y}_L^* \end{bmatrix}_{2(N-L)\times(L+1)} \tag{3.11}$$

where $\mathbf{y}_i \triangleq \begin{bmatrix} y(i) & y(i+1) & \ldots & y(i+N-L-1) \end{bmatrix}^T$ and SVD is carried out on $\mathbf{Y}$ to from the matrices $\mathbf{Y}_1$ and $\mathbf{Y}_2$ as follows:

$$\mathbf{Y} \triangleq \mathbf{U}\mathbf{S}\mathbf{V}^H \tag{3.12}$$

where $\mathbf{U} \triangleq \begin{bmatrix} \mathbf{u}_1, & \mathbf{u}_2, & \ldots, & \mathbf{u}_{2(N-L)} \end{bmatrix}$

$\mathbf{V} \triangleq \begin{bmatrix} \mathbf{v}_1, & \mathbf{v}_2, & \ldots, & \mathbf{v}_{L+1} \end{bmatrix}$

$\mathbf{S} \triangleq \begin{bmatrix} \mathbf{s}_1, & \mathbf{s}_2, & \ldots, & \mathbf{s}_{L+1} \end{bmatrix}$.

Here, $\mathbf{U}$ and $\mathbf{V}$ are left and right singular matrices respectively of $\mathbf{Y}$, and $\mathbf{s}_i = \begin{bmatrix} 0 & \ldots & 0 & \lambda_i & 0 & \ldots & 0 \end{bmatrix}^T$ is a column vector consisting of all zeros except a singular value at the ith element. Then,

$$\mathbf{Y}_1 = \sum_{i=1}^{P} \lambda_i \mathbf{u}_i \mathbf{v}_i^H \tag{3.13}$$

$$\mathbf{Y}_2 = \sum_{i=2}^{P+1} \lambda_i \mathbf{u}_i \mathbf{v}_i^H \tag{3.14}$$

where $P = N/2$, is the number of active subcarriers. The estimation of $\exp\left(-j\,2\pi/N\,(\varepsilon + 2k)\right)$, $k = 0,\ 1,\ \ldots, N/2-1$, is obtained from the eigenvalues of $\mathbf{Q}$, $\mathbf{Q} = \mathbf{Y}_1^+ \mathbf{Y}_2$, and thus the CFO can be estimated from Eqn. (3.9) and Eqn. (3.10).

The CFO estimation ranges of the proposed MP and ESPRIT methods depend on the position of the largest active subcarrier. $\exp\left(-j\,2\pi/N\,(\varepsilon+2k)\right)$ can be estimated if $2\pi/N\,(\varepsilon+2k)$ is within the range *0* to 2π. Since the largest active subcarrier position, $2k$, is at $N-2$ as shown in Figure 3.2, the range of ε becomes $0\le\varepsilon\le 2$. However, the ESPRIT method has a large ε estimation range than the MP method. Since ESPRIT method uses P from the total number of subcarriers, N, as active subcarriers, the largest subcarrier position of the ESPRIT method will be at P because the signal is transmitted with consecutive active subcarriers. Therefore, the estimation range of ESPRIT method will be $0\le\varepsilon\le N-P$ or $-\frac{N-P}{2}\le\varepsilon\le\frac{N-P}{2}$.

However, a major limitation in applying the MP technique to the CFO estimation in OFDM system is the FFT period, which defines the number of samples. We can obtain better performance if the number of samples can be extended without changing the frequency spacing $2\left(2\pi/N\right)$, between the adjacent subcarriers. In the OFDM case, the number of samples, *N*, is the total number of sub-carriers after taking IDFT while the number of samples in the sinusoidal case [56, 57] can be of any value. Therefore we employ oversampling method mentioned in [26] to extend the number of samples. As in [26], the initial time shift, τ, is used as shown in Figure 3.4. When τ is set to *0*, the original Eqn. (3.2) is obtained. By setting $\tau=1/2$, we can form a vector, $\mathbf{y}_{0.5}$, as shown below:

$$\mathbf{y}_0 \triangleq \left[\, y(0) \quad y(1) \quad \ldots \quad y(N-1)\,\right]^T \tag{3.15}$$

$$\mathbf{y}_{0.5} \triangleq \left[\, y(0.5) \quad y(1.5) \quad \ldots \quad y(N-0.5)\,\right]^T. \tag{3.16}$$

The time shift does not alter the frequency spacing between the adjacent subcarrier. This can be seen clearly in Figure 3.4. Straight line is represented for $\tau = 0$ and dotted line sampling is represented for $\tau = 1/2$.

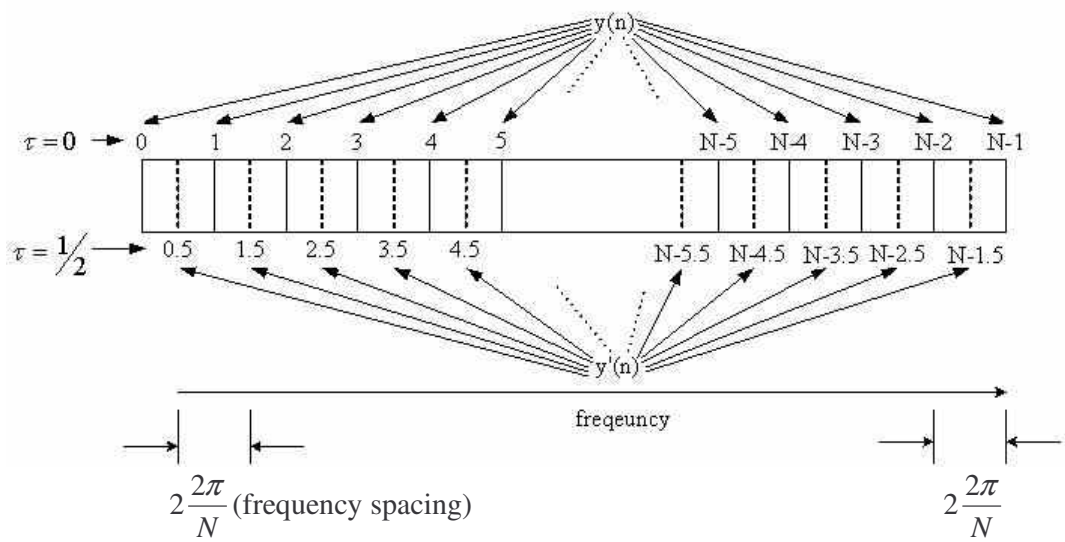

Figure 3.4 Received OFDM symbol with oversampling.

From the vectors $\mathbf{y}_0$ and $\mathbf{y}_{0.5}$, the Forward Backward matrices $\mathbf{Y}_0$ and $\mathbf{Y}_{0.5}$ can be constructed respectively as

$$\mathbf{Y}_0 \triangleq \begin{bmatrix} \mathbf{y}_{0,L} & \mathbf{y}_{0,L-1} & \cdots & \mathbf{y}_{0,0} \\ \mathbf{y}_{0,0}^* & \mathbf{y}_{0,1}^* & \cdots & \mathbf{y}_{0,L}^* \end{bmatrix}_{2(N-L)\times(L+1)} \tag{3.17}$$

$$\mathbf{Y}_{0.5} \triangleq \begin{bmatrix} \mathbf{y}_{0.5,L} & \mathbf{y}_{0.5,L-1} & \cdots & \mathbf{y}_{0.5,0} \\ \mathbf{y}_{0.5,0}^* & \mathbf{y}_{0.5,1}^* & \cdots & \mathbf{y}_{0.5,L}^* \end{bmatrix}_{2(N-L)\times(L+1)} \tag{3.18}$$

where $\mathbf{y}_{0,k} \triangleq \left[y_0(k) \quad y_0(k+1) \quad \ldots \quad y_0(N-L+k-1) \right]^T$ is the received vector at the initial time shift $\tau = 0$, and $\mathbf{y}_{0.5,k} \triangleq \left[y_{0.5}(k) \quad y_{0.5}(k+1) \quad \ldots \quad y_{0.5}(N-L+k-1) \right]^T$ is

the received vector at the initial time shift $\tau = 1/2$. By using the above two equations, we can construct $\mathbf{Y}_{os}$ as

$$\mathbf{Y}_{os} \triangleq \begin{bmatrix} \mathbf{Y}_0 \\ \mathbf{Y}_{0.5} \end{bmatrix} \tag{3.19}$$

$$\Rightarrow \quad \mathbf{Y}_{os} \triangleq \begin{bmatrix} \mathbf{y}_{0,L} & \mathbf{y}_{0,L-1} & \cdots & \mathbf{y}_{0,0} \\ \mathbf{y}^*_{0,0} & \mathbf{y}^*_{0,1} & \cdots & \mathbf{y}^*_{0,L} \\ \mathbf{y}_{0.5,L} & \mathbf{y}_{0.5,L\text{-}1} & \cdots & \mathbf{y}_{0.5,0} \\ \mathbf{y}^*_{0.5,0} & \mathbf{y}^*_{0.5,1} & \cdots & \mathbf{y}^*_{0.5,L} \end{bmatrix}_{4(N-L)\times(L+1)} .$$

From Eqn. (3.19), we can see that the number of rows in matrix $\mathbf{Y}_{os}$ becomes twice the number of rows in matrix $\mathbf{Y}$ in Eqn. (3.11). The SVD of $\mathbf{Y}_{os}$ is taken to form $\mathbf{Y}_{1os}$ and $\mathbf{Y}_{2os}$ as in Eqn. (3.12). By using $\mathbf{Y}_{1os}$ and $\mathbf{Y}_{2os}$, $\exp\left(-j2\pi/N(\varepsilon+2k)\right)$ is estimated as the generalized eigenvalues of the matrix pair $\left[\mathbf{Y}_{1os}, \mathbf{Y}_{2os}\right]$, and thus the CFO can be estimated from Eqn. (3.9) and Eqn. (3.10). Although the number of rows in $\mathbf{Y}_{1os}$ and $\mathbf{Y}_{2os}$ becomes double, the rank of each matrix is still $N/2$. Because of oversampling, we expect better estimation performance. This will be demonstrated using simulation results.

Generally, CFO estimation methods are categorized as blind (non-data aided) method and non-blind (data aided) method. If repeated symbols or periodically inserted known symbols are used for CFO estimation, this method would be categorized as non-blind method. Otherwise, this method is categorized as blind method.

The proposed MP method can be categorized as blind method if all signals can be transmitted with equispacing structure without considering bandwidth efficiency because the use of virtual carriers reduces bandwidth efficiency. If the bandwidth efficiency is considered as a first priority, the first OFDM symbol with equispacing can be defined as a training symbol so that the other OFDM symbol can be transmitted with

no virtual subcarriers. In that case, the proposed MP method can be categorized as non-blind method, which requires only one OFDM training symbol. In ESPRIT [36], it uses virtual subcarriers to estimate the CFO. Since it does not use training symbols, it is categorized as blind method. But ESPRIT method is not suitable to use when the bandwidth efficiency is considered as a first priority. This is because ESPRIT method requires approximately 10 OFDM symbols to have acceptable performance, and it is impractical to transmit 10 training symbols continuously in a real implementation.

3.3 Discussion and Simulation

In the previous section, MP method, which is one of the variations of POF method, is proposed for estimating the CFO in OFDM cases. Similarly, one of the variations of POF method is the ESPRIT algorithm. The following table represents the summary of both MP method and ESPRIT method [36] for CFO estimation in OFDM system for comparison purposes.

As shown in Table 3.1, SVD is common in both algorithms. Thus, Hua and Sarkar [54] compared the SVD results for both MP and ESPRIT methods and showed that both methods are equivalent to the first order approximation. However, Hua and Sarkar [54] compared only the different eigendecomposition or SVD based steps inherent in these algorithms. Hua and Sarkar [54] did not take into consideration the different matrix structures. Actually, while MP constructs the forward backward matrix, $\mathbf{Y}$, directly from the received OFDM symbol, ESPRIT method estimates the covariance matrix, $\hat{\mathbf{R}}$, from the received OFDM symbol. This covariance matrix is estimated by averaging over the number of samples taken from the received OFDM

Table 3.1 Summary of MP and ESPRIT [36] methods for CFO estimation in the conventional OFDM system

MP method	**ESPRIT method**
1. Construct the forward backward matrix $\mathbf{Y}$, equation (3.11), from the received OFDM symbol vector. 2. Take the Singular Value Decomposition (SVD) of $\mathbf{Y}$ to form the matrices $\mathbf{Y}_1$ and $\mathbf{Y}_2$, Eqn. (3.13) and Eqn. (3.14). 3. Find the eigenvalue of $\left[\mathbf{Y}_1^+ \mathbf{Y}_2\right]$ to estimate the CFO	1. Form the $(N-M)$ blocks in both the forward and backward direction from each received k^{th} OFDM block, $\mathbf{y}_k \triangleq \left[y_k(0) \ \ldots \ y_k(N-1)\right]^T$ as $\mathbf{y}_{Fk}^i \triangleq \left[y_k(i-1) \ \ldots \ y_k(i+M-1)\right]^T$ $\mathbf{y}_{Bk}^i \triangleq \left[y_k(N-i) \ \ldots \ y_k(M-i-M)\right]^H$. 2. Construct the covariance matrix $\hat{\mathbf{R}}$ as follows: $\hat{\mathbf{R}}_{M+1} \triangleq \frac{1}{K(N-M)} \sum_{k=1}^{K} \sum_{i=1}^{N-M} \left[\mathbf{y}_{Fk}^i \left(\mathbf{y}_{Fk}^i\right)^H + \mathbf{y}_{Bk}^i \left(\mathbf{y}_{Bk}^i\right)^H\right]$ 3. Take the SVD of $\hat{\mathbf{R}}$. $\hat{\mathbf{R}} = \hat{\mathbf{U}} \ \hat{\Sigma} \hat{\mathbf{V}}^H$. 4. Find the eigenvalue of $[\hat{\mathbf{U}}(1:M,1:P)^+ \hat{\mathbf{U}}(2:M+1,1:P)]$ to estimate the CFO.

symbols. If the number of samples increases, the estimated covariance matrix is no longer singular and the estimate becomes more accurate. Otherwise, the estimated covariance will be less accurate. This effect can be seen in the performance of ESPRIT

method by varying 1 to 10 OFDM symbols as shown in Figure 3.5. Thus, there is the trade off between number of samples and the performance of ESPRIT method [36]. In OFDM systems, the number of subcarriers is assumed as the number of samples in an OFDM symbol. Therefore, the estimated covariance matrix effect must be counted as an important factor in OFDM systems.

Moreover, in the proposed MP method the OFDM signals are transmitted using equispaced subcarriers that can give double frequency spacing, while the same signals are transmitted with consecutive subcarriers in ESPRIT method. Therefore, although the SVD is a common structure for both methods, the performance of both methods will not be identical in the OFDM system because of the different signal model and the different matrix structures developed for the respective method.

When we consider the computational complexity of both methods, the complexity of ESPRIT is usually higher than that of MP method. This is because ESPRIT method requires the computation of the covariance matrix while MP defines the forward backward matrix directly form the received OFDM symbol. Moreover, several OFDM symbols are required in ESPRIT method to obtain accurate estimated covariance matrix but MP method requires only one OFDM symbol with equispacing. The computational complexity for estimating a covariance matrix increases as the number of OFDM symbols increases. Hence, MP is computationally less expensive when compared with the ESPRIT method in the OFDM system. However, there is a limitation in applying MP method to the OFDM system: that is the number of active subcarriers can be used is only half of the total number of subcarriers.

Computer simulations were conducted to compare and analyze the performance of the proposed MP method with that of ESPRIT method [36], Schmidl and Cox method [17], and against CRB (For CRB, see Appendix B for detail). Here we consider

the total number of subcarriers, $N = 64$, with cyclic prefix length $N_G = 11$ and $P = N/2$ used subcarriers or active subcarriers for each OFDM symbol. The true normalized CFO is set at ε =0.1, and we evaluate the performance under frequency selective fading channel by choosing the channel impulse response [40] as $h = \left[e^{j1.38} \; 0.5e^{j0.30} \; 0.3e^{-j2.02} \right]^T$. The proposed MP method as well as Schmidl and Cox method [17] made use of the number of active subcarriers equal to half of the total number of subcarriers. To be fair, for the performance comparison work, the same number of active subcarriers for ESPRIT method is used to compare against these 3 methods.

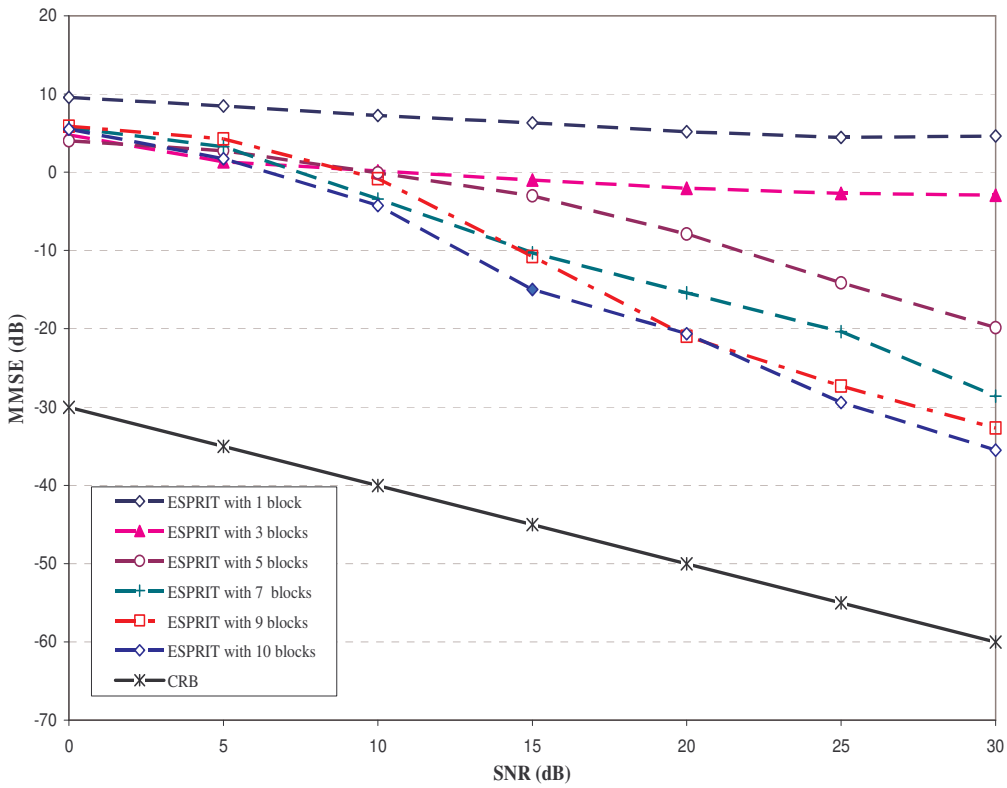

Figure 3.5 MMSE vs SNR for ESPRIT method varying the number of blocks from 1 block to 10 blocks.

We define the SNR ratio as in ESPRIT method [36]

$$SNR \triangleq \frac{\sigma_{x'}^2}{\sigma_w^2} \tag{3.20}$$

where $\sigma_{x'}^2$ is the variance of the OFDM symbol.

For each estimate of the CFO, we calculate the MMSE as the performance indicator as

$$MMSE = \frac{1}{M}\sum_{m=1}^{M}\left|\varepsilon - \hat{\varepsilon}(m)\right|^2 \tag{3.21}$$

where M is the total number of Monte Carlo runs, and $\hat{\varepsilon}(m)$ is the estimated CFO value at m^{th} run. In the simulation, we arbitrarily use 1000 Monte Carlo runs for each SNR. As we have claimed before, the estimated covariance matrix effect, which is used in ESPRIT method, can be seen in Figure 3.5. This figure compares the MMSE of the ESPRIT method by varying the number of OFDM symbols 1 to 10. From this figure, it is clear that the performance of ESPRIT method improves gradually when the number of OFDM symbols used in ESPRIT method is monotonically increased.

Figure 3.6 reveals that the proposed MP method with one block always outperforms the ESPRIT method with 10 blocks when the performance of the proposed MP method is compared with that of ESPRIT method. This clearly shows the superiority of the proposed method with equispacing. As we have discussed in Section 3.2, oversampling is applied onto the received OFDM symbol to improve the performance of the MP method. Here we can see that the oversampled MP method has better performance than the MP method for the whole SNR range. However, Schmidl and Cox method [17] performs better than all subspace-based method especially at low SNR.

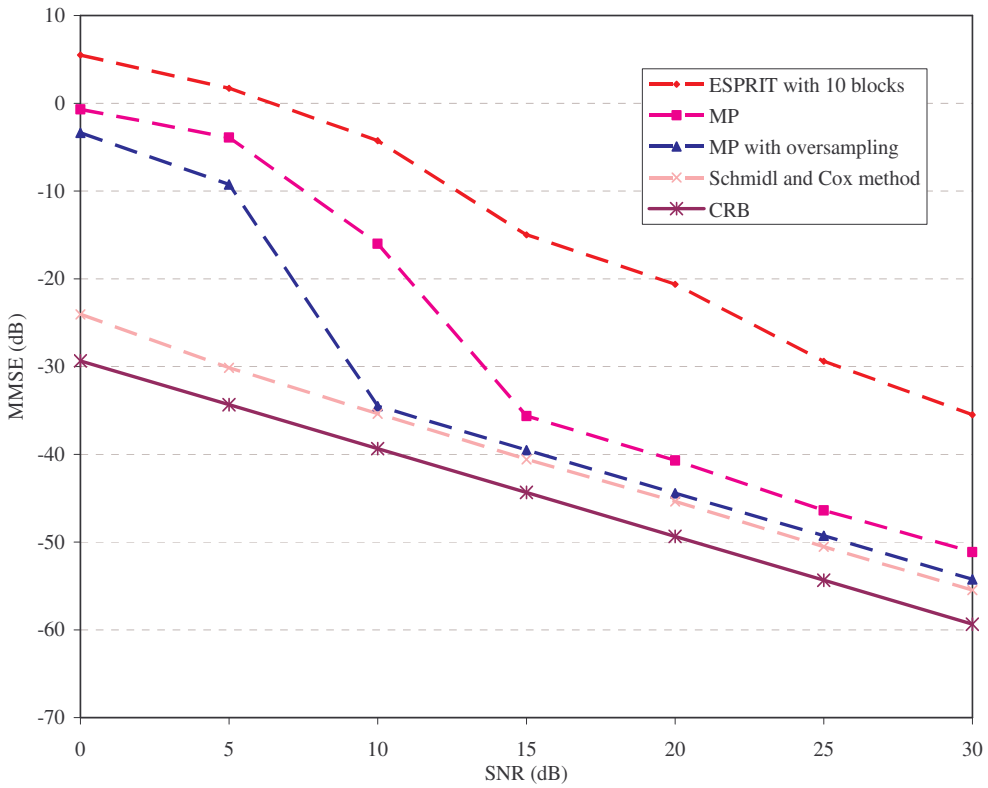

Figure 3.6 MMSE vs SNR over frequency selective fading channel.

If the bandwidth efficiency is considered as a first priority, the first symbol, which is used for the CFO estimation will be defined as a training symbol in the proposed method. In that case, the proposed method and the Schmidl and Cox method [17] will have the same bandwidth efficiency while ESPRIT method [36] has less bandwidth efficiency than Schmidl and Cox method [17]. However, the computational complexity of Schmidl and Cox method [17] is less than that of the MP method and the ESPRIT method [36]. This is because Schmidl and Cox method [17] does not use SVD. But more importantly we are interested in the subspace based method because it offers the accuracy of super resolution. Moreover, ESPRIT method, one of the subspace based method, not only requires more than one OFDM symbol to estimate the CFO but also has high MMSE. In fact, Schmidl and Cox method [17] is a non-subspace based

method. Since our proposed method is subspace based, the comparison between Schmidl and Cox method [17] and our proposed method will not be justified.

However, we compare our proposed method with Schmidl and Cox method [17] to determine the performance of CFO estimation since Schmidl method is one of the best CFO estimation. In OFDM system, we assume that the noise is zero-mean complex envelope of additive white Gaussian. Thus when Schmidl used the correlation function between the first half and second half OFDM symbol, the effect of noise can be reduced even at low SNR. In high SNR, oversampled MP method shows almost similar performance to Schmidl and Cox method [17] with about 1 dB degradation.

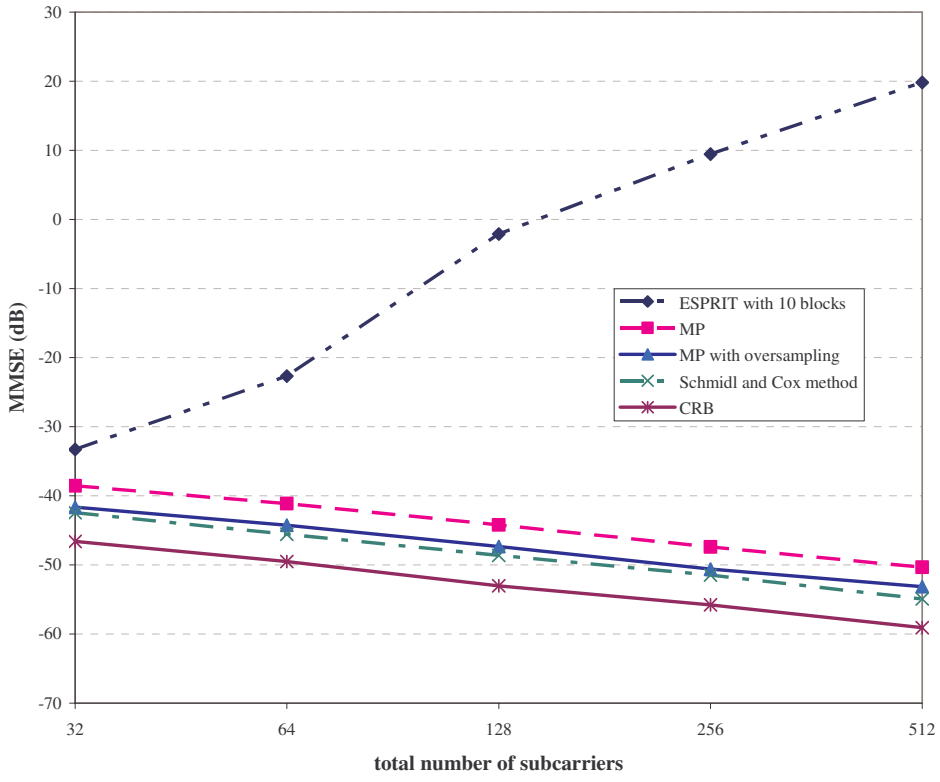

Figure 3.7 MMSE vs total number of active subcarriers over frequency selective fading channel at SNR=20dB.

Figure 3.7 shows the MMSE performance of the conventional OFDM system with ESPRIT (10 OFDM blocks), MP, MP with oversampling, and Schmidl and Cox methods under frequency selective fading channel with respect to the total number of subcarriers, *N*. In this case, the total number of subcarriers was varied from 32 to 512 and SNR is 20dB. From this figure, it is clear that the MP and MP with oversampling methods can estimate consistently for the total number of subcarriers range and the estimation accuracy as Schmidl and Cox method. But the ESPRIT method cannot estimate consistently, and the accuracy of ESPRIT method also decreases as the total number of subcarriers increases.

This is because of the properties of covariance matrix in ESPRIT method. Stoica and Soderstrom [61] analyzed the properties of MUSIC and ESPRIT methods for sinusoidal frequency estimation. According to the properties of the covariance elements in [61], the covariance elements of ESPRIT depend only on difference between frequencies and not the frequency values. In addition, Property 3 from [61] states that if two frequencies are close to each other, then the covariance elements of the ESPRIT method are large. In our OFDM system, the relationship between the number of subcarriers and the frequency spacing can be seen clearly from the received OFDM symbol, Eqn. (3.2).

In vector form,

$$\mathbf{y}_k \triangleq \left[y_k(0) \quad \ldots \quad y_k(N-1) \right]^T \triangleq \frac{1}{\sqrt{N}} \mathbf{E}\mathbf{W}\mathbf{s}'_k + \mathbf{w}_k \tag{3.22}$$

where $\mathbf{y}_k$ is the kth received OFDM symbol vector, N is the total number of subcarriers $\mathbf{w}_k$ is the AWGN noise vector at k^{th} received OFDM symbol and the definitions of $\mathbf{E}$, $\mathbf{W}$ and $\mathbf{s}'_k$ have mentioned in page (57).

In the above equation, when the number of subcarriers, N, increases, $2\pi/N$ will decrease proportionally. In fact, $2\pi/N$ is the frequency spacing between the adjacent subcarriers in OFDM system. If the adjacent subcarriers are close to each other, the matrix $\mathbf{EW}$ in ESPRIT method is nearly ranked deficient and thus the covariance elements are large. Therefore, the accuracy of ESPRIT method decreases as the number of subcarriers increases.

The reason for having consistent estimation by proposed MP method is the equispacing structure for the transmitted signal. Using equispacing structure for the transmitted signal causes not only double frequency spacing between the adjacent subcarriers but also the active subcarriers to be uniformly distributed over the whole frequency range, 0 to 2π . But for the ESPRIT method, the active subcarriers will not be uniformly distributed over the whole frequency range, 0 to 2π , because the signal is transmitted with consecutive subcarriers. (Equispacing subcarriers and consecutive subcarriers is shown in Figure 3.2 and 3.3)

In the presence of noise, the CFO estimation can be highly inaccurate, for example, the estimated value may be 180-degree out of phase. When the frequency spacing becomes narrower, it is observed that the effect of 180 degree out of phase becomes greater. However, in MP method the 180 degree out of phase effects offset each other in opposite direction since the transmitted signal is uniformly distributed within the range 0 to 2π . But in the ESPRIT method, the 180-degree out of phase effect cannot offset each other. This can be seen clearly in Figures 3.8 (a), (b) and (c). In Figure 3.8, (a) represents the case of $N = 32$, (b) is for $N= 64$ and (c) is for $N= 128$. The actual frequencies spacing with CFO between the adjacent subcarriers for both methods is shown in (i) and (ii) of Figures 3.8 (a), (b) and (c). The estimated frequencies spacing

with CFO between the adjacent subcarriers for both methods is shown in (iii) and (iv) of Figures 3.8 (a), (b) and (c).

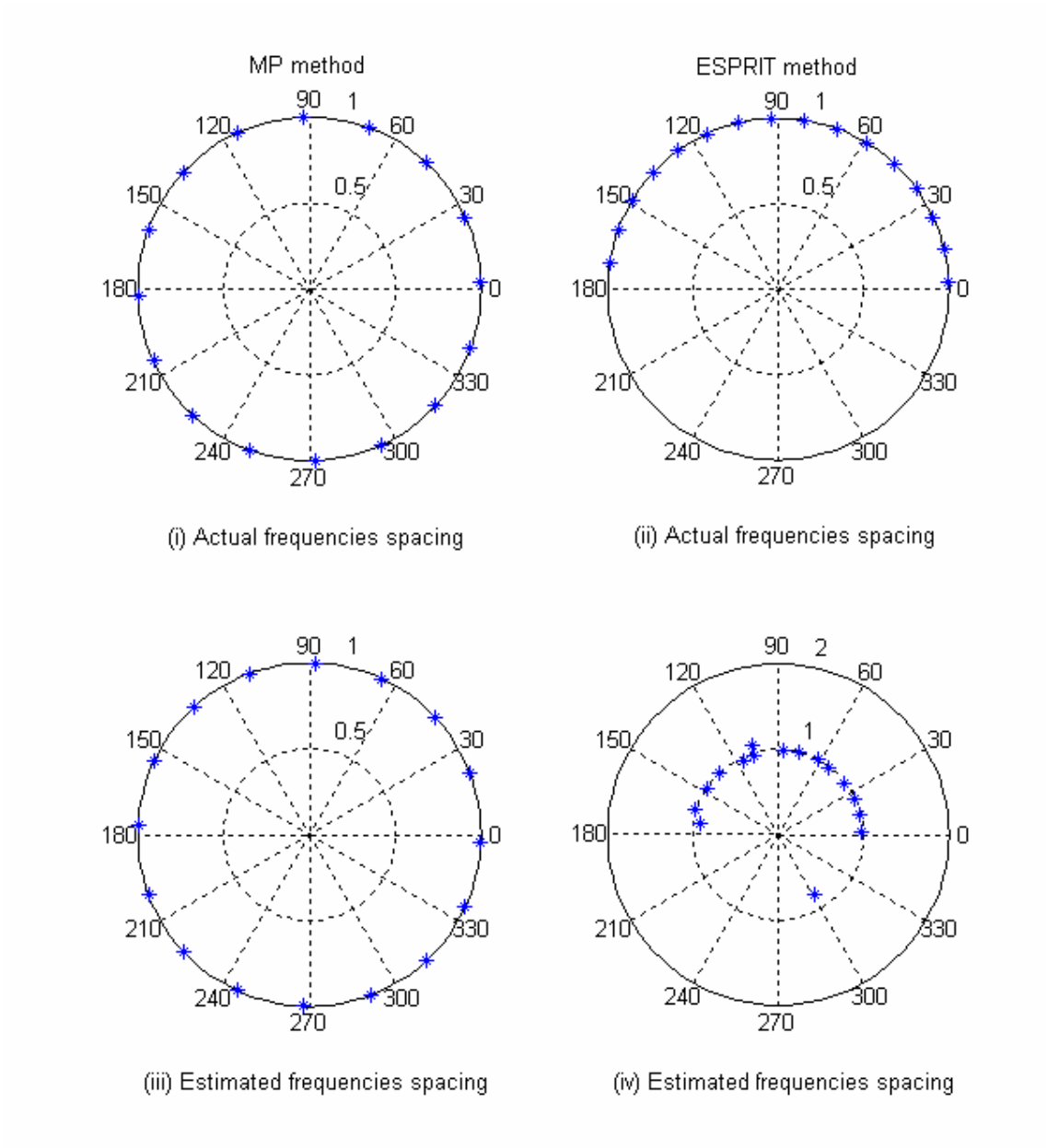

Figure 3.8 Actual and estimated frequencies spacing with CFO between the adjacent subcarriers of both MP and ESPRIT methods (a) $N = 32$ case

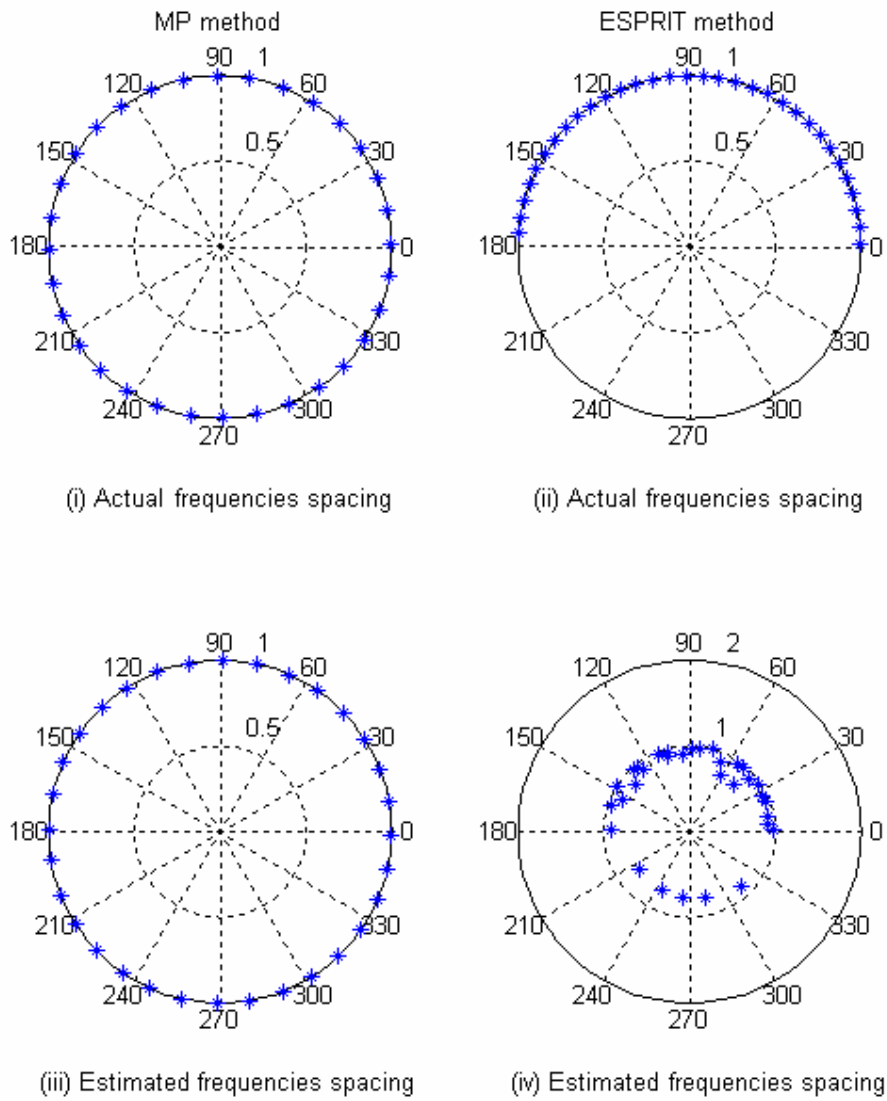

Figure 3.8 (b) $N = 64$ case

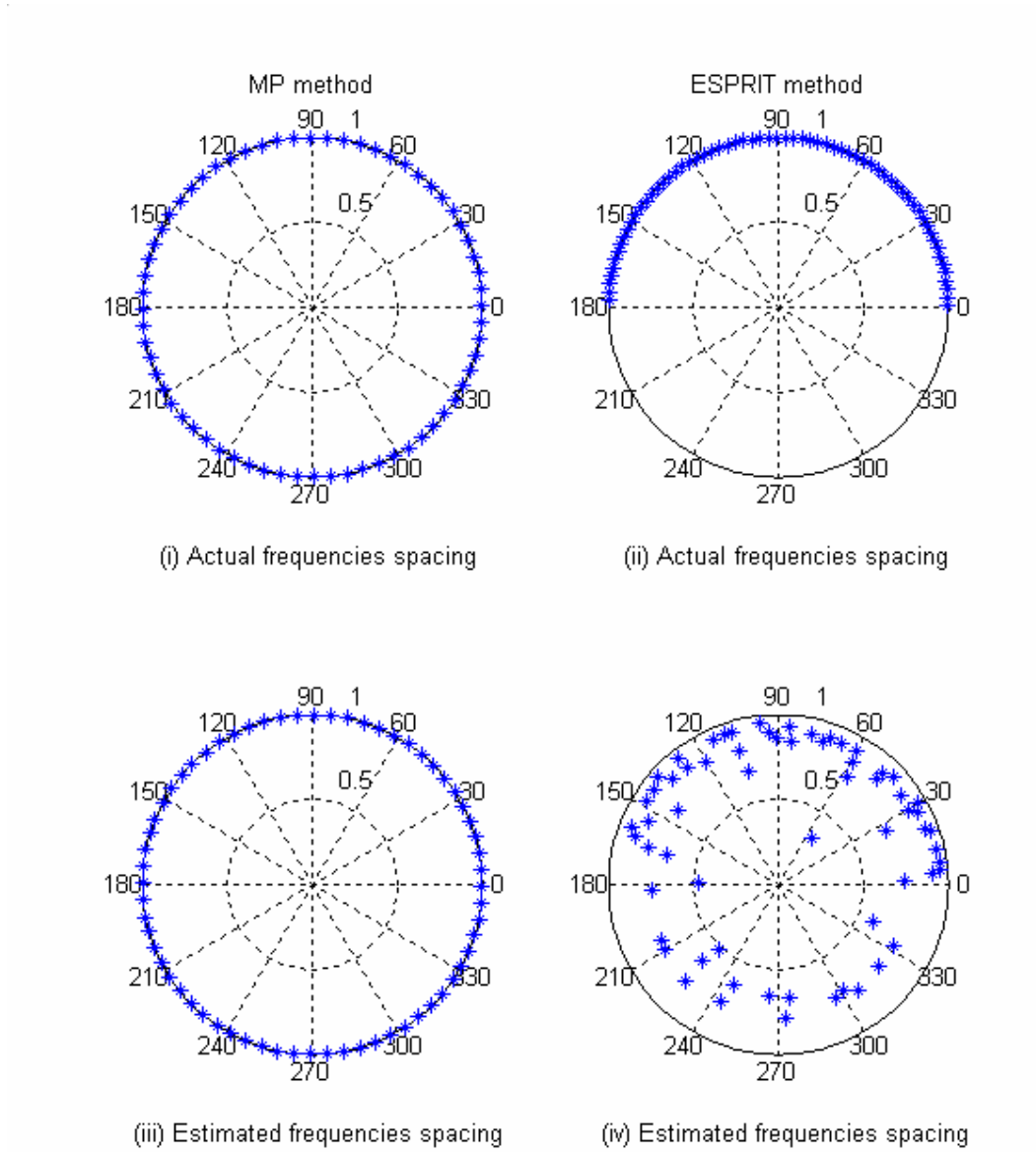

Figure 3.8 (c) $N = 128$ case

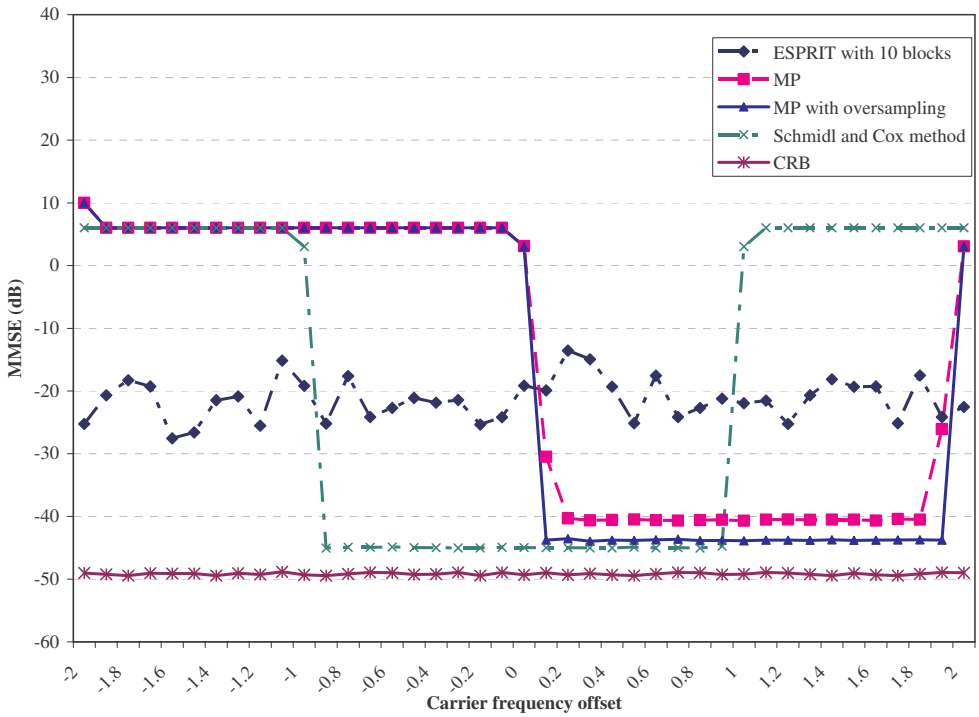

Figure 3.9 MMSE vs CFO over frequency selective fading channel with 10 block s ESPRIT

Figure 3.9 illustrates the CFO range of the proposed MP method and the ESPRIT method for the conventional OFDM system. The number of subcarriers is 64 and the SNR is 20 dB. It may be observed that the CFO range of the MP method is $0 \le \varepsilon \le 2$ as discussed in Section 3.2 and is the same range of Schmidl method. Although the CFO range of ESPRIT method is larger than that of MP method, ESPRIT method has poor estimation accuracy within the CFO estimation range.

3.4 Conclusion

This chapter proposed an efficient CFO estimation, which requires only one symbol in the OFDM system. We discussed the reason why the proposed MP method

required the equispace structure for the transmitted signal, and performs better than the ESPRIT method. Moreover, we also showed how to improve the performance of the proposed method by using oversampling technique. From the simulation results, we observed that the performance of the proposed MP method is superior to that of the ESPRIT method under frequency selective fading channel. We also showed the impact of the covariance matrix estimation accuracy in ESPRIT method.

CHAPTER 4

CARRIER FREQUENCY OFFSET ESTIMATION IN OFDM BASED WLAN STRUCTURE

The objectives of this chapter are two-fold. Firstly, this chapter shows in a clear way how an OFDM preamble data frame in WLAN can be modeled in accordance with the widely used uniform linear array DOA estimation. This potentially leads us to the possible exploitation of the plethora of DOA estimation algorithms for CFO estimation. Secondly, in this chapter we show how a subspace-based DOA algorithm, called MUSIC, can be successfully applied to the CFO estimation in OFDM based WLAN. Also, we derive the theoretical performance, which indicates the strength of the proposed estimation method.

In Section 4.1, we focus on the signal model that is derived from the preamble of the OFDM based WLANs. In Section 4.2, we show that this signal model is identical to the uniform linear array signal-processing model. We propose to use the MUSIC method, which is originally presented as a DOA estimator in array signal processing. In Section 4.3, theoretical performance analysis of the proposed method is derived. Finally, conclusion is made in Section 4.4.

4.1 Signal Model

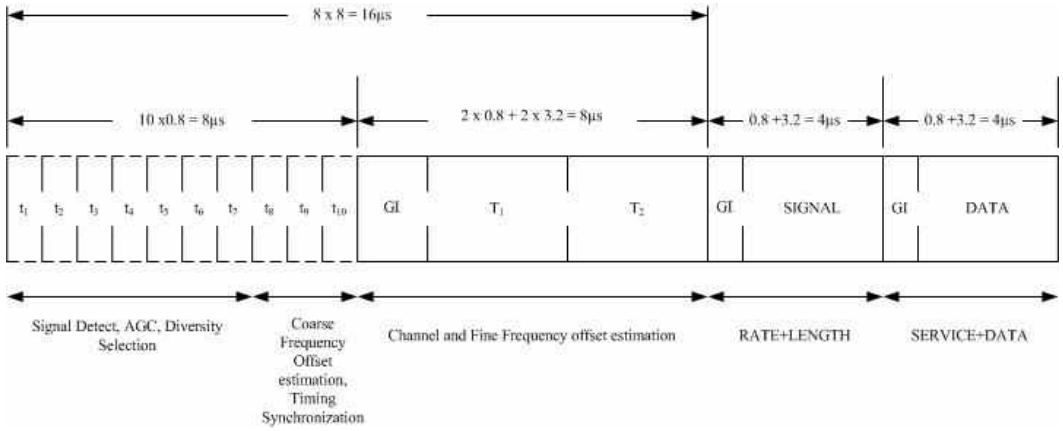

Figure 4.1 Data frame structure of OFDM based WLAN structure.

In OFDM based WLAN structure, the preamble section is used for channel estimation, CFO estimation, and timing synchronization. The details of the PLCP preamble field are as shown in Figure 4.1. The PLCP preamble composes of ten identical short training symbols, $t_1, t_2, ..., t_{10}$, which have 16 samples in each symbol; and two identical long training symbols, T_1, T_2, which have 64 samples in each symbol. The identical short training symbols are used for Automatic Gain Control convergence, diversity selection, timing acquisition and coarse CFO acquisition in the receiver. The identical long training symbols are used for channel and fine CFO estimation. The OFDM training symbols shall be followed by the SIGNAL field, which contains the RATE and the LENGTH fields of the TXVECTOR. The TXVECTOR represents a list of parameters that the Medium Access Control (MAC) sub-layer provides to the local PHY entity in order to transmit a MPDU (MAC Protocol Data Unit), as described in [5]. The data carrying portion consists of a variable number of OFDM symbols which have 64 samples in each symbol. Each OFDM symbol contains the active subcarriers, null

subcarriers inserted at equal distance, and the pilot subcarriers, which are typically used for updating the channel estimates [5].

In the preamble section, the cyclic prefix or GI is not available for all short training symbols. Since the short training symbols are series of identical symbols, the first short training symbol is assumed as the cyclic prefix or GI of the following nine short training symbols. In front of the long training symbol, there is a GI, which is copied from the last 32 samples of the long training symbol. We assume that the first short training symbol and GI have been removed before CFO estimation.

Although there is CFO, the frequency offset subcarrier is independent because the frequency change due to CFO is the same for all subcarriers. Therefore, the phase shift, which appeared due to CFO, is independent of the subcarriers frequencies themselves. Moreover, the length of channel impulse response is assumed to be shorter than a short training symbol. Since the variations are negligible during the transmission of a single block of data, the nine short training symbols will still be identical after taking the first short training symbol as a cyclic prefix to mitigate ISI. In the absence of noise, first short training symbol, (here we assume 2nd training symbol as a 1st training symbol because the actual 1st training symbol is removed as a cyclic prefix) becomes

$$x_S(1,n) = \frac{1}{\sqrt{N_L}} \sum_{k=0}^{N_L-1} H_k S_k e^{j\frac{2\pi}{N_L}kn} e^{j2\pi\varepsilon n} \tag{4.1}$$

where $n = 0,\ 1,\ \ldots,\ N_S - 1$, the subscripts S and L refer to the short and long training symbols, $N_S = 16$ is the number of samples in each short training symbol, $N_L = 64$ is the number of samples in each long training symbol or the number of samples after taking IFFT, H_k is the transfer function of the channel at the frequency of the kth

carrier, given as $H_k = \sum_{l=0}^{L_C-1} h(l)\exp\left(j\left(2\pi/N_L\right)kl\right)$, L_C is the number of multipaths, S_k is the kth element of the sequence which is taken from [5] and ε is the CFO.

The 2nd short training symbol becomes

$$x_s(2,n) = \frac{1}{\sqrt{N_L}} \sum_{k=0}^{N_L-1} H_k S_k e^{j\frac{2\pi}{N_L}k(n+N_S)} e^{j2\pi\varepsilon(n+N_S)}$$

$$= \frac{1}{\sqrt{N_L}} e^{j2\pi\varepsilon N_S} \sum_{k=0}^{N_L-1} H_k S_k e^{j\frac{2\pi}{N_L}k(n+N_S)} e^{j2\pi\varepsilon n} . \tag{4.2}$$

Because of the periodicity of the IFFT of the sequence, S_k, $\frac{1}{\sqrt{N_L}} \sum_{k=0}^{N_L-1} H_k S_k e^{j\frac{2\pi}{N_L}k(n+N_S)}$ value is equivalent to $\frac{1}{\sqrt{N_L}} \sum_{k=0}^{N_L-1} H_k S_k e^{j\frac{2\pi}{N_L}kn}$ value (see details in [5]). Thus it is easy to see that

$$x_S(2,n) = e^{j2\pi\varepsilon N_S} x_S(1,n) . \tag{4.3}$$

Therefore, the 3rd short training symbol and the rest of the short training symbol can also be easily shown as

$$x_S(3,n) = \frac{1}{\sqrt{N_L}} \sum_{k=0}^{N_L-1} H_k S_k e^{j\frac{2\pi}{N_L}k(n+2N_S)} e^{j2\pi\varepsilon(n+2N_S)}$$

$$= \frac{1}{\sqrt{N_L}} e^{j2\pi\varepsilon 2N_S} \sum_{k=0}^{N_L-1} H_k S_k e^{j\frac{2\pi}{N_L}k(n+2N_S)} e^{j2\pi\varepsilon n}$$

$$= e^{j2\pi\varepsilon 2N_S} x_s(1,n) \tag{4.4}$$

$$\vdots$$

$$x_S(9,n)=\frac{1}{\sqrt{N_L}}\sum_{k=0}^{N_L-1}H_kS_k e^{j\frac{2\pi}{N_L}k(n+8N_S)}e^{j2\pi\varepsilon(n+8N_S)}$$

$$=\frac{1}{\sqrt{N_L}}e^{j2\pi\varepsilon 8N_S}\sum_{k=0}^{N_L-1}H_kS_k e^{j\frac{2\pi}{N_L}k(n+8N_S)}e^{j2\pi\varepsilon n}$$

$$=e^{j2\pi\varepsilon 8N_S}x_s(1,n)\,. \tag{4.5}$$

According to Eqns. (4.1) – (4.5), we can form the relationship as follows:

$$x_S(m,n)=e^{j2\pi(m-1)N_S\varepsilon}x_S(1,n) \tag{4.6}$$

where $m=1,2,...,M_S-1$, $n=0,1,...,N_S-1$, $M_S=10$ is the total number of short training symbol.

Therefore, the received short training symbol with noise can be formulated as

$$\mathbf{y}_S(n)\triangleq\mathbf{a}_S(\varepsilon)\;x_S(1,n)+\mathbf{w}_S(n) \tag{4.7}$$

where $\mathbf{y}_S(n)\triangleq\left[y_S(1,n)\quad ...\quad y_S(M_S-1,n)\right]^T$ (4.8)

$$\mathbf{a}_S(\varepsilon)\triangleq\left[1\quad e^{j2\pi\varepsilon N_S}\quad ...\quad e^{j2\pi\varepsilon(M_S-2)N_S}\right]^T \tag{4.9}$$

$$\mathbf{w}_S(n)\triangleq\left[w_S(1,n)\quad ...\quad w_S(M_S-1,n)\right]^T \tag{4.10}$$

$x_s(1,n)$ is the noise free short training symbol at the nth sample after removing the cyclic prefix and before FFT, ε is the CFO and $w_S(m,n)$ is the zero-mean complex envelope of AWGN with variance σ^2, which appears at the short training symbols.

In the same way, the two long training symbols are also identical, (see Figure 4.1) and thus the following expression is also valid

$$\mathbf{y}_L(n) \triangleq \mathbf{a}_L(\varepsilon)\, x_L(1,n) + \mathbf{w}_L(n) \tag{4.11}$$

where $\mathbf{y}_L(n) \triangleq \left[y_L(1,n) \quad y_L(M_L,n) \right]^T$ (4.12)

$$\mathbf{a}_L(\varepsilon) \triangleq \left[1 \quad e^{j2\pi\varepsilon N_L} \right]^T \tag{4.13}$$

$$\mathbf{w}_L(n) \triangleq \left[w_L(1,n) \quad w_L(M_L,n) \right]^T \tag{4.14}$$

$$x_L(1,n) = \frac{1}{N_L} \sum_{k=0}^{N_L-1} H_k S_k e^{j\frac{2\pi}{N_L}kn} e^{j2\pi\varepsilon n} \tag{4.15}$$

$n = 0,1,2,...,N_L - 1$, $M_L = 2$ is the total number of long training symbol, $x_L(1,n)$ is the noise free long training symbol at the nth sample after removing the cyclic prefix and before FFT and $w_L(m,n)$ is the zero-mean complex envelope of AWGN with variance σ^2, which appears at the long training symbols.

4.2 Carrier Frequency Offset Estimation using MUSIC Technique

Now, the signal models for short training symbols and long training symbols are identical to the uniform linear array signal processing model [62] shown below

$$\mathbf{y}(n) \triangleq \mathbf{A}(\theta)\,\mathbf{x}(n) + \mathbf{w}(n) \tag{4.16}$$

where $n = 0,1,2,...,N-1$, $\mathbf{y}(n)$ is $M \times 1$ array output vector, $\mathbf{x}(n)$ is $p \times 1$ signal vector, $\mathbf{w}(n)$ is the complex additive white Gaussian noise with zero mean, M is the total number of sensors, p is the total number of sources, and N is the number of snapshots. Here, $\mathbf{A}(\theta)$ is the $M \times p$ steering matrix and has the following structure

$$\mathbf{A}(\theta) \triangleq \begin{bmatrix} \mathbf{a}(\theta_1) & \mathbf{a}(\theta_2) & \ldots & \mathbf{a}(\theta_p) \end{bmatrix} \tag{4.17}$$

$$\mathbf{a}(\theta_i) \triangleq \begin{bmatrix} 1 & e^{j\frac{2\pi}{\lambda}d\sin(\theta_i)} & \ldots & e^{j(M-1)\frac{2\pi}{\lambda}d\sin(\theta_i)} \end{bmatrix}^T \tag{4.18}$$

where d is the distance between the two adjacent sensors, θ_i is the direction of arrival of the ith signal and λ is the wavelength of the incident signal. Since Eqns (4.7) & (4.16) and (4.11) & (4.16) have a similar structure, the DOA estimation methods of array signal model can be used to estimate the CFO in OFDM based WLANs structure. The famous and most common subspace-based DOA methods are the MUSIC [44] and ESPRIT [50] algorithms. According to the signal models of short and long training symbols, ESPRIT can be applied only to the short training symbols and cannot be applied to the long training symbols because for the long training symbol case, it is as if we are dealing with a two sensor array case and hence we cannot construct the shift invariance structure as required in the ESPRIT algorithm. Thus, MUSIC algorithm can be used for this CFO estimation case. Therefore, one of the famous methods of array signal processing, MUSIC [44], is proposed to use in OFDM based WLANs structure according to the signal model of short and long training symbol Eqns. (4.7) & (4.11).

To use the MUSIC algorithm for the CFO in OFDM base WLAN system, the estimated covariance matrices of short and long training symbols are computed from the received training symbols, Eqn. (4.7) and Eqn. (4.12), as follows:

$$\hat{\mathbf{R}}_{y_i y_i} = E\left\{\mathbf{y}_i \mathbf{y}_i^H\right\} = \mathbf{a}_i \hat{\mathbf{R}}_{x_i x_i} \mathbf{a}_i^H + \sigma^2 \mathbf{I} \tag{4.19}$$

where $i = S$ or L, $\hat{\mathbf{R}}_{x_i x_i}$ is the estimated covariance matrix corresponding to the short training symbols or long training symbols, $\boldsymbol{x}_i$, and $\mathbf{a}_i$ is the steering vector of the short or long training symbols. We estimate $\hat{\mathbf{R}}_{y_i y_i}$ by $\left(1/N_i\right)\sum_{k=0}^{N_i-1} \mathbf{y}_i\left(k\right)\mathbf{y}_i^H\left(k\right)$.

We carried out the eigendecomposition of $\hat{\mathbf{R}}_{y_i y_i}$ in order to ascertain the noise and signal subspaces. They are

$$\hat{\mathbf{R}}_{y_i y_i} = \sum_{m=1}^{M_i} \hat{\lambda}_{i,m} \hat{\mathbf{e}}_{i,m} \hat{\mathbf{e}}_{i,m}^H \tag{4.20}$$

where $\hat{\mathbf{e}}_{i,1}$, $\hat{\mathbf{e}}_{i,2}$, ...,$\hat{\mathbf{e}}_{i,M_i}$ are the eigenvectors and $\hat{\lambda}_{i,1}$, $\hat{\lambda}_{i,2}$, ...,$\hat{\lambda}_{i,M_i}$ are the corresponding eigenvalues of the estimated covariance matrix $\hat{\mathbf{R}}_{y_i y_i}$.

Since the CFO estimation in OFDM based WLAN is similar to the linear array signal processing model with single source case, we define the matrices $\hat{\mathbf{E}}_{i\,sig}$ and $\hat{\mathbf{E}}_{i\,noise}$ whose columns span the signal and noise subspaces, respectively, of the estimated covariance matrix $\hat{\mathbf{R}}_{y_i y_i}$ as

$$\hat{\mathbf{e}}_{i,sig} \triangleq \hat{\mathbf{e}}_{i1}$$

$$\hat{\mathbf{E}}_{i\,noise} = \left[\hat{\mathbf{e}}_{i,noise\,1} \quad \ldots \quad \hat{\mathbf{e}}_{i,noise\,M_i-1}\right] \triangleq \left[\hat{\mathbf{e}}_{i2} \quad \ldots \quad \hat{\mathbf{e}}_{i\,M_i}\right]. \tag{4.21}$$

Therefore, we extract the CFO, ε , as the coordinates of the highest peak of the following MUSIC spectrum:

$$\mathbf{P}_i(\varepsilon) \triangleq \frac{1}{\mathbf{a}^H(\varepsilon)\hat{\mathbf{E}}_{i\,noise}\hat{\mathbf{E}}_{i\,noise}^H\mathbf{a}(\varepsilon)} \quad . \tag{4.22}$$

MUSIC method is based on the orthogonality between the signal and noise subspaces. However, the number of samples in all training symbols of OFDM based WLANs structure has fixed value. The number of samples in each short training symbol is only 16 although the number of samples in each long training symbol is 64. If we did not apply all short training symbols as the number of sensors, an estimated covariance matrix will have low quality because of the small sample sizes and the so called small number of sensors. Thus, estimated noise subspace may be poorly aligned with the true noise subspace. This effect causes MUSIC to pick spurious frequency value, and thus gives inaccurate CFO estimate. We can observe these effects in our simulation experiments.

4.3 Theoretical Analysis of MUSIC method in the OFDM based WLAN

In this section, we analytically examine the performance of the proposed method for the CFO estimation in OFDM based WLAN. We conduct a first order performance analysis on the MUSIC method for CFO estimation by evaluating the mean and variance of the CFO estimation error.

To evaluate the mean and variance of the CFO estimation error, firstly we need the following lemma, which results in the statistics of the eigenvectors of the estimated

covariance matrix, $\hat{\mathbf{R}}_{yy}$. Let us first introduce the notations, which will be used in Lemma and Theorem, as follows:

(1) $\hat{\Lambda}=\left[\hat{\lambda}_1\right]$ is the signal space eigenvalue of the estimated covariance matrix $\hat{\mathbf{R}}_{yy}$.

(2) $\Lambda=\left[\lambda_1\right]$ is the signal space eigenvalue of the ideal covariance matrix $\mathbf{R}_{yy}$.

(3) $\hat{\mathbf{\Sigma}}=diag\left[\hat{\lambda}_2 \quad \hat{\lambda}_3 \quad ... \quad \hat{\lambda}_M\right]$ is the diagonal matrix of the noise space eigenvalues of the estimated covariance matrix $\hat{\mathbf{R}}_{yy}$.

(4) $\mathbf{\Sigma}=diag\left[\lambda_2 \quad \lambda_3 \quad ... \quad \lambda_M\right]$ is the diagonal matrix of the noise space eigenvalues of the ideal covariance matrix $\mathbf{R}_{yy}$.

(5) $\hat{\mathbf{\Omega}}=\begin{bmatrix}\hat{\Lambda} & 0\\ 0 & \hat{\mathbf{\Sigma}}\end{bmatrix}$ is the diagonal matrix of the eigenvalues of the estimated covariance matrix $\hat{\mathbf{R}}_{yy}$.

(6) $\hat{\mathbf{e}}_{sig}$ is the signal subspace eigenvector, which is taken from the estimated covariance matrix $\hat{\mathbf{R}}_{yy}$.

(7) $\hat{\mathbf{E}}_{noise}=\left[\hat{\mathbf{e}}_{noise,1} \quad \hat{\mathbf{e}}_{noise,2} \quad \hat{\mathbf{e}}_{noise,(M-1)}\right]$ is the matrix that consists the noise subspace eigenvectors, which is taken from the estimated covariance matrix $\hat{\mathbf{R}}_{yy}$, where $\hat{\mathbf{e}}_{noise,i}$ is the ith column of $\hat{\mathbf{E}}_{noise}$.

(8) $\mathbf{e}_{sig}$ is the signal subspace eigenvector, which is taken from the ideal covariance matrix $\mathbf{R}_{yy}$.

(9) $\mathbf{E}_{noise}$ is the matrix that consists the noise subspace eigenvectors, which is taken from the ideal covariance matrix $\mathbf{R}_{yy}$.

(10) $O(.)$ is the approximation of the computational complexity and

(11) let $\mathbf{\Delta} \triangleq \mathbf{E}_{noise}^{H} \hat{\mathbf{R}}_{yy} \mathbf{E}_{noise} - \sigma^2 \mathbf{I}$, and $\mathbf{\Gamma} \triangleq \mathbf{e}_{sig}^{H} \hat{\mathbf{R}}_{yy} \mathbf{E}_{noise}$

In addition, for large N, $\hat{\mathbf{e}}_{sig} = \mathbf{e}_{sig} + O\left(1/\sqrt{N}\right)$, $\hat{\Lambda} = \Lambda + O\left(1/\sqrt{N}\right)$, $\hat{\mathbf{\Sigma}} = \Sigma + O\left(1/\sqrt{N}\right)$, and $\mathbf{E}_{noise}^{H} \hat{\mathbf{e}}_{sig} = O\left(1/\sqrt{N}\right)$.

Lemma 4.1: The orthogonal projections of $\left\{\hat{\mathbf{e}}_{noise,i}\right\}$ onto the column space of $\mathbf{e}_{sig}$ are asymptotically jointly Gaussian distributed (for independent and identically distributed (iid) case, N may not necessarily be too large [63]) with zero means and covariance matrices given by

$$E\left\{\left(\mathbf{e}_{sig}\mathbf{e}_{sig}^{H}\hat{\mathbf{e}}_{noise,i}\right)\left(\mathbf{e}_{sig}\mathbf{e}_{sig}^{H}\hat{\mathbf{e}}_{noise,j}\right)^{H}\right\} = \frac{1}{N} U\, \delta_{i,j} \tag{4.23}$$

where $U \triangleq \dfrac{\sigma^2 \lambda_1}{\left(\sigma^2 - \lambda_1\right)^2} \mathbf{e}_{sig}\mathbf{e}_{sig}^{H}$ and

$$E\left\{\left(\mathbf{e}_{sig}\mathbf{e}_{sig}^{H}\hat{\mathbf{e}}_{noise,i}\right)\left(\mathbf{e}_{sig}\mathbf{e}_{sig}^{H}\hat{\mathbf{e}}_{noise,j}\right)^{T}\right\} = 0 \quad \text{for all i,j.} \tag{4.24}$$

Proof: Firstly, we prove that $\mathbf{\Delta}$ and $\mathbf{\Gamma}$ are independent random matrices. According to the above definitions for large N and the eigenvalue decomposition of $\hat{\mathbf{R}}_{yy}$, we obtain

$$\begin{aligned}
\left(\mathbf{E}_{noise}^{H}\hat{\mathbf{E}}_{noise}\right)\left(\hat{\mathbf{E}}_{noise}^{H}\mathbf{E}_{noise}\right) &= \hat{\mathbf{E}}_{noise}^{H}\left(\mathbf{I} - \hat{\mathbf{e}}_{sig}\hat{\mathbf{e}}_{sig}^{H}\right)\mathbf{E}_{noise} \\
&= \hat{\mathbf{E}}_{noise}^{H}\mathbf{I}\,\mathbf{E}_{noise} - \hat{\mathbf{E}}_{noise}^{H}\hat{\mathbf{e}}_{sig}\hat{\mathbf{e}}_{sig}^{H}\,\mathbf{E}_{noise} \\
&= \mathbf{I} - \hat{\mathbf{E}}_{noise}^{H}\hat{\mathbf{e}}_{sig}\hat{\mathbf{e}}_{sig}^{H}\,\mathbf{E}_{noise}, \\
&\simeq \mathbf{I}.
\end{aligned} \tag{4.25}$$

Therefore,

$$\begin{aligned}
\mathbf{\Delta} &= \mathbf{E}_{noise}^{H}\hat{\mathbf{R}}_{yy}\mathbf{E}_{noise} - \sigma^2\mathbf{I} \\
&= \mathbf{E}_{noise}^{H}\left(\hat{\mathbf{e}}_{sig}\hat{\Lambda}\hat{\mathbf{e}}_{sig}^{H} + \hat{\mathbf{E}}_{noise}\hat{\mathbf{\Sigma}}\hat{\mathbf{E}}_{noise}^{H}\right)\mathbf{E}_{noise} - \sigma^2\mathbf{I}
\end{aligned}$$

$$=\left(\mathbf{E}_{noise}^{H}\hat{\mathbf{e}}_{sig}\right)\hat{\Lambda}\left(\hat{\mathbf{e}}_{sig}^{H}\mathbf{E}_{noise}\right)+\left(\mathbf{E}_{noise}^{H}\hat{\mathbf{E}}_{noise}\right)\hat{\mathbf{\Sigma}}\left(\hat{\mathbf{E}}_{noise}^{H}\mathbf{E}_{noise}\right)-\sigma^{2}\mathbf{I}$$

$$\simeq\left(\mathbf{E}_{noise}^{H}\hat{\mathbf{E}}_{noise}\right)\hat{\mathbf{\Sigma}}\left(\hat{\mathbf{E}}_{noise}^{H}\mathbf{E}_{noise}\right)-\sigma^{2}\mathbf{I}$$

$$=\left(\mathbf{E}_{noise}^{H}\hat{\mathbf{E}}_{noise}\right)\left(\hat{\mathbf{\Sigma}}-\sigma^{2}\mathbf{I}\right)\left(\hat{\mathbf{E}}_{noise}^{H}\mathbf{E}_{noise}\right)-\sigma^{2}.\left(\mathbf{I}-\left(\mathbf{E}_{noise}^{H}\hat{\mathbf{E}}_{noise}\right)\left(\hat{\mathbf{E}}_{noise}^{H}\mathbf{E}_{noise}\right)\right)$$

$$\simeq\left(\mathbf{E}_{noise}^{H}\hat{\mathbf{E}}_{noise}\right)\left(\hat{\Sigma}-\sigma^{2}\mathbf{I}\right)\left(\hat{\mathbf{E}}_{noise}^{H}\mathbf{E}_{noise}\right). \tag{4.26}$$

From Eqns. (4.25) and (4.26) we can see that asymptotically the columns of $\mathbf{E}_{noise}^{H}\hat{\mathbf{E}}_{noise}$ form an orthonormal basis for the eigenspace of $\mathbf{\Lambda}$.

$$\mathbf{\Gamma}=\mathbf{e}_{sig}^{H}\ \hat{\mathbf{R}}_{yy}\mathbf{E}_{noise}$$

$$=\mathbf{e}_{sig}^{H}\left(\hat{\mathbf{e}}_{sig}\hat{\Lambda}\,\hat{\mathbf{e}}_{sig}^{H}+\hat{\mathbf{E}}_{noise}\,\hat{\Sigma}\,\hat{\mathbf{E}}_{noise}^{H}\right)\mathbf{E}_{noise}$$

$$=\left(\mathbf{e}_{sig}^{H}\hat{\mathbf{e}}_{sig}\right)\hat{\Lambda}\left(\hat{\mathbf{e}}_{sig}^{H}\mathbf{E}_{noise}\right)+\left(\mathbf{e}_{sig}^{H}\hat{\mathbf{E}}_{noise}\right)\hat{\Sigma}\left(\hat{\mathbf{E}}_{noise}^{H}\mathbf{E}_{noise}\right)$$

$$\simeq\hat{\Lambda}\left(\hat{\mathbf{e}}_{sig}^{H}\mathbf{E}_{noise}\right)+\sigma^{2}\mathbf{I}\left(\mathbf{e}_{sig}^{H}\hat{\mathbf{E}}_{noise}\right)\left(\hat{\mathbf{E}}_{noise}^{H}\mathbf{E}_{noise}\right) \tag{4.27}$$

and $\left(\mathbf{e}_{sig}^{H}\hat{\mathbf{E}}_{noise}\right)\left(\hat{\mathbf{E}}_{noise}^{H}\mathbf{E}_{noise}\right)=\mathbf{e}_{sig}^{H}\left(\hat{\mathbf{E}}_{noise}\hat{\mathbf{E}}_{noise}^{H}\right)\mathbf{E}_{noise}$

$$=\mathbf{e}_{sig}^{H}\left(\mathbf{I}-\hat{\mathbf{e}}_{sig}\hat{\mathbf{e}}_{sig}^{H}\right)\mathbf{E}_{noise}$$

$$=\mathbf{e}_{sig}^{H}\mathbf{I}\,\mathbf{E}_{noise}-\left(\mathbf{e}_{sig}^{H}\hat{\mathbf{e}}_{sig}\right)\left(\hat{\mathbf{e}}_{sig}^{H}\mathbf{E}_{noise}\right)$$

$$\simeq-\left(\hat{\mathbf{e}}_{sig}^{H}\mathbf{E}_{noise}\right). \tag{4.28}$$

By substituting Eqn.(4.28) in Eqn.(4.27), we get the following

$$\mathbf{\Gamma}\simeq\hat{\Lambda}\left(\hat{\mathbf{e}}_{sig}^{H}\mathbf{E}_{noise}\right)-\sigma^{2}\mathbf{I}\left(\hat{\mathbf{e}}_{sig}^{H}\mathbf{E}_{noise}\right)$$

$$\simeq\left(\hat{\Lambda}-\sigma^{2}\mathbf{I}\right)\left(\hat{\mathbf{e}}_{sig}^{H}\mathbf{E}_{noise}\right). \tag{4.29}$$

According to Eqn. (4.28), $\hat{\mathbf{E}}_{noise}^{H}\mathbf{E}_{noise}$ can be considered as a fixed matrix. Therefore, $\mathbf{e}_{sig}^{H}\hat{\mathbf{E}}_{noise}$ has the same asymptotic distribution as $-\hat{\mathbf{e}}_{sig}^{H}\mathbf{E}_{noise}\mathbf{Q}$, where $\mathbf{Q}$ is

some fixed unitary matrix (from Eqn. (4.25). We conclude that $\mathbf{e}_{sig}^H \hat{\mathbf{E}}_{noise}$ and $-\hat{\mathbf{e}}_{sig}^H \mathbf{E}_{noise}$ have the same asymptotic distribution. Therefore, $\mathbf{e}_{sig}\left(\mathbf{e}_{sig}^H \hat{\mathbf{e}}_{noise,i}\right)$ and $-\mathbf{e}_{sig}\left(\hat{\mathbf{e}}_{sig}^H \mathbf{e}_{noise,i}\right)$ have also the same limiting distribution. Thus, the limiting distribution of $-\mathbf{e}_{sig}\left(\hat{\mathbf{e}}_{sig}^H \mathbf{e}_{noise,i}\right)$ is the same as that of $-\mathbf{e}_{sig}\left(\left(\Lambda-\sigma^2\mathbf{I}\right)^{-1}\mathbf{\Gamma}_i\right)$, where $\mathbf{\Gamma}_i$ is the column of $\mathbf{\Gamma}$.

Let $g(n) \triangleq \mathbf{e}_{sig}^H \mathbf{y}(n)$, $\mathbf{h}(n) \triangleq \mathbf{E}_{noise}^H \mathbf{y}(n) = \mathbf{E}_{noise}^H \mathbf{w}(n)$, where $\mathbf{y}(n) = \mathbf{y}_S(n)$ or $\mathbf{y}_L(n)$ and $\mathbf{w}(n) = \mathbf{w}_S(n)$ or $\mathbf{w}_L(n)$. In the following, we prove that the asymptotic distribution of the elements of $\hat{\mathbf{E}}_{noise}^H \mathbf{E}_{noise}$ and $\hat{\mathbf{e}}_{sig}^H \mathbf{E}_{noise}$ are independent.

$$
\begin{aligned}
E\left\{g(n)\mathbf{h}^H(m)\right\} &= \mathbf{e}_{sig}^H E\left\{\mathbf{y}(n)\mathbf{y}^H(m)\right\}\mathbf{E}_{noise} \\
&= \sigma^2 \mathbf{e}_{sig}^H \mathbf{E}_{noise}\,\delta_{n,m} \\
&= 0 \qquad\qquad \text{for all } n,m,
\end{aligned}
$$

$$
\begin{aligned}
E\left\{\mathbf{h}(n)\mathbf{h}^H(m)\right\} &= \mathbf{E}_{noise}^H E\left\{\mathbf{w}(n)\mathbf{w}^H(m)\right\}\mathbf{E}_{noise} \\
&= \sigma^2 \mathbf{I}\,\delta_{n,m},
\end{aligned}
$$

$$
\begin{aligned}
E\left\{\mathbf{h}(n)\mathbf{h}^T(m)\right\} &= \mathbf{E}_{noise}^H E\left\{\mathbf{w}(n)\mathbf{w}^T(m)\right\}\mathbf{E}_{noise}^* \\
&= 0 \qquad\qquad \text{for all } n,m,
\end{aligned}
$$

$$
\begin{aligned}
E\left\{g(n)\mathbf{h}^T(m)\right\} &= \mathbf{e}_{sig}^H E\left\{\mathbf{y}(n)\mathbf{w}^T(m)\right\}\mathbf{E}_{noise}^* \\
&= 0 \qquad\qquad \text{for all } n,m.
\end{aligned}
$$

Hence, we use $g(n)$ and $\mathbf{h}(n)$ into the expression of $\mathbf{\Delta}$ and $\mathbf{\Gamma}$ as follows:

$$
\begin{aligned}
\mathbf{\Delta} &= \mathbf{E}_{noise}^H \hat{\mathbf{R}}_{yy}\mathbf{E}_{noise} - \sigma^2\mathbf{I} \\
&= \frac{1}{N}\mathbf{E}_{noise}^H \sum_{n=0}^{N-1}\mathbf{y}(n)\mathbf{y}^H(n)\mathbf{E}_{noise} - \sigma^2\mathbf{I}
\end{aligned}
$$

$$=\frac{1}{N}\sum_{n=0}^{N-1}\mathbf{E}_{noise}^{H}\mathbf{y}(n)\mathbf{y}^{H}(n)\mathbf{E}_{noise}-\sigma^{2}\mathbf{I}$$

$$\mathbf{\Delta}_{i,j}=\frac{1}{N}\sum_{n=0}^{N-1}h_{i}(n)h_{j}^{H}(n)-\sigma^{2}\mathbf{I}\delta_{i.j} \tag{4.30}$$

where $h_i(n)$ is the ith element of $\mathbf{h}(n)$.Similarly,

$$\mathbf{\Gamma}=\mathbf{e}_{sig}^{H}\hat{\mathbf{R}}_{yy}\mathbf{E}_{noise}$$

$$=\frac{1}{N}\mathbf{e}_{sig}^{H}\sum_{n=0}^{N-1}\mathbf{y}(n)\mathbf{y}^{H}(n)\mathbf{E}_{noise}$$

$$\mathbf{\Gamma}_{p}=\frac{1}{N}\sum_{n=0}^{N-1}g(n)\mathbf{h}_{p}^{H}(n)\ . \tag{4.31}$$

Therefore, $E\{\mathbf{\Delta}_{i,j}\}=0$ for $i\neq j$ and $E\{\mathbf{\Gamma}_{p}\}=0$.

In a four complex jointly Gaussian random variables case, $\{x_1, x_2, x_3, x_4\}$ of which at least one of them is zero mean, the fourth order moment can be obtained as

$E\{x_1\ x_2\ x_3\ x_4\}=E\{x_1\ x_2\}E\{x_3\ x_4\}+E\{x_1\ x_3\}E\{x_2\ x_4\}+E\{x_1\ x_4\}E\{x_2\ x_3\}$.

Thus, by using the above expression, the following can be easily obtained

$$E\{\mathbf{\Delta}_{i,j}\mathbf{\Gamma}_{p}^{H}\}=\frac{1}{N^{2}}\sum_{n=0}^{N-1}\sum_{m=0}^{N-1}E\{(h_{i}(n)h_{j}^{H}(n)-\sigma^{2}\delta_{i,j})(g^{H}(m)h_{p}(m))\}$$

$$=0 \tag{4.32}$$

$$E\{\mathbf{\Delta}_{i,j}\mathbf{\Gamma}_{p}\}=\frac{1}{N^{2}}\sum_{n=0}^{N-1}\sum_{m=0}^{N-1}E\{(h_{i}(n)h_{j}^{H}(n)-\sigma^{2}\delta_{i,j})(g(m)h_{p}^{H}(m))\}$$

$$=0 \tag{4.33}$$

Hence, $\mathbf{\Delta}_{i,j}$ and $\mathbf{\Gamma}_{p}$ are statistically independent random variables.

Now, the covariance of the asymptotic distribution of $\mathbf{\Gamma}$ is derived as follows:

$$\lim_{N\to\infty}E\{\mathbf{\Gamma}_{i}\ \mathbf{\Gamma}_{j}^{H}\}=\lim_{N\to\infty}\frac{1}{N^{2}}\sum_{n=0}^{N-1}\sum_{m=0}^{N-1}E\{(g(n)h_{i}^{H}(n))\ (h_{j}(m)g^{H}(m))\}$$

$$= \lim_{N\to\infty} \frac{1}{N^2} \sum_{n=0}^{N-1} \sum_{m=0}^{N-1} E\left\{ g(n) g^H(m) \right\} E\left\{ h_i^H(n) h_j(m) \right\}$$

$$= \lim_{N\to\infty} \frac{1}{N^2} \sum_{n=0}^{N-1} \sum_{m=0}^{N-1} E\left\{ g(n) g^H(m) \right\} \sigma^2 \delta_{n,m} \delta_{i,j}$$

$$= \sigma^2 \lim_{N\to\infty} \frac{1}{N} \sum_{n=0}^{N-1} \mathbf{e}_{sig}^H E\left\{ \mathbf{y}(n) \mathbf{y}^H(n) \right\} \mathbf{e}_{sig} \delta_{i,j}$$

$$= \sigma^2 \lim_{N\to\infty} \frac{1}{N^2} \sum_{n=0}^{N-1} \mathbf{e}_{sig}^H \left\{ \mathbf{a}(\varepsilon) x(n) x^H(n) \mathbf{a}^H(\varepsilon) + \sigma^2 \right\} \mathbf{e}_{sig} \delta_{i,j}$$

$$= \sigma^2 \lim_{N\to\infty} \frac{1}{N^2} \sum_{n=0}^{N-1} \mathbf{e}_{sig}^H \left\{ \mathbf{a}(\varepsilon) x(n) x^H(n) \mathbf{a}^H(\varepsilon) \right\} \mathbf{e}_{sig} \delta_{i,j}$$

$$= \frac{\sigma^2}{N} \lambda_1 \delta_{i,j} \tag{4.34}$$

$$\lim_{N\to\infty} E\left\{ \mathbf{\Gamma}_i \mathbf{\Gamma}_j^T \right\} = \lim_{N\to\infty} \frac{1}{N^2} \sum_{n=0}^{N-1} \sum_{m=0}^{N-1} E\left\{ \left(g(n) h_i^H(n) \right) \left(h_j^*(m) g^T(m) \right) \right\}$$

$$= 0 . \tag{4.35}$$

The difference between Eqn. (4.23) and Eqn. (4.34) is $\left(\sigma^2 - \lambda_1\right)^{-2} \mathbf{e}_{sig} \mathbf{e}_{sig}^H$. Since this term does not relate with E, $\left(\mathbf{e}_{sig} \mathbf{e}_{sig}^H \hat{\mathbf{e}}_{noise,i}\right)$ and $-\mathbf{e}_{sig} \left(\lambda_1 - \sigma^2\right)^{-1} \mathbf{\Gamma}_i$ have the same asymptotic distribution. Eqn. (4.23) and Eqn. (4.24) now follow from Eqn. (4.34) and Eqn. (4.35). These complete the proof of the lemma.

Now we can state and prove a first order performance analysis on the MUSIC method for CFO estimation by evaluating the mean and variance of the CFO estimation error.

Theorem 4.1: The MUSIC estimation error $\left(\hat{\varepsilon} - \varepsilon\right)$ for the CFO in the OFDM based WLAN is asymptotically jointly Gaussian distributed with zero means and variance given by

$$E\left\{\left(\hat{\varepsilon}-\varepsilon\right)^2\right\} \triangleq \frac{\sigma^2 \lambda_1}{2N\left(\sigma^2-\lambda_1\right)^2} \frac{\mathbf{a}^H(\varepsilon)\left[\mathbf{e}_{sig}\mathbf{e}_{sig}^H\right]\mathbf{a}(\varepsilon)}{\mathbf{d}^H(\varepsilon)\,\mathbf{E}_{noise}\mathbf{E}_{noise}^H\,\mathbf{d}(\varepsilon)} \tag{4.36}$$

where $\mathbf{d}(\varepsilon) \triangleq \dfrac{d\,\mathbf{a}(\varepsilon)}{d\varepsilon}$.

Proof: Since $\hat{\varepsilon}$ is a minimum point of $P(\varepsilon) = \mathbf{a}^H(\varepsilon)\hat{\mathbf{E}}_{noise}\hat{\mathbf{E}}_{noise}^H\mathbf{a}(\varepsilon)$, we must have $\left.\dfrac{d\,P(\varepsilon)}{d\varepsilon}\right|_{\varepsilon=\hat{\varepsilon}} = 0$. Therefore

$$\begin{aligned}
P'(\hat{\varepsilon}) &= \left.\frac{d\,P(\varepsilon)}{d\varepsilon}\right|_{\varepsilon=\hat{\varepsilon}} \\
&= \frac{d}{d\varepsilon}\left[\mathbf{a}^H(\varepsilon)\hat{\mathbf{E}}_{noise}\hat{\mathbf{E}}_{noise}^H\mathbf{a}(\varepsilon)\right]\Big|_{\varepsilon=\hat{\varepsilon}} \\
&= \mathbf{d}^H(\hat{\varepsilon})\hat{\mathbf{E}}_{noise}\hat{\mathbf{E}}_{noise}^H\mathbf{a}(\hat{\varepsilon}) + \mathbf{a}^H(\hat{\varepsilon})\hat{\mathbf{E}}_{noise}\hat{\mathbf{E}}_{noise}^H\mathbf{d}(\hat{\varepsilon}) \\
&= 2\,\mathrm{Re}\left[\mathbf{a}^H(\hat{\varepsilon})\hat{\mathbf{E}}_{noise}\hat{\mathbf{E}}_{noise}^H\mathbf{d}(\hat{\varepsilon})\right]
\end{aligned}$$

and we also have

$$\begin{aligned}
P''(\hat{\varepsilon}) &= \frac{d^2P(\varepsilon)}{d\varepsilon^2} \\
&= \mathbf{d}^H(\hat{\varepsilon})\hat{\mathbf{E}}_{noise}\hat{\mathbf{E}}_{noise}^H\mathbf{a}(\hat{\varepsilon}) + \mathbf{a}^H(\hat{\varepsilon})\hat{\mathbf{E}}_{noise}\hat{\mathbf{E}}_{noise}^H\mathbf{d}(\hat{\varepsilon}) \\
&= \frac{d}{d\varepsilon}\left(\frac{d\,\mathbf{a}(\varepsilon)}{d\varepsilon}\right)\hat{\mathbf{E}}_{noise}\hat{\mathbf{E}}_{noise}^H\mathbf{a}(\varepsilon) + \mathbf{d}^H(\varepsilon)\hat{\mathbf{E}}_{noise}\hat{\mathbf{E}}_{noise}^H\mathbf{d}(\varepsilon) + \\
&\quad \mathbf{d}^H(\varepsilon)\hat{\mathbf{E}}_{noise}\hat{\mathbf{E}}_{noise}^H\mathbf{d}(\varepsilon) + \mathbf{a}^H(\varepsilon)\hat{\mathbf{E}}_{noise}\hat{\mathbf{E}}_{noise}^H\frac{d}{d\varepsilon}\left(\frac{d\,\mathbf{a}(\varepsilon)}{d\varepsilon}\right) \\
&= 2\,\mathrm{Re}\left[\mathbf{a}^H(\varepsilon)\hat{\mathbf{E}}_{noise}\hat{\mathbf{E}}_{noise}^H\frac{d}{d\varepsilon}\left(\frac{d\,\mathbf{a}(\varepsilon)}{d\varepsilon}\right) + \mathbf{d}^H(\varepsilon)\hat{\mathbf{E}}_{noise}\hat{\mathbf{E}}_{noise}^H\mathbf{d}(\varepsilon)\right].
\end{aligned}$$

with $P'(\hat{\varepsilon}) = 0$, we can write

$$0 = P'(\hat{\varepsilon}) \approx P'(\varepsilon) + P''(\varepsilon)\left(\hat{\varepsilon}-\varepsilon\right)$$

$$2\,\mathrm{Re}\left[\mathbf{a}^H(\varepsilon)\hat{\mathbf{E}}_{noise}\hat{\mathbf{E}}_{noise}^H\mathbf{d}(\varepsilon)\right]+2\,\mathrm{Re}\left[\mathbf{a}^H(\varepsilon)\hat{\mathbf{E}}_{noise}\hat{\mathbf{E}}_{noise}^H\frac{d}{d\varepsilon}\left(\frac{d\,\mathbf{a}(\varepsilon)}{d\varepsilon}\right)+\mathbf{d}^H(\varepsilon)\hat{\mathbf{E}}_{noise}\hat{\mathbf{E}}_{noise}^H\mathbf{d}(\varepsilon)\right]=0$$

$$2\,\mathrm{Re}\left[\mathbf{a}^H(\varepsilon)\hat{\mathbf{E}}_{noise}\hat{\mathbf{E}}_{noise}^H\mathbf{d}(\varepsilon)\right]+2\left[\mathbf{d}^H(\varepsilon)\hat{\mathbf{E}}_{noise}\hat{\mathbf{E}}_{noise}^H\mathbf{d}(\varepsilon)\right](\hat{\varepsilon}-\varepsilon)\simeq 0$$

$$(\hat{\varepsilon}-\varepsilon)=-\frac{\mathrm{Re}\left[\mathbf{a}^H(\varepsilon)\hat{\mathbf{E}}_{noise}\hat{\mathbf{E}}_{noise}^H\mathbf{d}(\varepsilon)\right]}{\left[\mathbf{d}^H(\varepsilon)\hat{\mathbf{E}}_{noise}\hat{\mathbf{E}}_{noise}^H\mathbf{d}(\varepsilon)\right]} \tag{4.37}$$

where the terms, $2\,\mathrm{Re}\left[\mathbf{a}^H(\varepsilon)\hat{\mathbf{E}}_{noise}\hat{\mathbf{E}}_{noise}^H\frac{d}{d\varepsilon}\left(\frac{d\,\mathbf{a}(\varepsilon)}{d\varepsilon}\right)\right](\hat{\varepsilon}-\varepsilon)$, neglected in the approximations because this term tend to zero faster than the retained terms. But, we have,

$$\begin{aligned}\mathbf{a}^H\hat{\mathbf{E}}_{noise}\hat{\mathbf{E}}_{noise}^H &= \mathbf{a}^H\mathbf{e}_{sig}\mathbf{e}_{sig}^H\hat{\mathbf{E}}_{noise}\hat{\mathbf{E}}_{noise}^H\mathbf{E}_{noise}\mathbf{E}_{noise}^H\\ &= \mathbf{a}^H\mathbf{e}_{sig}\mathbf{e}_{sig}^H\left(\mathbf{I}-\hat{\mathbf{e}}_{sig}\hat{\mathbf{e}}_{sig}^H\right)\mathbf{E}_{noise}\mathbf{E}_{noise}^H\\ &= -\mathbf{a}^H\mathbf{e}_{sig}\left(\mathbf{e}_{sig}^H\hat{\mathbf{e}}_{sig}\right)\left(\hat{\mathbf{e}}_{sig}^H\mathbf{E}_{noise}\right)\mathbf{E}_{noise}^H\\ &\simeq -\mathbf{a}^H\mathbf{e}_{sig}\left(\hat{\mathbf{e}}_{sig}^H\mathbf{E}_{noise}\right)\mathbf{E}_{noise}^H\,.\end{aligned}$$

We have shown earlier that $-\hat{\mathbf{e}}_{sig}^H\mathbf{E}_{noise}$ is asymptotically equivalent to $\mathbf{e}_{sig}^H\hat{\mathbf{E}}_{noise}$ (see Eqn. (4.28)).

Therefore,

$$\begin{aligned}\mathbf{a}^H(\varepsilon)\hat{\mathbf{E}}_{noise}\hat{\mathbf{E}}_{noise}^H\mathbf{d}(\varepsilon) &= -\mathbf{a}^H(\varepsilon)\mathbf{e}_{sig}\left(\hat{\mathbf{e}}_{sig}^H\mathbf{E}_{noise}\right)\mathbf{E}_{noise}^H\mathbf{d}(\varepsilon)\\ &= \mathbf{a}^H(\varepsilon)\mathbf{e}_{sig}\left(\mathbf{e}_{sig}^H\hat{\mathbf{E}}_{noise}\right)\mathbf{E}_{noise}^H\mathbf{d}(\varepsilon)\end{aligned}$$

and from Eqn.(4.21), we get

$$\mathbf{a}^H(\varepsilon)\hat{\mathbf{E}}_{noise}\hat{\mathbf{E}}_{noise}^H\mathbf{d}(\varepsilon) = \mathbf{a}^H(\varepsilon)\left[\mathbf{e}_{sig}\mathbf{e}_{sig}^H\hat{\mathbf{e}}_{noise,1} \quad \dots \quad \mathbf{e}_{sig}\mathbf{e}_{sig}^H\hat{\mathbf{e}}_{noise,(M-1)}\right]\begin{bmatrix}\mathbf{e}_{noise,1}^H\mathbf{d}(\varepsilon)\\ \cdot\\ \cdot\\ \cdot\\ \mathbf{e}_{noise,(M-1)}^H\mathbf{d}(\varepsilon)\end{bmatrix}$$

$$= \sum_{k=1}^{M-1}\left[\mathbf{e}_{noise,k}^H\mathbf{d}(\varepsilon)\right]\left[\mathbf{a}^H(\varepsilon)\mathbf{e}_{sig}\mathbf{e}_{sig}^H\hat{\mathbf{e}}_{noise,k}\right]. \tag{4.38}$$

By substituting Eqn. (4.38) into Eqn. (4.37), we have

$$\left(\hat{\varepsilon}-\varepsilon\right) = -\frac{\mathrm{Re}\left[\sum_{k=1}^{M-1}\left[\mathbf{e}_{noise,k}^H\mathbf{d}(\varepsilon)\right]\left[\mathbf{a}^H(\varepsilon)\mathbf{e}_{sig}\mathbf{e}_{sig}^H\hat{\mathbf{e}}_{noise,k}\right]\right]}{\mathbf{d}^H(\varepsilon)\hat{\mathbf{E}}_{noise}\hat{\mathbf{E}}_{noise}^H\mathbf{d}(\varepsilon)}. \tag{4.39}$$

To derive the variance of the CFO estimation error $\left(\hat{\varepsilon}-\varepsilon\right)$, let $u = \sum_{k=1}^{M-1}\left[\mathbf{e}_{noise,k}^H\mathbf{d}(\varepsilon)\right]\left[\mathbf{a}^H(\varepsilon)\mathbf{e}_{sig}\mathbf{e}_{sig}^H\hat{\mathbf{e}}_{noise,k}\right]$ and we note that for two scalar-valued complex variables, u and v, we have

$$\mathrm{Re}\left(u\right)\mathrm{Re}\left(v\right) = \frac{1}{2}\left[\mathrm{Re}\left(uv\right)+\mathrm{Re}\left(uv^H\right)\right]. \tag{4.40}$$

Thus,

$$\begin{aligned} E\left\{u\,u^H\right\} = &\sum_{k=1}^{M-1}\sum_{l=1}^{M-1}\left[\mathbf{e}_{noise,k}^H\mathbf{d}(\varepsilon)\right]\left[\mathbf{d}^H(\varepsilon)\mathbf{e}_{noise,l}\right] \\ &\mathbf{a}^H(\varepsilon)\ E\left\{\left(\mathbf{e}_{sig}\mathbf{e}_{sig}^H\hat{\mathbf{e}}_{noise,k}\right)\left(\mathbf{e}_{sig}\mathbf{e}_{sig}^H\hat{\mathbf{e}}_{noise,l}\right)^H\right\}\mathbf{a}(\varepsilon). \end{aligned} \tag{4.41}$$

By invoking Lemma 4.1, $E\left\{\left(\mathbf{e}_{sig}\mathbf{e}_{sig}^H\hat{\mathbf{e}}_{noise,k}\right)\left(\mathbf{e}_{sig}\mathbf{e}_{sig}^H\hat{\mathbf{e}}_{noise,k}\right)^H\right\} = \frac{1}{N}U$, Eqn. (4.41) becomes

$$E\left\{u\,u^H\right\} = \frac{1}{N}\sum_{k=1}^{M-1}\left[\mathbf{d}^H(\varepsilon)\mathbf{e}_{noise,k}\mathbf{e}_{noise,k}^H\mathbf{d}(\varepsilon)\right]\mathbf{a}^H(\varepsilon)U\,\mathbf{a}(\varepsilon)$$

$$= \frac{1}{N}\left(\mathbf{d}^H(\varepsilon)\mathbf{E}_{noise}\mathbf{E}_{noise}^H\mathbf{d}(\varepsilon)\right)\left(\mathbf{a}^H(\varepsilon)U\,\mathbf{a}(\varepsilon)\right). \tag{4.42}$$

But

$$E\left\{u\,u^T\right\} = \sum_{k=1}^{M-1}\sum_{k=1}^{M-1}\left[\mathbf{e}_{noise,k}^H \mathbf{d}(\varepsilon)\right]\left[\mathbf{d}^H(\varepsilon)\mathbf{e}_{noise,k}\right]$$

$$\mathbf{a}^H(\varepsilon)\; E\left\{\left(\mathbf{e}_{sig}\mathbf{e}_{sig}^H\hat{\mathbf{e}}_{noise,k}\right)\left(\mathbf{e}_{sig}\mathbf{e}_{sig}^H\hat{\mathbf{e}}_{noise,k}\right)^T\right\}\mathbf{a}^T(\varepsilon)$$

$$= 0\,. \tag{4.43}$$

Therefore, this completes the proof of the Theorem. It can be seen from Eqn. (4.36) the CFO variance takes a large value when λ_1 is close to σ^2. This case arises only at the low SNR scenario.

4.4 Conclusion

In this chapter, the signal model of the preamble section in OFDM based WLAN is derived as the signal model of the DOA estimation in the uniform linear array signal processing. Thus, the advantage of deriving this signal model is that the DOA estimation algorithms in the uniform linear array signal processing can be applied directly to the CFO estimation of OFDM based WLAN. Moreover, we also apply one of the DOA estimations, which is based on subspace method, to estimate the CFO in the OFDM based WLAN over frequency selective fading channel. In addition, we derive a first order perturbation analysis of the proposed method for the CFO estimation in the OFDM based WLAN. In the next Chapter, we validate the performance of the proposed MUSIC algorithm by extensive computer simulations.

CHAPTER 5

COMPUTER EXPERIMENTS AND DISCUSSIONS

The objectives of this chapter are two-fold. Firstly, as we have shown in the Chapter 4 the signal model of an OFDM based WLAN is identical to a uniform linear array signal model, here we present a maximum entropy method for CFO estimation. Secondly, we present results of our extensive computer simulations in order to validate the MUSIC CFO estimation method and the maximum entropy estimator.

5.1 Maximum Entropy Application for the CFO Estimation in OFDM based WLAN

In Chapter 4, we have shown that the signal model of the preamble section of the OFDM based WLAN can be modeled in accordance to the widely used uniform linear array DOA estimation, and we showed how to apply the MUSIC method, one of the subspace based DOA algorithms, successfully to the CFO problem in OFDM based WLAN. In Chapter 2, we have reviewed that maximum entropy, which is originally developed by Burg [55], and show how it can be applied to estimate the DOA of an

uniform linear array signal processing. Similarly, maximum entropy method has been suggested by numerous authors as a good objective measure for optimally modeling the power spectrum of a wide-sense stationary random process. In this chapter, we show here how maximum entropy method can be applied directly to the CFO estimation in OFDM based WLAN.

The main idea of maximum entropy method for DOA or CFO estimation is to determine a filter vector, **w**, that can be applied to the vector at the output of linear array sensors or the received data vector of the short and long training symbols. Using this idea the mth element of the array sensor is estimated in a least square sense by a linear combination of the other sensor elements,

$$\underset{\mathbf{w}}{MINIMISE}\left\{\mathbf{w}^H \hat{\mathbf{R}}_{yy} \mathbf{w}\right\} \text{ subject to a constraint } \mathbf{w}^H \mathbf{l}_m = 1$$

where $\mathbf{l}_m$ is a real vector consisting of all zeros except a 1 for the mth element, and $\hat{\mathbf{R}}_{yy}$ is the estimated covariance matrix of the received OFDM symbol. The optimum weight becomes as

$$\mathbf{w}_{ME} = \frac{\hat{\mathbf{R}}_{yy}^{-1} \mathbf{l}_m}{\mathbf{l}_m^H \hat{\mathbf{R}}_{yy}^{-1} \mathbf{l}_m} \tag{5.1}$$

and the minimum power is given by

$$\sigma_{ME}^2 = \frac{1}{\mathbf{l}_m^H \hat{\mathbf{R}}_{yy}^{-1} \mathbf{l}_m} \tag{5.2}$$

If we consider the smoothing error as

$$\begin{aligned} \psi_m(n) &= y_m(n) - \hat{y}_m(n) \\ &= y_m(n) + \sum_{\substack{i=0 \\ i \neq m}}^{M-1} w_i^* y_i(n) \end{aligned} \tag{5.3}$$

Eqn. (5.3) reseambles an Auto Regressive (AR) process generated by an all pole filter excited by a white noise. Therefore, the maximum entropy power spectral estimate of the output of the array sensor at $m = 0$ is given as

$$P_{ME}(\omega) = \frac{\left(\mathbf{l}_0^H \ \hat{\mathbf{R}}_{yy}^{-1} \ \mathbf{l}_0\right)^{-1}}{\left|1 + \sum_{k=1}^{M} w_k \exp(-j\omega k)\right|^2}. \tag{5.4}$$

Since $\mathbf{a}(\varepsilon)$ is defined in Eqns. (4.9) and (4.13) as the steering vector, we can write the maximum entropy power spectrum as

$$P_{ME}(\hat{\varepsilon}) = \frac{\left(\mathbf{l}_0^H \ \hat{\mathbf{R}}_{yy}^{-1} \ \mathbf{l}_0\right)^{-1}}{\left|\mathbf{w}_{ME}^H \ \mathbf{a}(\hat{\varepsilon})\right|^2}. \tag{5.5}$$

The steps in estimating the CFO using the above maximum entropy method are as follows:

(1) Estimate the covariance matrix $\hat{\mathbf{R}}_{y_i y_i}$ form the received short and long training symbols, where $i = S$ or L, with S and L representing the short and long training symbols, respectively.

(2) Take the inverse of the estimated covariance matrix $\hat{\mathbf{R}}_{y_i y_i}$ to obtain $\hat{\mathbf{R}}_{y_i y_i}^{-1}$.

(3) Construct a real $M_i \times 1$ vector consisting of all zeros except a 1 for the first element, $\mathbf{l}_0 = [1, \ 0, \ ..., \ 0]^T$.

(4) Construct the optimum weight vector, $\mathbf{w}_{ME}$, according to Eqn. (5.1).

(5) After estimating and constructing all necessary matrix and vectors, we can find the highest peak of the maximum entropy power spectrum by varying the frequency range from $-\frac{1}{2N_s} \le \varepsilon \le \frac{1}{2N_s}$ as

$$P_{ME}\left(\hat{\varepsilon}\right)=\frac{\left(\mathbf{l}_0^H\ \hat{\mathbf{R}}_{yy}^{-1}\ \mathbf{l}_0\right)^{-1}}{\left|\mathbf{w}_{ME}^H\ \mathbf{a}\left(\hat{\varepsilon}\right)\right|^2}.$$

5.2 Computer Experiments - MUSIC based CFO Estimation

In this section, computer simulations are conducted to compare and analyze the performance of the MUSIC method proposed in Section 4.2 for the CFO estimation of OFDM based WLAN under frequency selective fading channel. In each simulation example, we use minimum mean square error (MMSE) of CFO estimation as the performance measure defined as follows:

$$MMSE \triangleq \frac{1}{M}\sum_{m=1}^{M}\left|\varepsilon-\hat{\varepsilon}(m)\right|^2 \tag{5.6}$$

We arbitrarily use 1000 independent Monte Carlo runs for each SNR. (SNR is defined by the ratio of the average energy per sample to the variance of the additive white Gaussian noise.) we use the same SNR range in NLS method [40].

The simulation platform is as follows:

(a) Using the IEEE standard 802.11a preamble section [5], which contains 10 identical short training symbols and 2 identical long training symbols, we generate the short and long training symbols as follows:

Short OFDM training symbols are generated by using the following sequence $S_{S(-26,26)}$

$$S_{S(-26,26)}=\sqrt{\frac{13}{6}}\begin{Bmatrix}0,\ 0,\ 1+j,\ 0,\ 0,\ 0,\ -1-j,\ 0,\ 0,\ 0,\ 1+j,\ 0,\ 0,\ 0,\ -1-j,\\ 0,\ 0,\ 0,\ -1-j,\ 0,\ 0,\ 0,\ 1+j,\ 0,\ 0,\ 0,\ 0,\ 0,\ 0,\ 0,\ -1-j,\\ 0,0,\ 0,\ -1-j,\ 0,\ 0,\ 0,\ 1+j,\ 0,\ 0,\ 0,\ 1+j,\ 0,\ 0,\ 0,\ 1+j,\\ 0,\ 0,\ 0,1+j,\ 0,\ 0,\end{Bmatrix}. \tag{5.7}$$

The multiplication by a factor of $\sqrt{\frac{13}{6}}$ is in order to normalize the average power of the resulting OFDM symbols, which utilizes 12 out of 52 subcarriers. For a 64 point IFFT, the coefficients 1 to 26 are mapped to the same numbered IFFT inputs, while the coefficients -26 to -1 are mapped into IFFT inputs numbered 38 to 63. The rest of the inputs 27 to 37 and the 0 input are set to zero. The arrangement of the sequence to perform IFFT is shown in Figure 5.1.

Sequence arrangement S'_S	0	$S_{S(1)}$ ~ $S_{S(26)}$	0	$S_{S,(-26)}$ ~ $S_{S(-1)}$
IFFT input	0	1~26	27~37	39~63

Figure 5.1 Sequence arrangement for the IFFT input.

The OFDM signal is generated by taking the IFFT function in Matlab as follows:

$$x_S(n) = \text{IFFT}\left(S'_S\right). \tag{5.8}$$

Because of S'_S and the arrangement to perform IFFT, there are 4 identical portions in $x_S(n)$. Therefore, in one IFFT period, we obtain four identical short training symbols. After taking IFFT, the output of the IFFT is cyclically extended to obtain 10 identical short training symbols.

The following sequence is used for the long training symbols

$$S_{L(-26,26)} = \left\{ \begin{matrix} 1,\ 1,\ -1,\ -1,\ 1,\ 1,\ -1,\ 1,\ -1,\ 1,\ 1,\ 1,\ 1,\ 1,\ 1, \\ -1,\ -1,\ 1,\ 1,\ -1,\ 1,\ -1,\ 1,\ 1,\ 1,\ 1,\ 0,\ 1,\ -1, \\ -1,\ 1,\ 1,\ -1,\ 1,\ -1,\ 1,\ -1,\ -1,\ -1,\ -1,\ -1,\ 1, \\ 1,\ -1,\ -1,\ 1,\ -1,\ 1,\ -1,\ 1,\ 1,\ 1,\ 1 \end{matrix} \right\}. \tag{5.9}$$

The steps of arranging the sequence and performing IFFT for the long training symbols are the same with the steps for the short training symbols.

After generating the one long training symbol, this symbol is cyclically extended to obtain the 2 long training symbols and the Guard Interval (GI), which is the copy of the last 32 samples of the long training symbol.

Finally, the preamble section is formed by concatenating the section of ten short training symbols and the two long training symbols with GI as the following Figure 5.2.

10 identical short training symbols	GI	2 identical long training symbols

Figure 5.2 Preamble section of the OFDM based WLAN.

(b) Since we compare the performance of the proposed method with that of the NLS method [40], we also used $h = \left[\exp(j1.38) \quad 0.5\exp(j0.3) \quad 0.3\exp(-j2.2)\right]$ channel impulse function from [40]. Channel remains invariant during the reception of one packet, which is true as the packet receiving time is short due to high bit rate but is independent from one packet to another. In Matlab, we define the channel transfer function at the frequency of kth subcarrier as follows:

$$H_k = \sum_{l=0}^{L_c-1} h(l)\ \exp\left(-j\frac{2\pi}{N}kl\right) \tag{5.10}$$

At the receiver, the OFDM preamble section without CFO is formed as

$$\mathbf{x} = \left[\mathbf{x}'_S;\ \mathbf{x}'_S;\ \mathbf{x}'_S(1:32);\ \mathbf{x}'_L(33:64);\ \mathbf{x}'_L;\ \mathbf{x}'_L\right] \tag{5.11}$$

where $\mathbf{x}'_S = diag\left[H_0 \quad H_1 \quad \ldots \quad H_{N-1}\right] * \mathbf{x}_S$

$$\mathbf{x}'_L = diag\left[H_0 \quad H_1 \quad \ldots \quad H_{N-1}\right] * \mathbf{x}_L$$

$$\mathbf{x}_S = \left[x_S(0) \quad x_S(1) \quad \ldots \quad x_S(N-1)\right]^T$$

$$\mathbf{x}_L = \left[x_L(0) \quad x_L(1) \quad \ldots \quad x_L(N-1) \right]^T .$$

After that, the OFDM preamble section, which has CFO, with noise is formed in Matlab as

$$\mathbf{x}_{CFO} = \mathbf{x} * \exp\left(j * 2\pi * \varepsilon * length(\mathbf{x}) \right) + \mathbf{w} \tag{5.12}$$

ε is the CFO, and $\mathbf{w}$ is vector of the zero mean complex envelope of AWGN with variance σ^2.

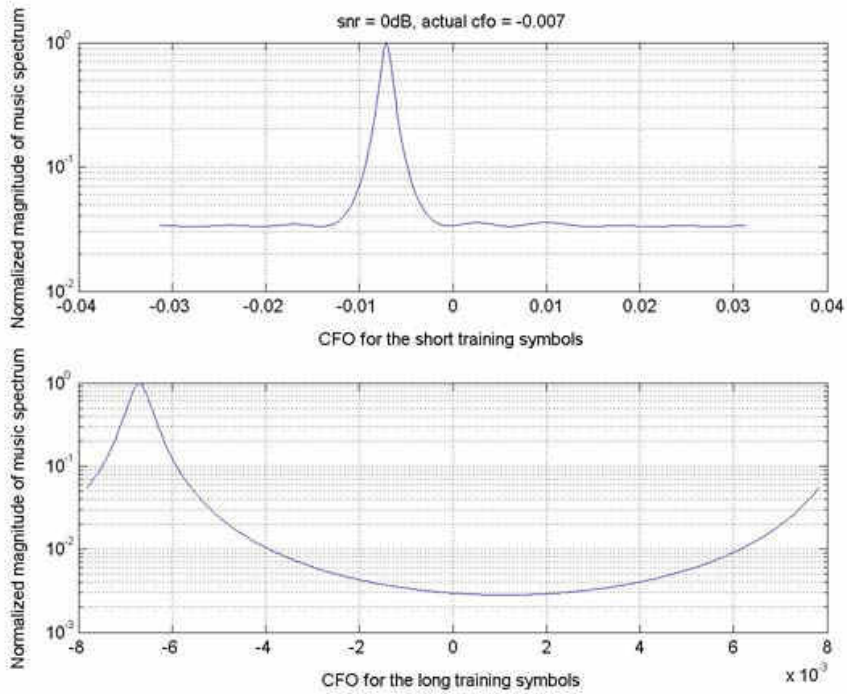

Figure 5.3(a) The MUSIC spectrum vs CFO for the short and long training symbols at the actual CFO = -0.007

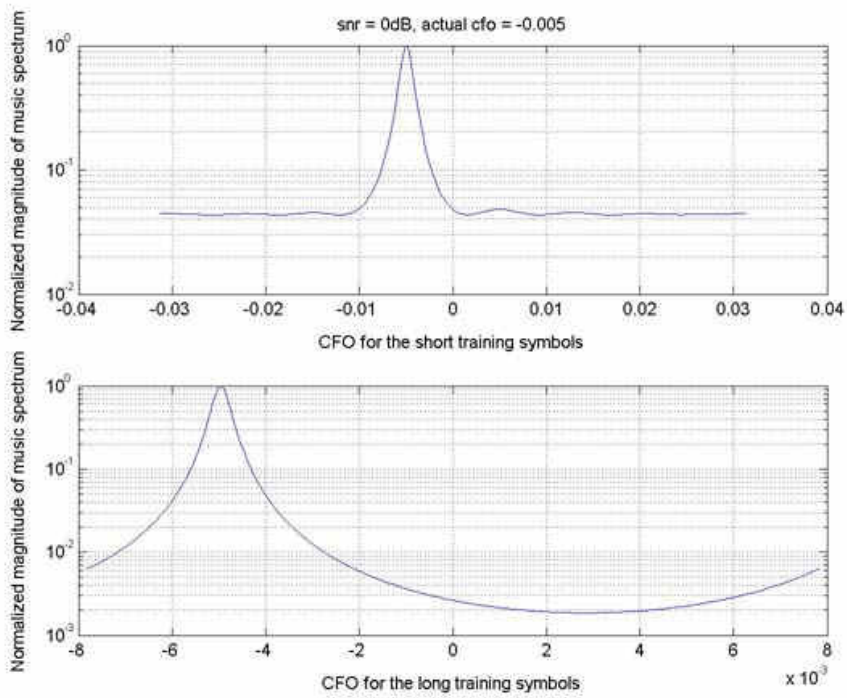

Figure 5.3(b) The MUSIC spectrum vs CFO for the short and long training symbols at the actual CFO = -0.005

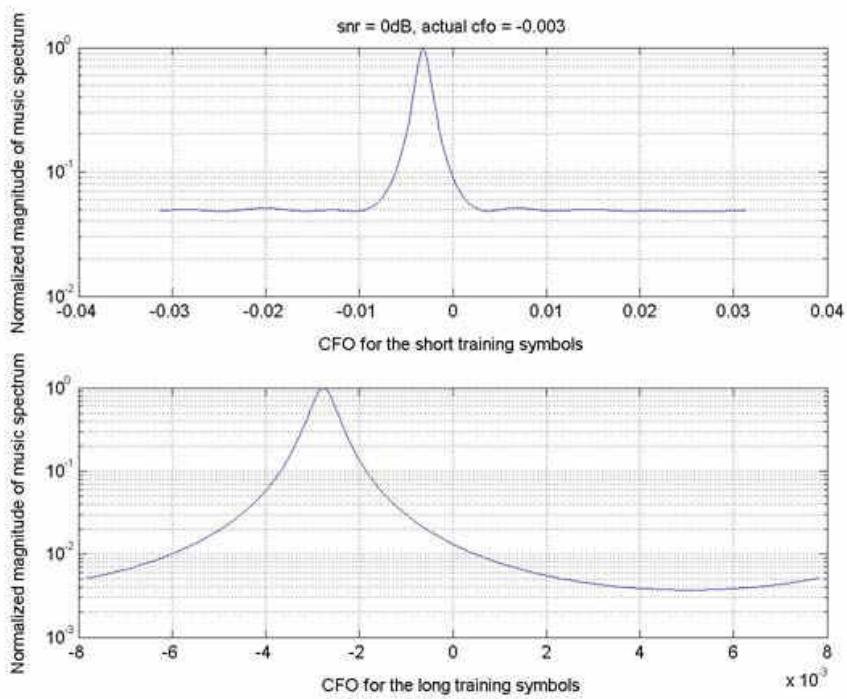

Figure 5.3(c) The MUSIC spectrum vs CFO for the short and long training symbols at the actual CFO = -0.003

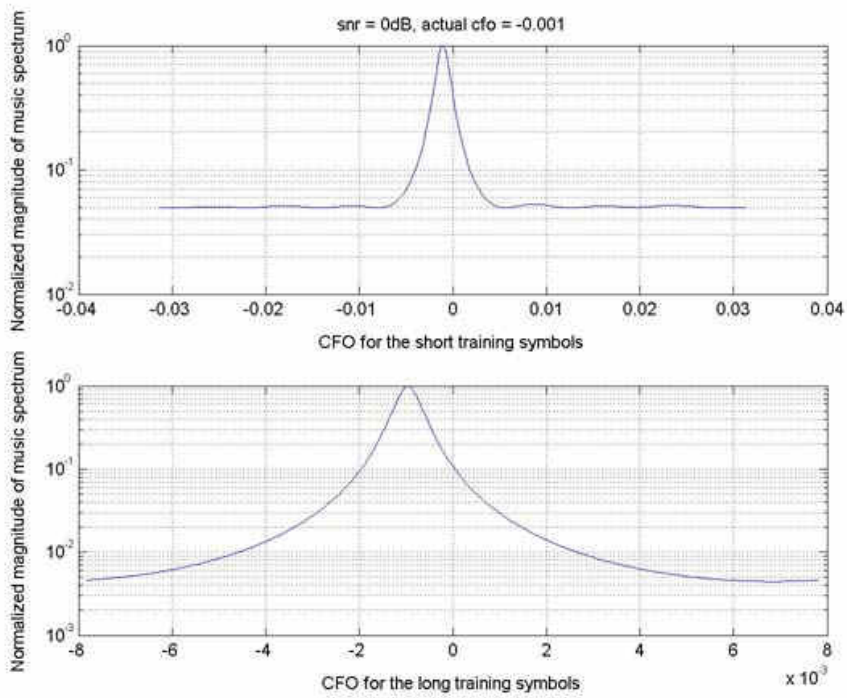

Figure 5.3(d) The MUSIC spectrum vs CFO for the short and long training symbols at the actual CFO = -0.001

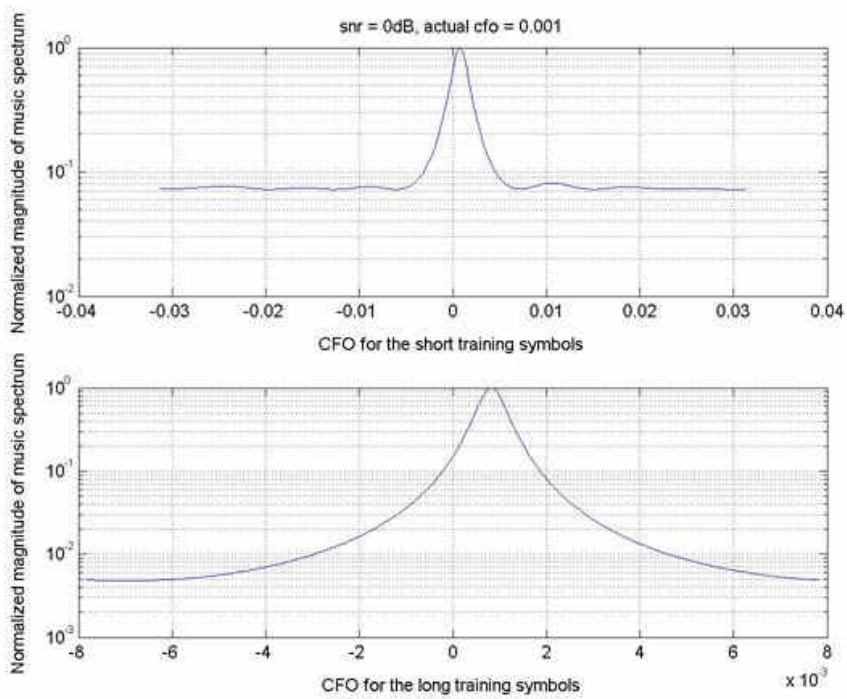

Figure 5.3(e) The MUSIC spectrum vs CFO for the short and long training symbols at the actual CFO = 0.001

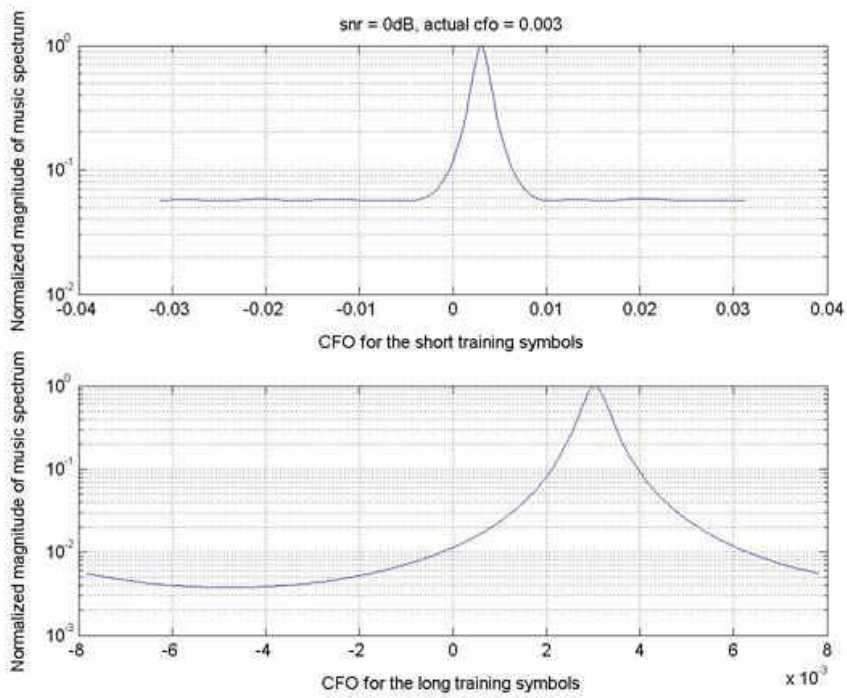

Figure 5.3(f) The MUSIC spectrum vs CFO for the short and long training symbols at the actual CFO = 0.003

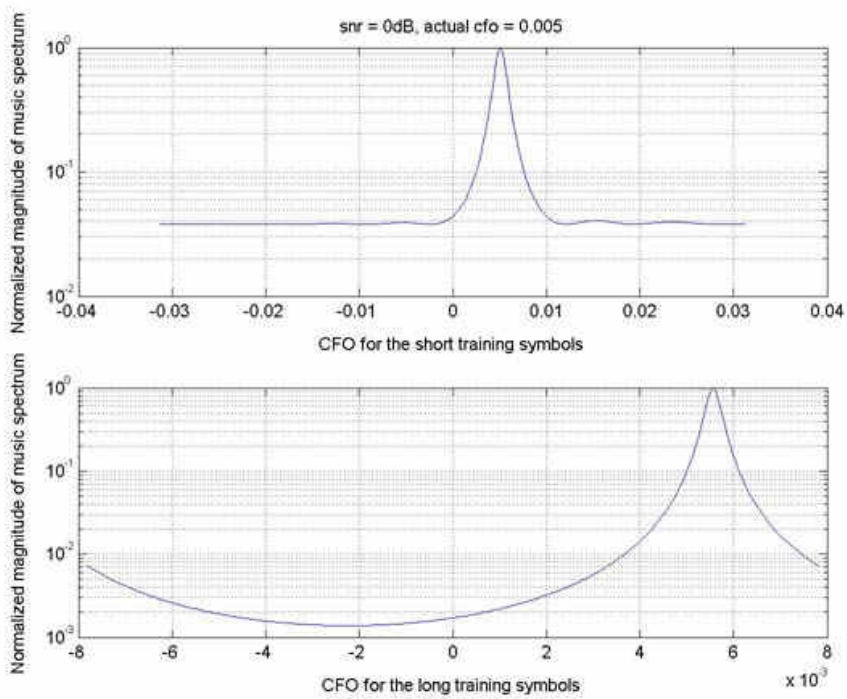

Figure 5.3(g) The MUSIC spectrum vs CFO for the short and long training symbols at the actual CFO = 0.005

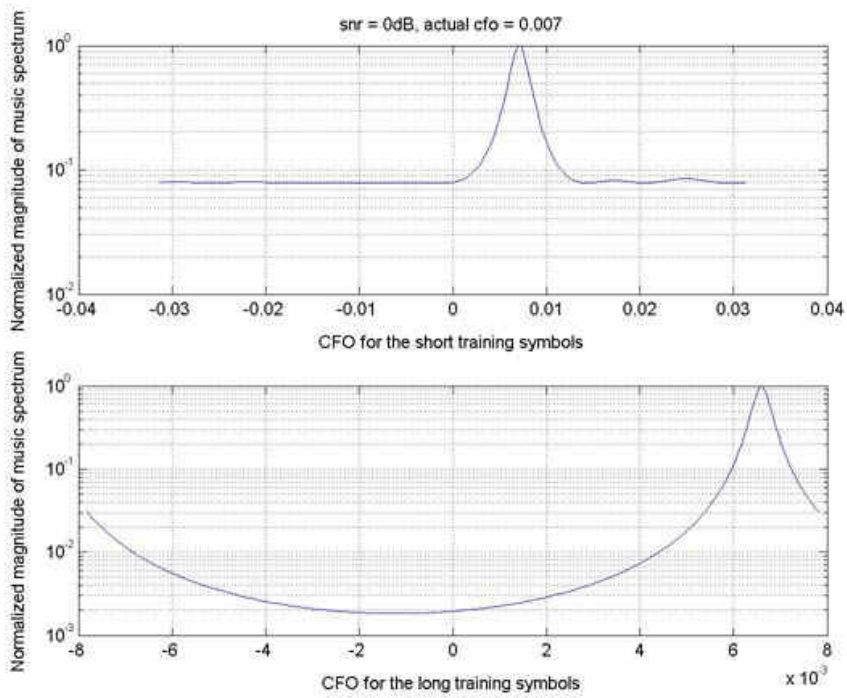

Figure 5.3(h) The MUSIC spectrum vs CFO for the short and long training symbols at the actual CFO = 0.007

Figure 5.3 shows the MUSIC spectrum for the short and long training symbols. These spectra are generated at SNR 0dB. These figures show the CFO for the respective training symbols vs normalized magnitude value of the MUSIC spectrum (dB) under frequency selective fading channel. The CFO range for the short training symbols varies from $-1/2N_S$ to $1/2N_S$ and the CFO range for the long training symbols varies form $-1/2N_L$ to $1/2N_L$ in each figure. To see the resolutions of the MUSIC spectrum clearly, we run the simulation for different actual CFO value from -0.007 to 0.007 with an increment step of 0.002. The result for each CFO is shown in Figures 5.3 (a) to (h). From these Figures, we can see that the highest peak of the spectrum is sharp and very close to the actual CFO value.

Table 5.1 (a) Mean, variance and standard deviation of CFO estimation errors of the MUSIC method at SNR = -10dB.

short training symbols

actual CFO	error mean $\times 10^{+3}$	error variance $\times 10^{+5}$	error standard deviation $\times 10^{+3}$
-0.007	5.4025	6.9892	8.3601
-0.006	3.5821	6.5175	8.0731
-0.004	2.1582	6.8665	8.2864
-0.002	1.9321	5.5469	7.4477
-0.001	1.8173	5.3512	7.3152
0.001	1.9795	6.0115	7.7534
0.002	1.8557	5.7087	7.5556
0.004	2.1787	5.1843	7.2002
0.006	3.6891	6.7286	8.2028
0.007	5.459	6.909	8.312

long training symbols

actual CFO	error mean $\times 10^{+3}$	error variance $\times 10^{+5}$	error standard deviation $\times 10^{+3}$
-0.007	3.4731	6.2259	7.8904
-0.006	3.5402	3.2806	5.7277
-0.004	3.594	1.0722	3.2744
-0.002	3.237	0.7287	2.6995
-0.001	3.1815	0.6149	2.4798
0.001	3.6119	0.7164	2.6766
0.002	3.3538	0.6648	2.5783
0.004	3.1812	1.119	3.3451
0.006	3.555	3.4507	5.8743
0.007	3.6423	6.1768	7.8593

Table 5.1(b) Mean, variance and standard deviation of CFO estimation errors of the MUSIC method at SNR = -3dB.

short training symbols

actual CFO	error mean $\times 10^{+4}$	error variance $\times 10^{+7}$	error standard deviation $\times 10^{+4}$
-0.007	2.7092	1.1231	3.3512
-0.006	2.7239	1.1312	3.3633
-0.004	2.6678	1.1042	3.323
-0.002	2.7024	1.1466	3.3861
-0.001	2.7161	1.2364	3.5162
0.001	2.643	1.1601	3.4061
0.002	2.6503	1.1224	3.3502
0.004	2.6948	1.1236	3.352
0.006	2.6799	1.1086	3.3296
0.007	2.6349	1.0565	3.2503

long training symbols

actual CFO	error mean $\times 10^{+4}$	error variance $\times 10^{+7}$	error standard deviation $\times 10^{+4}$
-0.007	13.7794	149.2041	38.6269
-0.006	4.5415	3.2551	5.7053
-0.004	4.5874	3.3838	5.817
-0.002	4.5798	3.3311	5.7716
-0.001	4.4284	3.1821	5.641
0.001	4.3291	2.9402	5.4224
0.002	4.3804	3.0562	5.5283
0.004	4.5975	3.3196	5.7616
0.006	4.8284	6.9373	8.329
0.007	13.8883	152.7569	39.0841

Table 5.1(c) Mean, variance and standard deviation of CFO estimation errors of the MUSIC method at SNR = 0dB.

short training symbols

actual CFO	error mean $\times 10^{+4}$	error variance $\times 10^{+8}$	error standard deviation $\times 10^{+4}$
-0.007	1.8841	5.2734	2.2964
-0.006	1.9375	5.4528	2.3351
-0.004	1.9112	5.3736	2.3181
-0.002	1.8239	5.2693	2.2955
-0.001	1.805	5.6152	2.3696
0.001	1.7199	5.1767	2.2752
0.002	1.7956	5.2111	2.2828
0.004	1.9604	5.5544	2.3568
0.006	1.9496	5.3586	2.3149
0.007	1.8741	5.1496	2.2693

long training symbols

actual CFO	error mean $\times 10^{+4}$	error variance $\times 10^{+8}$	error standard deviation $\times 10^{+4}$
-0.007	4.1759	226.556	15.0518
-0.006	2.8359	12.606	3.5505
-0.004	2.7813	11.9487	3.4567
-0.002	2.8231	12.4865	3.5336
-0.001	2.7366	11.7859	3.4331
0.001	2.7702	12.1862	3.4909
0.002	2.7619	11.967	3.4593
0.004	2.8487	12.6614	3.5583
0.006	2.7049	11.4382	3.382
0.007	4.6915	292.6783	17.1078

Table 5.1(d) Mean, variance and standard deviation of CFO estimation errors of the MUSIC method at SNR = 3dB.

short training symbols

actual CFO	error mean $\times 10^{+4}$	error variance $\times 10^{+8}$	error standard deviation $\times 10^{+4}$
-0.007	1.4374	2.812	1.6769
-0.006	1.4626	2.7649	1.6628
-0.004	1.4679	2.8566	1.6902
-0.002	1.316	2.843	1.6861
-0.001	1.2519	2.9705	1.7235
0.001	1.2096	2.8008	1.6736
0.002	1.2766	2.6486	1.6275
0.004	1.4883	2.9577	1.7198
0.006	1.4801	2.835	1.6838
0.007	1.4181	2.7081	1.6456

long training symbols

actual CFO	error mean $\times 10^{+4}$	error variance $\times 10^{+8}$	error standard deviation $\times 10^{+4}$
-0.007	1.9019	26.5849	5.1561
-0.006	1.7444	4.772	2.1845
-0.004	1.7689	5.0166	2.2398
-0.002	1.8223	5.3624	2.3157
-0.001	1.7428	4.8098	2.1931
0.001	1.7791	4.9334	2.2211
0.002	1.7842	5.0225	2.2411
0.004	1.783	4.9308	2.2205
0.006	1.7406	4.7787	2.186
0.007	1.9356	26.9513	5.1915

Table 5.1(e) Mean, variance and standard deviation of CFO estimation errors of the MUSIC method at SNR = 8dB.

short training symbols

actual cfo	error mean $\times 10^{+4}$	error variance $\times 10^{+8}$	error standard deviation $\times 10^{+4}$
-0.007	1.0931	1.3981	1.1824
-0.006	1.2117	1.5622	1.2499
-0.004	1.1402	1.4012	1.1837
-0.002	0.7798	1.0227	1.0113
-0.001	0.5866	0.9561	0.9778
0.001	0.5545	0.8811	0.9386
0.002	0.7919	1.052	1.0257
0.004	1.1789	1.5003	1.2249
0.006	1.203	1.5016	1.2254
0.007	1.0723	1.3316	1.154

long training symbols

actual cfo	error mean $\times 10^{+4}$	error variance $\times 10^{+8}$	error standard deviation $\times 10^{+4}$
-0.007	0.9407	1.3904	1.1791
-0.006	0.9428	1.3503	1.162
-0.004	0.9398	1.3554	1.1642
-0.002	0.9535	1.4486	1.2036
-0.001	0.9408	1.4209	1.192
0.001	0.9602	1.4191	1.1913
0.002	0.9861	1.5021	1.2256
0.004	0.9396	1.405	1.1853
0.006	0.9081	1.2996	1.14
0.007	0.9503	1.413	1.1887

Tables 5.1 (a) to (e) present the mean, variance, and standard deviation of the MUSIC CFO estimation error of the short and long training symbols for different SNR values. These values are calculated as follows:

$$\Delta\varepsilon(m) = \varepsilon - \hat{\varepsilon}(m) \tag{5.13}$$

$$\mu_{MUSIC} \triangleq \frac{1}{M}\sum_{m=1}^{M}\left|\triangle\varepsilon(m)\right| \tag{5.14}$$

$$\sigma_{MUSIC}^{2} \triangleq \frac{1}{M}\sum_{m=1}^{M}\left|\triangle\varepsilon(m)\right|^{2} \tag{5.15}$$

$$\sigma_{MUSIC} \triangleq \sqrt{\sigma_{MUSIC}^{2}} = \sqrt{\frac{1}{M}\sum_{m=1}^{M}\left|\triangle\varepsilon(m)\right|^{2}} \tag{5.16}$$

where $\triangle\varepsilon(m)$ is the error of the estimated CFO at m^{th} run, ε is the actual CFO value, μ_{MUSIC} is the mean of the MUSIC estimator error, σ_{MUSIC}^{2} is the variance of the MUSIC estimator error, and σ_{MUSIC} is the standard deviation of the MUSIC estimator error. Table 5.1(a) refers to SNR -10dB, Table 5.1(b) refers to SNR -3dB, Table 5.1(c) refers to SNR 0dB, Table 5.1(d) refers to SNR 3dB, and Table 5.1(e) refers to SNR 8dB. To estimate these values, we use actual CFO values from -0.007 to 0.007 range and arbitrarily use 1000 runs for each SNR. From these tables, we can see that the mean, variance and standard deviation of the error are consistent with the SNR value. That is, mean, variance and standard deviation of the error gradually decrease as the SNR value is monotonically increased.

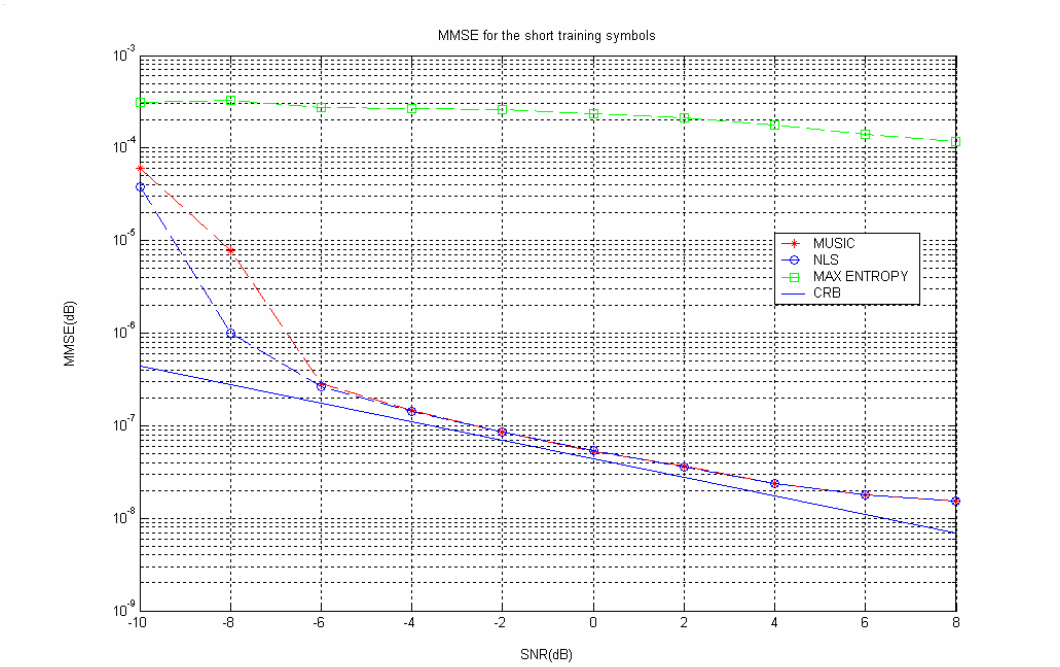

Figure 5.4 (a) MMSE(dB) vs SNR(dB) of the short training symbols for the frequency selective fading channel.

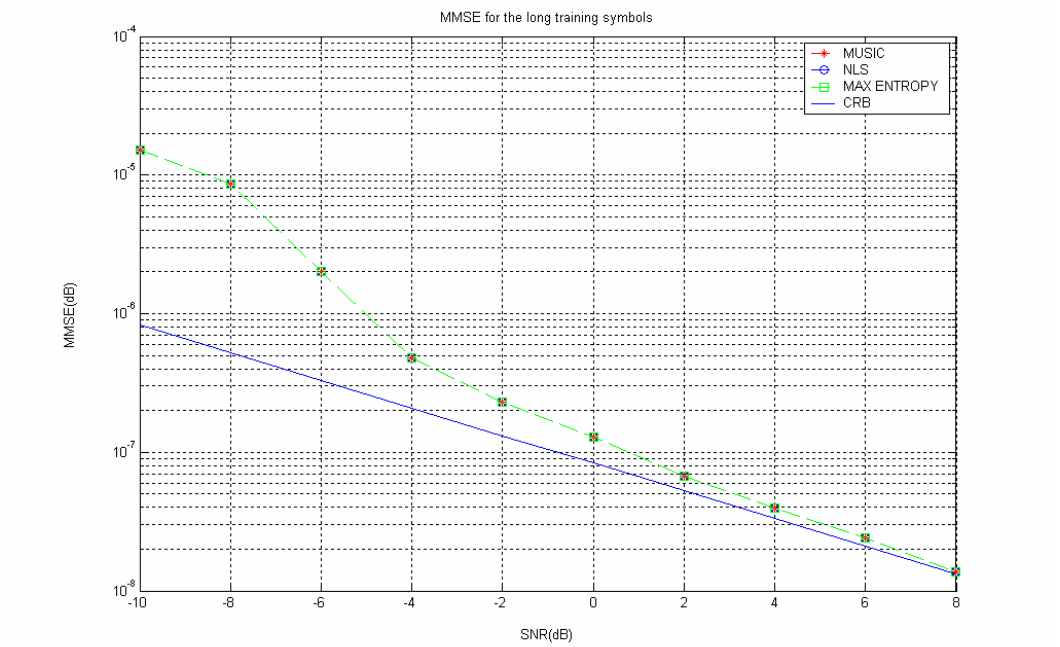

Figure 5.4 (b) MMSE(dB) vs SNR(dB) of the long training symbols for the frequency selective fading channel.

Figure 5.4(a) presents the MMSE of the CFO estimation for the 9 short training symbols under frequency selective fading channel with respect to the SNR. SNR was varied from -10 to 8 dB. The MMSE performance of the NLS method [40], MUSIC algorithm, and maximum entropy method are compared against the CRB. From this figure, it is clear that the performance of the MUSIC method is better than that of the maximum entropy method over the whole SNR range. Naidu [64] also discusses the effect of maximum entropy in DOA estimation. He concludes that the effect of finite data will result in (i) a loss in resolution, (ii) a shift in the position of peaks, an erroneous estimate of the direction of arrival (DOA). Thus, in our CFO estimation of the OFDM based WLAN, maximum entropy spectrum, $\mathbf{P}_{ME}(\varepsilon)$, has a highest peak at an incorrect frequency value because of the inadequate number of samples, $N_S = 16$, in the short training symbols. When we compared the performance of the MUSIC method with that of NLS method, MUSIC method has almost identical performance with the NLS estimation method except between the SNR range -10dB to -6dB.

Figure 5.4(b), as another comparison, the MMSE of the proposed MUSIC method, maximum entropy method and the NLS method [40] are evaluated for long training symbols over the frequency selective fading channel. Since the number of samples, $N_L = 64$, in the long training symbols is large, maximum entropy spectrum has a high peak at a correct frequency value. Hence, the maximum entropy method has the same performance with the MUSIC method for the CFO estimation of the long training symbols. From this figure, it can be seen clearly that the MUSIC method and the maximum entropy method have similar performance with the NLS method for the fine CFO estimation in long training symbols. Thus, with these MMSE comparisons, we can see that the maximum entropy method is more variable and it needs much larger data to obtain accurate estimation results.

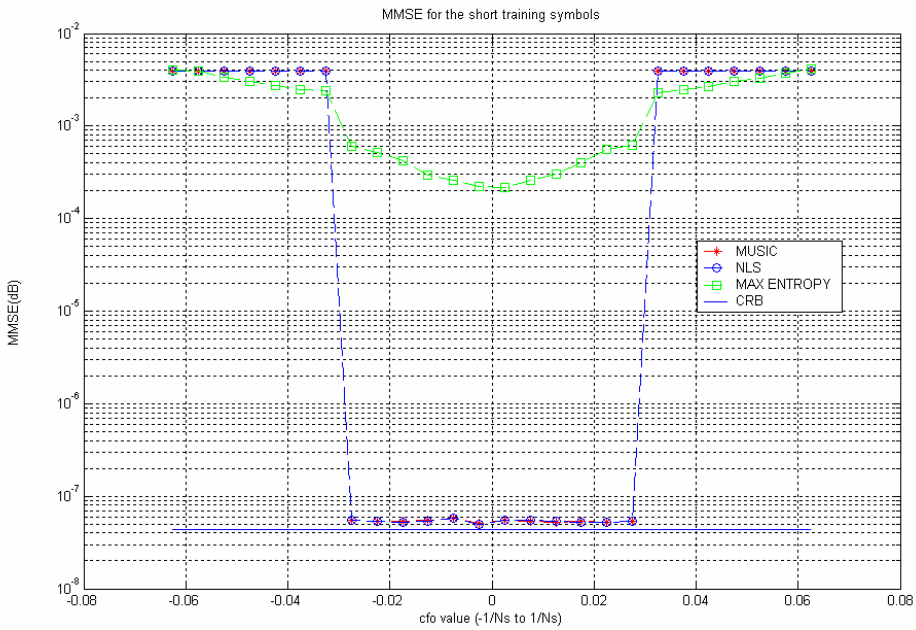

Figure 5.5 (a) CFO estimation range of the short training symbols at SNR = 0dB.

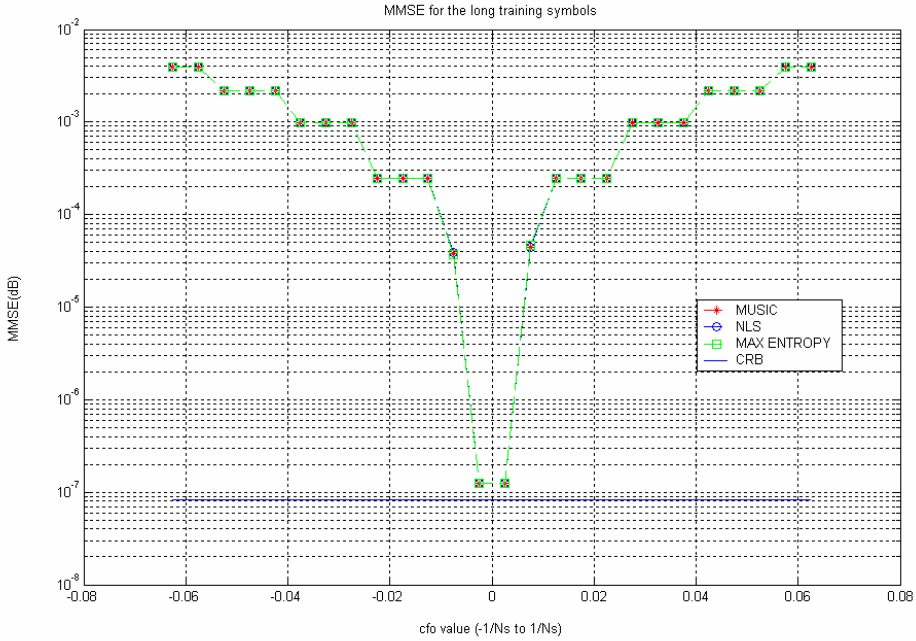

Figure 5.5 (b) CFO estimation range of the long training symbols at SNR = 0dB.

Figure 5.5(a) and Figure 5.5(b) show the MMSE resulting from CFO estimation by MUSIC method, maximum entropy method and the NLS method [40]. The SNR

value is set at 0dB. Figure 5.5(a) illustrates this for the short training symbols and Figure 5.5(b) demonstrates this for the long training symbols. These figures show that the CFO estimation ranges are the same for these methods with both short and long training symbols.

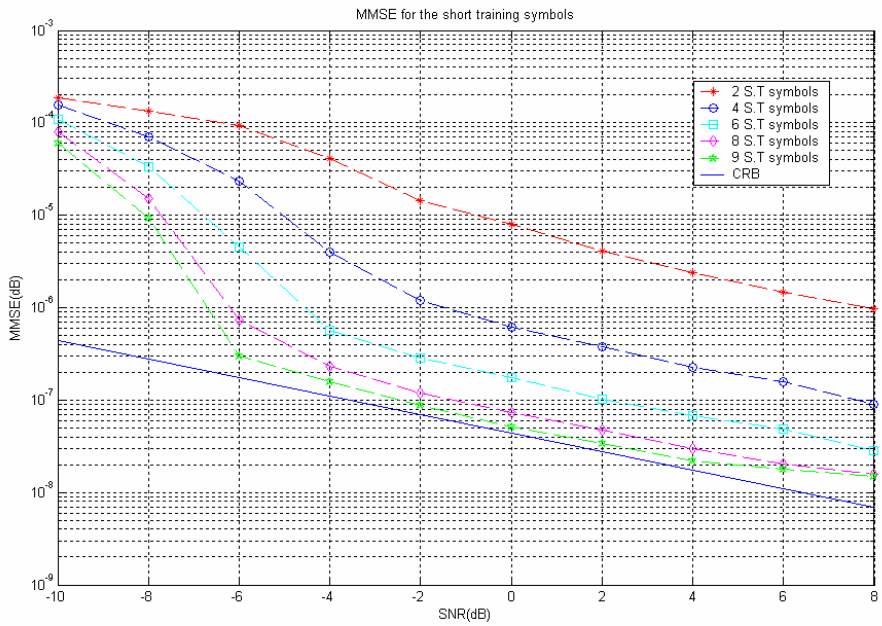

Figure 5.6 MMSE (dB) vs SNR (dB) for the MUSIC method with different number of short training symbols.

The performance of the MUSIC method is examined by varying the number of short training symbols. This result is shown in Figure 5.6, which illustrated the MMSE of the CFO estimation with respect to the SNR. For this case, the number of short training symbols is varied from 2 to 9. From the figure, it can be seen clearly that the performance of the proposed MUSIC method monotonically increases with increasing the number of short training symbols. This is because MUSIC method is based on the orthogonality between the signal and noise subspaces. For the short training symbols,

when all the short training symbols are not applied as the number of sensors, an estimated covariance matrix will have low quality because of the small sample sizes and small number of short training symbols. Thus, estimated noise subspace may be poorly aligned with the true noise subspace and MUSIC picks the spurious CFO value. In addition, from this figure, we can see clearly that the MMSE in individual MUSIC method has a large value at the low SNR although the number of short training symbols is increased as mentioned in the theoretical performance analysis.

5.3 Conclusion

In this chapter, we present a maximum entropy method for CFO estimation. Next, extensive computer simulations have been performed to validate the MUSIC CFO estimation method and the maximum entropy method. Firstly, we show the resolution of the MUSIC spectrum for the CFO estimation to see that the highest peak of the spectrum is sharp and very close to the actual CFO value. In addition, we also show that the consistency of the mean, variance and standard deviation of the CFO estimation error of the MUSIC method with different SNR values. Moreover, the MMSE results show that the performance of the MUSIC estimator is comparable with the performance of the NLS estimator even with small data size and low SNR. Finally, we also show that the MUSIC method, the maximum entropy method and the NLS method have the same CFO estimation range. From the simulation results, we observed that the maximum entropy method needs a larger number of data than the MUSIC method to obtain accurate estimation results although both methods have the same estimation range.

CHAPTER 6

CONCLUSIONS AND FUTURE WORK

6.1 Conclusions

In this thesis, the subspace methods for DOA estimation in the uniform linear array signal processing are adapted to estimate the CFO in OFDM systems. The accuracy of super resolution subspace methods has motivated this work. We propose and analyze the estimation methods for two types of OFDM systems:

(i) conventional OFDM systems, and

(ii) OFDM based WLAN system.

For the conventional OFDM systems, we propose a novel CFO estimation by using the matrix pencil method. The proposed matrix pencil method uses only one OFDM symbol while ESPRIT method, another subspace based method, uses about 10 OFDM symbols to obtain good performance. From our numerical studies, the performance of the matrix pencil method with one OFDM symbol significantly out performs the ESPRIT method with 10 OFDM symbols under frequency selective fading channel condition. We also discuss why the proposed matrix pencil method has better performance than ESPRIT method although both methods are subspace based

approaches. In addition, we improve the performance of the matrix pencil method by using oversampling. The proposed matrix pencil method approaches the Cramer-Rao bound except at low SNR.

For the OFDM based WLAN, we derive the signal model of the preamble section as the signal model of the DOA estimation in the uniform linear array signal processing. The advantage of deriving this signal model is that the DOA estimation algorithms in the uniform linear array signal processing can be applied directly to the CFO estimation of OFDM based WLAN. Thus, we proposed MUSIC method to estimate the CFO. We derive a first order perturbation analysis of the MUSIC method for the CFO estimation in the OFDM based WLAN.

We also present a maximum entropy method for CFO estimation. Moreover, the numerical investigation of the achievable performance of the MUSIC method, are also given by extensive simulation under frequency selective fading channel condition. All the results are compared with CRB. In addition, we also show that the consistency of the mean, variance and standard deviation of the CFO estimation error of the MUSIC method with different SNR values. MMSE results show that the performance of the MUSIC estimator is comparable with the performance of the NLS estimator even with small data size and low SNR. Finally, we also show that the MUSIC method, the maximum entropy method and the NLS method have the same CFO estimation range. From the simulation results, we observed that the maximum entropy method needs longer data than the MUSIC method to obtain accurate estimation results although both methods have the same estimation range.

In OFDM systems, the accuracy of the CFO estimation is an important issue. The proposed subspace based methods for both OFDM systems provide the accuracy of a super resolution approach and the advantage of computational simplicity.

6.2 Future Work

There are still several topics of research which should be studied before OFDM can be used in data transmission.

- The proposed subspace methods focus only on the problem of CFO estimation in OFDM systems and assume that the timing offset is completely eliminated. If the timing synchronization is not perfect or have not been estimated, timing offset also needs to be estimated and compensated. In this case, a two dimensional subspace method can be considered, one dimension for timing offset estimation and another for CFO estimation.
- In this research, we assume that we concentrate on the CFO due to the local oscillator instabilities and neglect Doppler Effect which arises from nonstationary movement of source/destination and obstacles between them. Therefore, research could be conducted to estimate the CFO which is caused by Doppler Effect.
- OFDM signal may exhibit a high instantaneous signal peak with respect to the average signal level. This may result in a high out of band harmonic distortion power unless the transmitter's amplifier operates in their extremely high linear region. Research could be conducted either to reduce the high peak to average power ratio or to improve the amplification stage of the transmitter.
- The presence of phase noise from the oscillators is also an important limiting factor for an OFDM system performance when the bandwidth of the phase noise is high compared to the OFDM subcarrier spacing. Therefore, the effect of phase noise on the OFDM signal should also be analyzed.

LIST OF PUBLICATIONS

1. K. K. Khaing, A. Rahim Leyman, Y. H. Chew, *"A Subspace-based Carrier Frequency Offset Estimation for OFDM based WLAN"* in preparation for submission to IEEE Communication Letters.
2. K. K. Khaing, A. Rahim Leyman, Y. H. Chew, *"A High Efficiency Subspace-based Estimator of Carrier Frequency Offset for OFDM system"* in preparation for submission to IEEE Trans. On Vehicular Technology

REFERENCES

[1] J. G. Proakis, *Digital Communications,* Fourth Edition, McGraw-Hill, 2001.

[2] M. C. D. Maddocks, I. R. Pullen, and J. A. Green, "Digital Audio Broadcasting, Measuring Techniques and Coverage Performance for a Medium Power VHF Single Frequency Network," *BBC R&D Report* BBC RD 1995/2.

[3] H. Sari, G. Karam, and I. Jeanclaude, "Transmission Techniques for Digital Terrestrial TV Broadcasting," *IEEE Commun. Mag*., vol. 33, no. 2, pp. 100-109, Feb. 1995.

[4] J. S. Chow, J. C. Tu, and J. M. Cioffi, "A Discrete Multitone Transceiver System for HDSL Applications," *IEEE Journal on Selected Areas in Communications*, vol. 9, pp. 895-908, Aug. 1991.

[5] Wireless LAN Medium Access Control (MAC) and Physical Layer (PHY) Specifications, IEEE Std. 802.11a, 1999.

[6] ETSI Technical Specification, "Broadband Radio Access Network; Hiperlan Type 2; Physical Layer," document code "ETSI 101 475 V1.1.1".

[7] R. V. Nee and R. Prasad, *OFDM for Wireless Multimedia Communications,* Boston: Artech House, 2000.

[8] S. Hara and R. Prasad, *Multicarrier Techniques for 4G Mobile Communications,* Boston, MA: Artech House, 2003.

[9] L. Hanzo, M. Munster, B. J. Choi, and T. Keller, *OFDM and MC-CDMA for Broadband Multi-user Communications, WLANs and Broadcasting,* Chichester; New York: John Wiley & Sons, 2003.

[10] L. Hanzo, W. Webb, and T. Keller, *Single- and Multi-carrier Quadrature Amplitude Modulation: Principles and Applications for Personal Communications, WLANs and Broadcasting,* Chichester, [England]; New York: John Wiley & Sons, 2000.

[11] A. R. S. Bahai and B. R. Saltzberg, *Multi-Carrier Digital Communications: Theory and Applications of OFDM,* New York: Kluwer Academic/ Plenum, 1999.

[12] H. Minn and V. K. Bhargava, "A Simple and Efficient Timing Offset Estimation for OFDM Systems," *in Proc. IEEE Veh. Technol. Conf.,* vol. 1, May, 2000, pp. 51-55.

[13] S. B. Weinstein and P. M. Ebert, "Data Transmission by Frequency Division Multiplexing using the Discrete Fourier Transform," *IEEE Trans. Commun.,* vol. 19, no. 5, pp. 628-634, Oct. 1971.

[14] T. S. Rappaport, *Wireless Communications Principles & Practice,* Upper Saddle River, N.J.: Prentice Hall, 1996.

[15] T. Pollet, M. V. Bladel, and M. Moeneclaey, "BER Sensitivity of OFDM Systems to Carrier Frequency Offset and Wiener Phase Noise," *IEEE Trans. Commun.*, vol. 43, no. 2/3/4, pp. 191-193, Feb./Mar./Apr. 1995.

[16] P. H. Moose, "A Technique for Orthogonal Frequency Division Multiplexing Frequency Offset Correction," *IEEE Trans. Commun.,* vol. 42, no. 10, pp. 2908-2914, Oct. 1994.

[17] T. M. Schmidl and D. C. Cox, "Robust Frequency and Timing Synchronization for OFDM," *IEEE Trans. Commun.,* vol. 45, no. 12, pp. 1613-1621, Dec. 1997.

[18] M. Morelli and U. Mengali, "An Improved Frequency Offset Estimator for OFDM Applications," *IEEE Commun. Lett.,* vol. 3, no. 3, pp. 75-77, Mar. 1999.

[19] Y. S. Lim and J. H. Lee, "An Efficient Carrier Frequency Offset Estimation Scheme for an OFDM System," *in Proc. IEEE Veh. Technol. Conf.,* vol. 5, Sept. 2000, pp. 2453-2457.

[20] Y. H. Kim, I. Song, S. Yoon, and S. R. Park, "An Efficient Frequency Offset Estimator for OFDM Systems and Its Performance Characteristics," *IEEE Trans. Veh. Technol.,* vol. 50, no. 5, pp. 1307-1308, Sept. 2001.

[21] B. S. Seo, S. C. Kim, and J. Park, "Fast Coarse Estimator of Carrier Frequency Offset for OFDM systems," *IEE Electron. Lett.,* vol. 38, no. 24, pp. 1520-1521, Nov. 2002.

[22] T. M. Schmidl and D. C. Cox, "Blind Synchronization for OFDM," *IEE Electron. Lett.,* vol. 33, no. 2, pp. 113-114, Jan. 1997.

[23] J. J. Van De Beek, M. Sandell, and P. O. Borjesson, "ML Estimation of Time and Frequency Offset in OFDM Systems," *IEEE Trans. Signal Processing,* vol. 45, no. 7, pp. 1800-1805, Jul. 1997.

[24] N. Lashkarian and S. Kiaei, "Globally Optimum ML Estimation of Timing and Frequency Offset in OFDM Systems," *in Proc. IEEE Int. Conf. Commun.,* vol. 2, Jun. 2000, pp. 1044-1048.

[25] Y. S. Choi, P. J. Voltz, and F. A. Cassara, "ML Estimation of Carrier Frequency Offset for Multicarrier Signals in Rayleigh Fading Channels," *IEEE Trans. Veh. Technol.,* vol. 50, no. 2, pp. 644-655, Mar. 2001.

[26] B. Chen and H. Wang, "Blind OFDM Carrier Frequency Offset Estimation via Oversampling," *in Proc. 35th Asilomar Conf. Signals, Syst., Comput.,* vol. 2, Nov. 2001, pp. 1465-1469.

[27] M. Ghogho, A. Swami, and G. B. Giannakis, "Optimized Null-Subcarrier Selection for CFO Estimation in OFDM over Frequency-Selective Fading Channels," *in Proc. GLOBECOM,* vol. 1, Nov. 2001, pp. 202- 206.

[28] M. Ghogho and A. Swami, "Semi-Blind Frequency Offset Synchronization for OFDM," *in Proc. IEEE Int. Conf. of Acoust., Speech, Signal Processing,* vol. 3, May, 2002, pp. 2333-2336.

[29] H. Bolcskei, "Blind Estimation of Symbol Timing and Carrier Frequency Offset in Wireless OFDM Systems," *IEEE Trans. Commun.,* vol. 49, no. 6, pp. 988-998, Jun. 2001.

[30] F. Gini and G. B. Giannakis, "Frequency Offset and Symbol Timing Recovery in Flat-Fading Channels: A Cyclostationary Approach," *IEEE Trans. Commun.,* vol. 46, no. 3, pp. 400-411, Mar. 1998.

[31] D. S. Han, J. H. Seo, and J. J. Kim, "Fast Carrier Frequency Offset Compensation in OFDM Systems," *IEEE Trans. Consumer Electronics,* vol. 47, no. 3, pp. 364-369, Aug. 2001.

[32] M. Luise, M. Marselli, and R. Reggiannini, "Low-Complexity Blind Carrier Frequency Recovery for OFDM Signals over Frequency-Selective Radio Channels," *IEEE Trans. Commun.,* vol. 50, no. 7, pp. 1182-1188, Jul. 2002.

[33] M. Oerder and H. Meyr, "Digital Filter and Square Timing Recovery," *IEEE Trans. Commun.,* vol. 36, no. 5, pp. 605-612, May, 1988.

[34] H. Liu and U. Tureli, "A High-Efficiency Carrier Estimator for OFDM Communications," *IEEE Commun. Lett.,* vol. 2, no. 4, pp. 104-106, Apr. 1998.

[35] B. Chen, "Maximum Likelihood Estimation of OFDM Carrier Frequency Offset," *IEEE Signal Processing Lett.,* vol. 9, no. 4, pp. 123-126, Apr. 2002.

[36] U. Tureli, H. Liu, and M. D. Zoltowski, "OFDM Blind Carrier Frequency Offset Estimation: ESPRIT," *IEEE Trans. Commun.,* vol. 48, no. 9, pp. 1459-1461, Sept. 2000.

[37] Bob O'Hara and Al Petrick, *The IEEE 802.11 Handbook: A Designer's Companion,* New York: Standards Information Network, IEEE Press, 1999.

[38] B. Y. Prasetyo, F. Said, and A. H. Aghvami, "Fast Burst Synchronization Technique for OFDM-WLAN systems," *in Proc. IEEE Commun.,* vol. 147, no. 5, Oct. 2000, pp. 292-298.

[39] C. J. You and J. H. Horng, "Optimum Frame and Frequency Synchronization for OFDM Systems," *in Proc. IEEE Int. Conf. Consumer Electronics,* Jun. 2001, pp. 226-227.

[40] J. Li, G. Liu, and G. B. Giannakis, "Carrier Frequency Offset Estimation for OFDM-based WLANs," *IEEE Signal Processing Lett.,* vol. 8, no. 3, pp. 80-82, Mar. 2001.

[41] S. Y. Liu and J. W. Chong, "A Study of Joint Tracking Algorithm of Carrier Frequency Offset and Sampling Clock Offset for OFDM based WLANs," *in Proc. IEEE Int. Conf. Commun., Circuits, and Syst.,* vol. 1, 29 Jun-1 Jul. 2002, pp. 109-113.

[42] C-S. Peng and K-A. Wen, "Synchronization for Carrier Frequency Offset in WLAN 802.11a System," *in Proc. IEEE 5th Int. Symposium on Wireless Personal Multimedia Communication,* vol. 3, Oct. 2002, pp. 1083-1087.

[43] A. Miaoudakis, A. Koukourgiannis, and G. Kalivas, "Carrier Frequency Offset Estimation and Correction for Hiperlan/2 WLANs," *in Proc. IEEE 7th Int. Symposium Computer, Communication,* 1-4 Jul. 2002, pp. 693-698.

[44] R. O. Schmidt, "Multiple Emitter Location and Signal Parameter Estimation," *IEEE Trans. Antennas Propagat.*, vol. AP-34, no. 3, pp. 276-280, Mar. 1986.

[45] D. Spielman, A. Paulraj, and T. Kailath, "Performance Analysis of the MUSIC Algorithm," *in Proc. IEEE Int. Conf. Acoust., Speech, Signal Processing,* vol. 11, Apr. 1986, pp. 1909-1912.

[46] B. Friedlander, "A Sensitivity Analysis of the MUSIC Algorithm," *IEEE Trans. Acoust., Speech, Signal Processing,* vol. 38, pp. 1740-1751, Oct. 1990.

[47] P. Stoica and T. Soderstrom, "Statistical Analysis of MUSIC and Subspace Rotation Estimates of Sinusoidal Frequencies," *IEEE Trans. Signal Processing,* vol. 39, no. 8, pp. 1836-1847, Aug. 1991.

[48] P. Stoica and A. Nehorai, "MUSIC, Maximum Likelihood, and Cramer-Rao Bound: Further Results and Comparisons," *IEEE Trans. Acoust., Speech, Signal Processing,* vol. 37, no. 5, pp. 720-741, May, 1989.

[49] P. Stoica and A. Nehorai, "MUSIC, Maximum Likelihood, and Cramer-Rao Bound: Further Results and Comparisons," *IEEE Trans. Acoust., Speech, Signal Processing,* vol. 38, no. 12, pp. 2140-2150, Dec. 1990.

[50] R. Roy and T. Kailath, "ESPRIT-Estimation of Signal Parameters via Rotational Invariance Techniques," *IEEE Trans. Acoust., Speech, Signal Processing,* vol. 37, no. 7, pp. 984-995, Jul. 1989.

[51] Y. Hua and T. K. Sarkar, "Matrix Pencil Method and Its Performance," *in Proc. IEEE Int. Conf. Acoust., Speech, Signal Processing,* vol. 4, Apr. 1988, pp. 2476-2479.

[52] R. Kumaresan and D. W. Tufts, "Estimating the Parameters of Exponentially Damped Sinusoids and Pole-Zero Modeling in Noise," *IEEE Trans. Acoust., Speech, Signal Processing,* vol. 30, no. 6, pp. 833-840, Dec. 1982.

[53] Y. Hua and T. K. Sarkar, "Matrix Pencil Method for Estimating Parameters of Exponentially Damped/Undamped Sinusoids in Noise," *IEEE Trans. Acoust., Speech, Signal Processing,* vol. 38, no. 4, pp. 814-824, May, 1990.

[54] Y. Hua and T. K. Sarkar, "On SVD for Estimation Generalized Eigenvalues of Singular Matrix Pencil in Noise," *IEEE Trans. Signal Processing,* vol. 39, no. 4, pp. 892-900, Apr. 1991.

[55] J. B. Burg, "Maximum Entropy Spectral Analysis," PhD thesis, Dept. of Geophysics, Stanford University, Stanford CA, 1975.

[56] R. N. McDonough, *Application of Maximum Likelihood Method and the Maximum Entropy method to Array Signal Processing,* Springer Verlag., New York, 1979.

[57] N. Owsley, *Sonar Array Processing,* Prentice Hall Inc., New Jersey, 1985.

[58] S. W. Lang and J. H. Mcclellan, "Frequency Estimation with Maximum Entropy Spectral Estimators," *IEEE Trans. Acoust., Speech, Signal Processing,* vol. 28, no. 6, pp. 716-724, Dec. 1980.

[59] J. L. Lacoume, M. Gharbi, and C. Latombe, "Close Frequencies Resolution by Maximum Entropy Spectral Estimators," *IEEE Int., Conf. Acoust., Speech, Signal Processing,* vol. 7, May, 1982, pp. 1034-1037.

[60] C. K. E. Lau, R. S. Adve, and T. K. Sakar, "Combined CDMA and Matrix Pencil Direction of Arrival Estimation," *in Proc. IEEE Veh. Technol., Conf.*, vol. 1, Sept. 2002, pp. 496-499.

[61] P. Stoica and T. Soderstrom, "Statistical Analysis of MUSIC and ESPRIT Estimates of Sinusoidal Frequencies," *IEEE Int. Conf. Acoust., Speech, Signal Processing,* vol. 5, Apr. 1991, pp. 3273-3276.

[62] H. Krim and M. Viberg, "Two Decades of Array Signal Processing Research," *IEEE Signal Processing Mag.,* vol. 13, no. 4, pp. 67-94, Jul. 1996.

[63] A. Papoulis, *Probability, Random Variables, and Stochastic Processes*, Third Edition, McGraw-Hill, 1991.

[64] P. S. Naidu, *Sensor Array Signal Processing,* Boca Raton, Fla: CRC Press, c2001.

APPENDICES

APPENDIX A

CARRIER FREQUENCY OFFSET EFFECT ON THE RECEIVED OFDM SYMBOL

In Section 3.1, we have shown and discussed the effect of CFO, Eqn. (3.4) on the received OFDM symbol. The detailed derivation of this equation is given here. The received OFDM symbol with CFO after removing cyclic prefix is as follows:

$$y(n) = \frac{1}{\sqrt{N}} \sum_{k=0}^{N-1} H_k S_k \exp\left(j \frac{2\pi}{N} (k+\varepsilon) n \right) + w(n). \tag{A.1}$$

Without eliminating the CFO, ε, and by applying DFT on the received OFDM symbol, we obtain

$$\begin{aligned} Y_l &= \frac{1}{\sqrt{N}} \sum_{n=0}^{N-1} y(n) e^{-j\frac{2\pi ln}{N}} \\ &= \frac{1}{\sqrt{N}} \sum_{n=0}^{N-1} \frac{1}{\sqrt{N}} \sum_{k=0}^{N-1} H_k S_k e^{j\frac{2\pi}{N}(k+\varepsilon)n} e^{-j\frac{2\pi}{N}nl} + \frac{1}{\sqrt{N}} \sum_{n=0}^{N-1} w(n) e^{-j\frac{2\pi}{N}nl} \\ &= \frac{1}{N} \sum_{n=0}^{N-1} \sum_{k=0}^{N-1} H_k S_k e^{j\frac{2\pi}{N}(k-l-\varepsilon)n} + W_l \end{aligned} \tag{A.2}$$

where $W_l = \frac{1}{\sqrt{N}} \sum_{n=0}^{N-1} w(n) e^{-j\frac{2\pi}{N}nl}$ (FFT of $w(n)$). Let $k - l - \varepsilon = x$. From Eqn. (A.2) we have

$$Y_l = \frac{1}{N} \sum_{k=0}^{N-1} H_k S_k \sum_{n=0}^{N-1} e^{j\frac{2\pi}{N}xn} + W_l . \tag{A.3}$$

The quantity $\sum_{n=0}^{N-1} e^{j\frac{2\pi}{N}xn}$ from Eqn. (A.3) can be expended as

$$\begin{aligned}
\sum_{n=0}^{N-1} e^{j\frac{2\pi}{N}xn} &= 1 + e^{j\frac{2\pi}{N}x} + e^{j\frac{4\pi}{N}x} + ... + e^{J\frac{2\pi}{N}x(N-1)} \\
&= \frac{e^{j\frac{2\pi}{N}x(N)} - 1}{e^{j\frac{2\pi}{N}x} - 1} \qquad \text{(Geometric Series)} \\
&= \frac{e^{j2\pi x} - 1}{e^{j\frac{2\pi}{N}x} - 1} \\
&= \frac{e^{j\pi x}\left(e^{j\pi x} - e^{-j\pi x}\right)}{e^{j\frac{\pi}{N}x}\left(e^{j\frac{\pi}{N}x} - e^{-j\frac{\pi}{N}x}\right)} \\
&= \frac{e^{j\pi x}\sin(\pi x)}{e^{j\frac{\pi}{N}x}\sin\left(\frac{\pi}{N}x\right)} \\
&= \frac{\sin(\pi x)}{\sin\left(\frac{\pi}{N}x\right)} e^{j\pi x\left(1-\frac{1}{N}\right)} \\
&= \frac{\sin(\pi x)}{\sin\left(\frac{\pi}{N}x\right)} e^{j\frac{\pi}{N}x(N-1)} .
\end{aligned} \tag{A.4}$$

We use Eqn. (A.4) into the expression of Y_l as follows:

$$Y_l = \frac{1}{N} \sum_{k=0}^{N-1} H_k S_k \frac{\sin(\pi x)}{\sin\left(\frac{\pi}{N}x\right)} e^{j\frac{\pi}{N}x(N-1)} + W_l$$

substituting $k-l-\varepsilon=x$ into the Y_l, the CFO effect on the received OFDM symbol can be expressed as

$$Y_l=\frac{1}{N}\sum_{k=0}^{N-1} H_k S_k \frac{\sin\left(\pi\left(k-l-\varepsilon\right)\right)}{\sin\left(\frac{\pi}{N}\left(k-l-\varepsilon\right)\right)} e^{j\frac{\pi}{N}(k-l-\varepsilon)(N-1)}+W_l$$

$$=\frac{1}{N}H_l S_l \frac{\sin\left(\pi\varepsilon\right)}{\sin\left(\frac{\pi}{N}\varepsilon\right)} e^{j\frac{\pi}{N}\varepsilon(N-1)}$$

$$+\frac{1}{N}\sum_{\substack{k=0\\k\neq l}}^{N-1} H_k S_k \frac{\sin\left(\pi\left(k-l-\varepsilon\right)\right)}{\sin\left(\frac{\pi}{N}\left(k-l-\varepsilon\right)\right)} e^{j\frac{\pi}{N}(k-l-\varepsilon)(N-1)}+W_l .$$

APPENDIX B

CRAMER-RAO BOUND

In any parameter estimation problem, the CRB is useful in determining a lower bound of the estimator. In this section, we derive the CRB that will be used to compare the performance of the proposed methods in Chapter 3, and 5. In Chapter 5, it is used to evaluate the estimation accuracy of the CFO. We derive the CRB for both OFDM based WLAN structure and the conventional OFDM system.

The CRB states that the lower bound of the mean squared error of an unbiased estimator is the reciprocal of the Fisher Information Matrix, $\mathbf{F}$

$$\mathbf{CRB} \triangleq \mathbf{F}^{-1} \quad .$$

(a) CRB of the Conventional OFDM System

In Section 3.3, CRB has been made as a reference for performance comparison of MP and ESPRIT method. The detailed derivation of the CRB is given here. For the derivation of CRB, we use Eqn. (3.1):

$$y(n) = \frac{1}{\sqrt{N}} \sum_{k=0:2}^{N-1} H_k S_k \, e^{j\frac{2\pi}{N}(k+\varepsilon)n} + w(n)$$

$$= x'(n) \, e^{j\frac{2\pi}{N}\varepsilon n} + w(n) \tag{3.1}$$

where $x'(n) = \frac{1}{\sqrt{N}} \sum_{k=0}^{N-1} H_k S_k \, e^{j\frac{2\pi}{N}kn}$. Because of the Gaussian noise, Eqn. (3.1) satisfies the following statistical model:

$$y(n) \sim N_C(x'(n) e^{j\frac{2\pi}{N}kn}, \sigma^2) \tag{B.1}$$

where N_C denotes the complex circularly Gaussian probability density function and σ^2 is the noise variance. Using Eqn. (3.1), the unknown parameter can be defined as

$$\boldsymbol{\beta} \triangleq \left\{ \varepsilon, b, \theta, \sigma^2 \right\}^T \tag{B.2}$$

where ε is the normalized carrier frequency offset, b is the average magnitude value of $x'(n)$, θ is the average phase value of $x'(n)$ and σ^2 is the noise variance. The Fisher Information Matrix can be formed by using these parameters as follows:

$$\mathbf{F} = \begin{bmatrix} F_{\varepsilon\varepsilon} & F_{\varepsilon b} & F_{\varepsilon\theta} & 0 \\ F_{b\varepsilon} & F_{bb} & F_{b\theta} & 0 \\ F_{\theta\varepsilon} & F_{\theta b} & F_{\theta\theta} & 0 \\ 0 & 0 & 0 & F_{\sigma^2\sigma^2} \end{bmatrix} \tag{B.3}$$

where $F_{l,k}$ is Fisher Information element of l,k parameter, l or k is the one of the parameters of Eqn. (B.2). The element of the Fisher Information Matrix, $\mathbf{F}$, is given by

$$F_{l,k} = N \left\{ \frac{1}{\sigma^2} \frac{\partial \sigma^2}{\partial \beta_l} \frac{1}{\sigma^2} \frac{\partial \sigma^2}{\partial \beta_k} \right\} + 2\, Re \left\{ \sum_{n=0}^{N-1} \frac{\partial \left(x'(n) \, e^{j\frac{2\pi}{N}\varepsilon n} \right)^H}{\partial \beta_l} \frac{1}{\sigma^2} \frac{\partial \left(x'(n) \, e^{j\frac{2\pi}{N}\varepsilon n} \right)}{\partial \beta_k} \right\} \tag{B.4}$$

By using Eqn. (B.4) for the unknown parameters, $\varepsilon, b, \theta, \sigma^2$, in Eqn. (B.2), we have

$$F_{\varepsilon\varepsilon} = 0 + 2\ Re\left\{ \sum_{n=0}^{N-1} \frac{\partial\left(x'(n)\ e^{j\frac{2\pi}{N}\varepsilon n} \right)^H}{\partial\varepsilon} \frac{1}{\sigma^2} \frac{\partial\left(x'(n)\ e^{j\frac{2\pi}{N}\varepsilon n} \right)}{\partial\varepsilon} \right\}$$

$$= \frac{2}{\sigma^2}\ Re\left\{ \sum_{n=0}^{N-1} x'(n)^* \left(\frac{2\pi}{N}\ n \right)^2 x'(n) \right\} \tag{B.5}$$

$$F_{\varepsilon b} = 0 + 2\ Re\left\{ \sum_{n=0}^{N-1} \frac{\partial\left(x'(n)\ e^{j\frac{2\pi}{N}\varepsilon n} \right)^H}{\partial\varepsilon} \frac{1}{\sigma^2} \frac{\partial\left(x'(n)\ e^{j\frac{2\pi}{N}\varepsilon n} \right)}{\partial b_n} \right\}$$

$$= \frac{2}{\sigma^2}\ Re\left\{ \sum_{n=0}^{N-1} x'(n)^* \left(-j\frac{2\pi}{N} n \right)\ e^{j\theta_n} \right\} = 0 \tag{B.6}$$

where b_n is the magnitude of $x'(n)$ at the nth sample and θ_n is the phase of $x'(n)$ at the nth sample.

$$F_{\varepsilon\theta} = 0 + 2\ Re\left\{ \sum_{n=0}^{N-1} \frac{\partial\left(x'(n)\ e^{j\frac{2\pi}{N}\varepsilon n} \right)^H}{\partial\varepsilon} \frac{1}{\sigma^2} \frac{\partial\left(x'(n)\ e^{j\frac{2\pi}{N}\varepsilon n} \right)}{\partial\theta_n} \right\}$$

$$= \frac{2}{\sigma^2}\ Re\left\{ \sum_{n=0}^{N-1} x'(n)^* \left(\frac{2\pi}{N}\ n \right) x'(n) \right\} \tag{B.7}$$

$$F_{b\varepsilon} = 0 + 2\ Re\left\{ \sum_{n=0}^{N-1} \frac{\partial\left(x'(n)\ e^{j\frac{2\pi}{N}\varepsilon n} \right)^H}{\partial b_n} \frac{1}{\sigma^2} \frac{\partial\left(x'(n)\ e^{j\frac{2\pi}{N}\varepsilon n} \right)}{\partial \varepsilon} \right\}$$

$$= \frac{2}{\sigma^2}\ Re\left\{ \sum_{n=0}^{N-1} e^{-j\theta_n}\ x'(n) \left(j\frac{2\pi}{N} n \right) \right\} = 0 \tag{B.8}$$

$$F_{bb} = 0 + 2\ Re\left\{ \sum_{n=0}^{N-1} \frac{\partial\left(x'(n)\ e^{j\frac{2\pi}{N}\varepsilon n} \right)^H}{\partial b_n} \frac{1}{\sigma^2} \frac{\partial\left(x'(n)\ e^{j\frac{2\pi}{N}\varepsilon n} \right)}{\partial b_n} \right\}$$

$$= \frac{2}{\sigma^2}\ Re\left\{ \sum_{n=0}^{N-1} 1 \right\} = \frac{2}{\sigma^2} N \tag{B.9}$$

$$F_{b\theta} = 0 + 2\ Re\left\{ \sum_{n=0}^{N-1} \frac{\partial\left(x'(n)\ e^{j\frac{2\pi}{N}\varepsilon n} \right)^H}{\partial b_n} \frac{1}{\sigma^2} \frac{\partial\left(x'(n)\ e^{j\frac{2\pi}{N}\varepsilon n} \right)}{\partial \theta_n} \right\}$$

$$= \frac{2}{\sigma^2}\ Re\left\{ \sum_{n=0}^{N-1} e^{-j\theta_n}\ x'(n)\ (j) \right\} = 0 \tag{B.10}$$

$$F_{\theta\varepsilon} = 0 + 2\ Re\left\{ \sum_{n=0}^{N-1} \frac{\partial\left(x'(n)\ e^{j\frac{2\pi}{N}\varepsilon n} \right)^H}{\partial \theta_n} \frac{1}{\sigma^2} \frac{\partial\left(x'(n)\ e^{j\frac{2\pi}{N}\varepsilon n} \right)}{\partial \varepsilon} \right\}$$

$$= \frac{2}{\sigma^2}\ Re\left\{ \sum_{n=0}^{N-1} x'(n)^*\ x'(n) \left(\frac{2\pi}{N} n \right) \right\} \tag{B.11}$$

$$F_{\theta b} = 0 + 2\ Re\left\{ \sum_{n=0}^{N-1} \frac{\partial\left(x'(n)\ e^{j\frac{2\pi}{N}\varepsilon n} \right)^H}{\partial \theta_n} \frac{1}{\sigma^2} \frac{\partial\left(x'(n)\ e^{j\frac{2\pi}{N}\varepsilon n} \right)}{\partial b_n} \right\}$$

$$= \frac{2}{\sigma^2}\ Re\left\{ \sum_{n=0}^{N-1} (-j)\, x'(n)^*\ e^{j\theta_n} \right\} = 0 \tag{B.12}$$

$$F_{\theta\theta} = 0 + 2\ Re\left\{ \sum_{n=0}^{N-1} \frac{\partial\left(x'(n)\ e^{j\frac{2\pi}{N}\varepsilon n} \right)^H}{\partial \theta_n} \frac{1}{\sigma^2} \frac{\partial\left(x'(n)\ e^{j\frac{2\pi}{N}\varepsilon n} \right)}{\partial \theta_n} \right\}$$

$$= \frac{2}{\sigma^2}\ Re\left\{ \sum_{n=0}^{N-1} x'(n)^* x'(n) \right\} \tag{B.13}$$

$$F_{\sigma^2\sigma^2} = \frac{N}{\sigma^4} + 2\ Re\left\{ \sum_{n=0}^{N-1} \frac{\partial\left(x'(n)\ e^{j\frac{2\pi}{N}\varepsilon n} \right)^H}{\partial \sigma^2} \frac{1}{\sigma^2} \frac{\partial\left(x'(n)\ e^{j\frac{2\pi}{N}\varepsilon n} \right)}{\partial \sigma^2} \right\}$$

$$= \frac{N}{\sigma^4} \tag{B.14}$$

and the CRB function of the unknown parameters is

$$\mathbf{CRB} \triangleq \mathbf{F}^{-1}$$

$$\begin{bmatrix} CRB_{\varepsilon\varepsilon} & CRB_{\varepsilon b} & CRB_{\varepsilon\theta} & 0 \\ CRB_{b\varepsilon} & CRB_{bb} & CRB_{b\theta} & 0 \\ CRB_{\theta\varepsilon} & CRB_{\theta b} & CRB_{\theta\theta} & 0 \\ 0 & 0 & 0 & CRB_{\sigma^2\sigma^2} \end{bmatrix} = \begin{bmatrix} F_{\varepsilon\varepsilon} & F_{\varepsilon b} & F_{\varepsilon\theta} & 0 \\ F_{b\varepsilon} & F_{bb} & F_{b\theta} & 0 \\ F_{\theta\varepsilon} & F_{\theta b} & F_{\theta\theta} & 0 \\ 0 & 0 & 0 & F_{\sigma^2\sigma^2} \end{bmatrix}^{-1} . \tag{B.15}$$

Since our interest is the CRB of the CFO estimation, we find the CRB for only CFO as

$$CRB_{CFO} = \mathbf{CRB}(1,1) = CRB_{\varepsilon\varepsilon} . \tag{B.16}$$

(b) CRB of the OFDM based WLAN System

Since the performances of the proposed methods are compared with CRB in Section 5.2, a detailed derivation of the CRB is presented here. The Eqns. (4.7) and (4.11) satisfy the following statistical model:

$$\mathbf{y}(n) \sim N_C\left(\mathbf{a}(\varepsilon)x(n),\, \sigma^2\mathbf{I}\right) \tag{B.17}$$

The unknown parameters can be defined from Eqns. (4.7) and (4.11) as

$$\boldsymbol{\beta} = \left\{\, \varepsilon,\, b,\, \theta,\, \sigma^2 \,\right\}^T \tag{B.18}$$

where b is the average magnitude value of $x(n)$, θ is the average phase value of $x(n)$. In this case, $x(n)$ means $x_S(1,n)$ of the short training symbols, and $x_L(1,n)$ of the long training symbols. Therefore, the elements of the Fisher Information Matrix for OFDM based WLAN are given by

$$\begin{aligned} F_{\varepsilon\varepsilon} &= 0 + 2\, Re\left\{ \sum_{n=0}^{N-1} \frac{\partial\left(\mathbf{a}(\varepsilon)x(n)\right)^H}{\partial\varepsilon}\, \frac{1}{\sigma^2}\, \frac{\partial\left(\mathbf{a}(\varepsilon)x(n)\right)}{\partial\varepsilon} \right\} \\ &= \frac{2}{\sigma^2}\, Re\left\{ \sum_{n=0}^{N-1} x(n)^*\, \mathbf{D}^H\, \mathbf{D}\, x(n) \right\} \end{aligned} \tag{B.19}$$

where $\mathbf{D} = \dfrac{\partial\mathbf{a}(\varepsilon)}{\partial\varepsilon}$

$$\begin{aligned} F_{\varepsilon b} &= 0 + 2\, Re\left\{ \sum_{n=0}^{N-1} \frac{\partial\left(\mathbf{a}(\varepsilon)x(n)\right)^H}{\partial\varepsilon}\, \frac{1}{\sigma^2}\, \frac{\partial\left(\mathbf{a}(\varepsilon)x(n)\right)}{\partial b_n} \right\} \\ &= \frac{2}{\sigma^2}\, Re\left\{ \sum_{n=0}^{N-1} x(n)^*\, \mathbf{D}^H\, \mathbf{a}(\varepsilon)e^{j\theta_n} \right\} \end{aligned} \tag{B.20}$$

$$F_{\varepsilon\theta} = 0 + 2\ Re\left\{ \sum_{n=0}^{N-1} \frac{\partial\left(\mathbf{a}(\varepsilon)x(n)\right)^H}{\partial\varepsilon} \frac{1}{\sigma^2} \frac{\partial\left(\mathbf{a}(\varepsilon)x(n)\right)}{\partial\theta_n} \right\}$$

$$= \frac{2}{\sigma^2}\ Re\left\{ \sum_{n=0}^{N-1} x(n)^* \mathbf{D}^H \mathbf{a}(\varepsilon)x(n)(j) \right\} \tag{B.21}$$

$$F_{b\varepsilon} = 0 + 2\ Re\left\{ \sum_{n=0}^{N-1} \frac{\partial\left(\mathbf{a}(\varepsilon)x(n)\right)^H}{\partial b_n} \frac{1}{\sigma^2} \frac{\partial\left(\mathbf{a}(\varepsilon)x(n)\right)}{\partial\varepsilon} \right\}$$

$$= \frac{2}{\sigma^2}\ Re\left\{ \sum_{n=0}^{N-1} e^{-j\theta_n} \mathbf{a}^H(\varepsilon)\mathbf{D}\ x(n) \right\} \tag{B.22}$$

$$F_{bb} = 0 + 2\ Re\left\{ \sum_{n=0}^{N-1} \frac{\partial\left(\mathbf{a}(\varepsilon)x(n)\right)^H}{\partial b_n} \frac{1}{\sigma^2} \frac{\partial\left(\mathbf{a}(\varepsilon)x(n)\right)}{\partial b_n} \right\}$$

$$= \frac{2}{\sigma^2}\ Re\left\{ \sum_{n=0}^{N-1} \mathbf{a}^H(\varepsilon)\mathbf{a}(\varepsilon) \right\} = \frac{2}{\sigma^2}\ N\left(\mathbf{a}^H(\varepsilon)\mathbf{a}(\varepsilon)\right) \tag{B.23}$$

$$F_{b\theta} = 0 + 2\ Re\left\{ \sum_{n=0}^{N-1} \frac{\partial\left(\mathbf{a}(\varepsilon)x(n)\right)^H}{\partial b_n} \frac{1}{\sigma^2} \frac{\partial\left(\mathbf{a}(\varepsilon)x(n)\right)}{\partial\theta_n} \right\}$$

$$= \frac{2}{\sigma^2}\ Re\left\{ \sum_{n=0}^{N-1} e^{-j\theta_n} \mathbf{a}^H(\varepsilon)\mathbf{a}(\varepsilon)x(n)\ (j) \right\} = 0 \tag{B.24}$$

$$F_{\theta\varepsilon} = 0 + 2\ Re\left\{ \sum_{n=0}^{N-1} \frac{\partial\left(\mathbf{a}(\varepsilon)x(n)\right)^H}{\partial\theta_n} \frac{1}{\sigma^2} \frac{\partial\left(\mathbf{a}(\varepsilon)x(n)\right)}{\partial\varepsilon} \right\}$$

$$= \frac{2}{\sigma^2}\ Re\left\{ \sum_{n=0}^{N-1} (-j)\,x(n)^* \mathbf{a}^H(\varepsilon)\mathbf{D}\,x(n) \right\} \tag{B.25}$$

$$F_{\theta b} = 0 + 2\ Re\left\{ \sum_{n=0}^{N-1} \frac{\partial\left(\mathbf{a}(\varepsilon)x(n)\right)^H}{\partial\theta_n} \frac{1}{\sigma^2} \frac{\partial\left(\mathbf{a}(\varepsilon)x(n)\right)}{\partial b_n} \right\}$$

$$= \frac{2}{\sigma^2} Re\left\{ \sum_{n=0}^{N-1} (-j)\, x(n)^* \mathbf{a}^H(\varepsilon)\mathbf{a}(\varepsilon) e^{j\theta_n} \right\} = 0 \tag{B.26}$$

$$F_{\theta\theta} = 0 + 2\ Re\left\{ \sum_{n=0}^{N-1} \frac{\partial\left(\mathbf{a}(\varepsilon)x(n)\right)^H}{\partial\theta_n} \frac{1}{\sigma^2} \frac{\partial\left(\mathbf{a}(\varepsilon)x(n)\right)}{\partial\theta_n} \right\}$$

$$= \frac{2}{\sigma^2} Re\left\{ \sum_{n=0}^{N-1} x(n)^* \mathbf{a}^H(\varepsilon)\mathbf{a}(\varepsilon) x(n) \right\} \tag{B.27}$$

$$F_{\sigma^2\sigma^2} = \frac{N}{\sigma^4} + 2\ Re\left\{ \sum_{n=0}^{N-1} \frac{\partial\left(\mathbf{a}(\varepsilon)x(n)\right)^H}{\partial\sigma^2} \frac{1}{\sigma^2} \frac{\partial\left(\mathbf{a}(\varepsilon)x(n)\right)}{\partial\sigma^2} \right\}$$

$$= \frac{N}{\sigma^4}\ . \tag{B.28}$$

We can find the CRB for CFO estimation in OFDM based WLAN by using Eqns. (B.15) and (B.16).